KOGNITIVE NEUROPHYSIOLOGIE DES MENSCHEN

HUMAN COGNITIVE NEUROPHYSIOLOGY

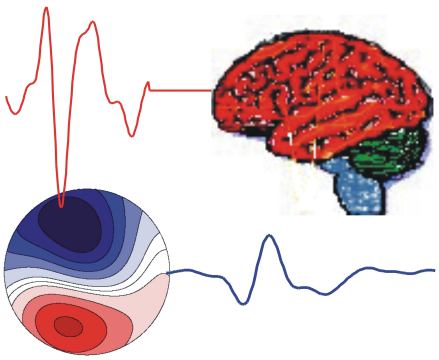

Impressum
Herausgeber: Wolfgang Skrandies

wolfgang.skrandies@physiologie.med.uni-giessen.de

ISSN 1867-576X

Kognitive Neurophysiologie des Menschen wurde im Jahr 2008 gegründet. Hier sollen wissenschaftliche Artikel zu Themen der kognitiven Neurophysiologie des Menschen erscheinen Sowohl Beiträge über Methoden als auch Ergebnisse der Grundlagen- und klinischen Forschung werden akzeptiert. Jedes Manuskript wird von 3 unabhängigen Gutachtern beurteilt und so rasch wie möglich publiziert werden.
Die Zeitschrift ist ein elektronisches "Open Access"-Journal, ohne kommerzielle Interessen; `http://geb.uni-giessen.de/geb/volltexte/2008/6504/.`
Eine dauerhafte Präsenz der Zeitschrift im Internet wird durch die Universität Giessen gewährleistet.

Human Cognitive Neurophysiology was founded in 2008. This journal will publish contributions on methodological advances as well as results from basic and applied research on cognitive neurophysiology. Both German and English manuscripts will be accepted. Each manuscript will be reviewed by three independent referees.
This is an electronic "Open Access"-Journal with no commercial interest, published at `http://geb.uni-giessen.de/geb/volltexte/2008/6504/.`
Online presence is guaranteed by the University of Giessen.

Instructions for Authors

Only original and unpublished work will be considered for publication unless it is explicitly stated that the topic is a review. All manuscripts will be peer-reviewed. Both German and English versions are acceptable. After publication, the copyright will be with the editor of the journal. Usage of published material for review papers will be granted. Manuscripts (as `WORD` or `TEX files`) should be sent to `wolfgang.skrandies@physiologie.med.uni-giessen.de`.

Organization of manuscripts: The title page with a concise title should give the authors' names, address(es), and e-mail address of the corresponding author. The manuscript should include an abstract in English (maximum 300 words). Organize your work in the sections Introduction, Methods, Results, Discussion, and Literature. Please also supply a short list of keywords that may help to find your publication.

Illustrations: All figures should be submitted as `jpeg` or `Coreldraw` files. Please supply figure legends that explain the content of the figures in detail. Since this is an electronic journal color figures will be published free-of-charge.

The *Literature* should only include papers that have been published or accepted for publication. The reference list should be in alphabetical order by author. In the text, references should be cited by author(s) and year (e.g. Johnson, Hsiao, & Twombly, 1995; Pascual-Marqui, Michel, & Lehmann, 1994; Zani & Proverbio, 2002).

Examples of reference format

Johnson, K., Hsiao, S., & Twombly, L. (1995). Neural mechanisms of tactile form recognition. In M. Gazzaniga (Ed.), *The Cognitive Neurosciences* (p. 253-267). Cambridge, Mass.: MIT Press.

Pascual-Marqui, R., Michel, C., & Lehmann, D. (1994). Low resolution electromagnetic tomography: a new method for localizing electrical activity in the brain. *International Journal of Psychophysiology*, *18*, 49-65.

Zani, A., & Proverbio, A. (Eds.). (2002). *The Cognitive Electrophysiology of Mind and Brain*. San Diego: Elsevier.

Inhalt — Contents

Abstract

B. Kopp, C. Moschner & K. Wessel (Braunschweig, Germany) — Event-related Brain Potentials and the Functional Specialization of Human Cerebral Hemispheres During Processing of Hierarchical Visual Stimuli

Neuropsychological evidence indicates that local and global features of visual stimuli are processed differentially by the two cerebral hemispheres. Whereas local levels of hierarchical stimuli should be processed more efficiently in the left hemisphere, the right hemisphere should be more efficient in processing global information. Event-related brain potentials (ERPs) and lateralized readiness potentials (LRPs) were measured in a go-nogo task using hierarchical letters. Participants had to respond to conjunctions of target shapes at global and local levels (i.e., a divided attention task). Responses were required only if target features were met on both levels. Neither the behavioral results nor the ERP or LRP findings supported global precedence, probably because the stimuli contained local, but not global, shapes at fixation, thereby counteracting the usually faster global processing. ERPs provided evidence that the left and right parietal regions were differentially activated during attentional allocation to the local and global levels, respectively. Specifically, the posterior N2 at around 350 ms post-stimulus, but not the earlier exogenous ERP components (P1, N1), showed the expected hemispheric lateralization. Response-locked ERPs manifested a novel response-synchronized lateralized posterior positivity (rLPP) which peaked simultaneously with the key-press. The rLPP may be an electrophysiological correlate of hemispheric monitoring.

Keywords: Lateralized event-related brain potentials (ERPs); Lateralized readiness potentials (LRPs); Navon letters; Global precedence; Hemispheric specialization

Event-related Brain Potentials and the Functional Specialization of Human Cerebral Hemispheres During Processing of Hierarchical Visual Stimuli

B. Kopp, C. Moschner & K. Wessel, Cognitive Neurology, University of Technology Carolo-Wilhelmina, and Department of Neurology, Braunschweig Hospital, 38126 Braunschweig, Germany
b.kopp@klinikum-braunschweig.de

Introduction

Zaidel (2001) provided one of the best descriptions of hemispheric brain asymmetry: "Today, cerebral asymmetry remains a cornerstone of human neuropsychology and serves as a model system for a fundamental question in cognitive neuroscience: how do separate subsystems of the mind/brain maintain their independence, on the one hand, and interact, on the other?" (p. 1322). In this article, we address these questions by analyzing event-related brain potentials (ERPs; Luck, 2005) recorded from healthy individuals during processing of hierarchical visual stimuli.

Hemispheric specialization may be divided by modality, material, or stage of processing, with the left hemisphere (LH) specialized for auditory, verbal or output processing and the right hemisphere (RH) for visual, nonverbal, or input processing (cf., Corballis, 1997; Hugdahl & Davidson, 2003; Zaidel & Iacoboni, 2003). According to a widely held theory of hemispheric specialization, the LH is dominant for language and praxis, whereas the RH is dominant for visuospatial functions. More recent views describe hemispheric specialization in terms of information-processing styles: the LH is analytic and the RH is holistic (cf., Robertson & Ivry, 2000). Another view holds that the LH analyzes local and the RH analyzes global levels of hierarchical stimuli (Sergent, 1982). In this context, the LH might be specialized for processing relatively high spatial and temporal frequencies whereas the RH might be specialized for relatively low frequencies (Hellige, 1993). According to the filtering-by-frequency hypothesis, the LH operates as a high-pass filter, allowing more high frequency information to pass on for further processing, and the RH operates as a low pass-filter, allowing more low frequency information to pass on for further processing (Ivry & Robertson, 1998). Asymmetric frequency filtering yields non-identical representations in the two hemispheres and, therefore, the two hemispheres are not simply performing redundant analyses: the LH representation should be more efficient for identifying the local information whereas the RH representation should be more efficient for identifying the global information in hierarchical perception tasks. The high frequency/local vs. low frequency/global hemispheric dissociation received empirical support mainly from behavioral studies in hemisphere-damaged patients: Patients with lesions in the temporoparietal junction exhibited marked problems with the analysis of global aspects of such stimuli following right-hemispheric lesions and with the analysis of local aspects following left-hemispheric lesions (Robertson, 1995; Robertson, Lamb, & Knight, 1988).

While in the real world global (e.g., a forest) and local levels (e.g., the trees) of a visual scene are often quite different, most experimental studies of processing of hierarchical visual stimuli have been composed of relatively similar elements at both levels. In particular, the hierarchical letter paradigm (Navon, 1977) is often used for investigating hemispheric specialization of local processing and global processing: Large letters made up of small letters, like those shown in Figure 1, are presented to subjects who are required to identify the large (global) letters or the small (local) letters, respectively. Response time (RT) studies usually reveal three effects: 1. A global precedence effect (also denoted level effect) because subjects usually respond to global shapes more rapidly than to local shapes (Miller & Navon, 2002). 2. A congruency effect because congruent stimuli (e.g., a large H made of little „H“s) are easier to identify than incongruent stimuli (e.g., a large H made of little „E“s; Zaidel, Iacoboni, Zaidel, & Bogen, 2003). 3. The congruency effect is, however, asymmetric because conflicting information from an irrelevant global shape is disruptive when subjects discriminate among local shapes, whereas conflicting information from irrelevant local shapes has little effect when subjects discriminate among global shapes

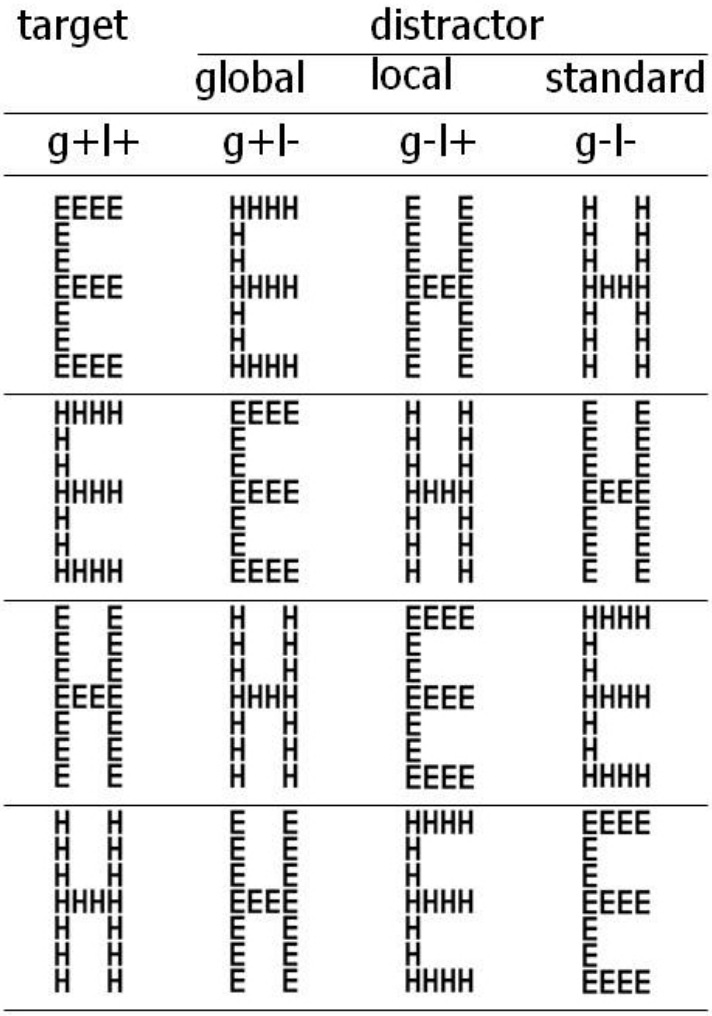

Figure 1: *Columns show targets (leftmost column), global distractors (left column), local distractors (right column), and standard distractors (rightmost column). Rows show the four possible ways to define a particular stimulus set: Uppermost row: When the target (g+l+) equals the global and local "E", the global "E", local "H" serves as global (g+l–) distractor, the global "H", local "E" as local (g–l+) distractor, and the global and local "H" as standard (g–l–) distractor. Upper row: When the target (g+l+) equals the global "E", local "H", the global and local "E" serves as global (g+l–) distractor, the global and local "H" as local (g–l+) distractor, and the global "H", local "E" as standard (g–l–) distractor. Lower row: When the target (g+l+) equals the global "H", local "E", the global and local "H" serves as global (g+l–) distractor, the global and local "E" as local (g–l+) distractor, and the global "E", local "H" as standard (g–l–) distractor. Lowermost row: When the target (g+l+) equals the global and local "H", the global "H", local "E" serves as global (g+l–) distractor, the global "E", local "H" as local (g–l+) distractor, and the global and local "E" as standard (g–l–) distractor.*

(Miller & Navon, 2002). Together, these phenomena are consistent with the hypothesis that global information is available earlier than local information (Miller & Navon, 2002).

RT studies provide, however, very limited evidence for hemispheric specialization of processing of hierarchical visual stimuli (van Kleeck, 1989; Yovel, Yovel, & Levy, 2001). A number of stimulus and task factors of hierarchical stimulus paradigms are known to influence hemispheric asymmetry:

1. When stimuli are presented either in the left or right visual fields, hemispheric asymmetry is attenuated compared to central stimulus presentation (Han et al., 2002; Lux et al., 2004).

2. The nature of the stimulus material affects hemispheric asymmetry: Verbal stimuli (hierarchical letters) produce more pronounced evidence for hemispheric specialization than nonverbal (hierarchical figures) stimuli (Han, Fan, Chen, & Zhuo, 1997; Han, He, Yund, & Woods, 2001).

3. Hemispheric asymmetry usually shows up in active cognitive tasks (Reinvang, Magnussen, & Greenlee, 2002), particularly when the task is attentionally demanding or computationally complex (Banich & Belger, 1990; Banich, 1998).

4. Stimulus congruency affects hemispheric asymmetry: Incongruent stimuli produce more pronounced evidence for hemispheric specialization than congruent stimuli, particularly when response conflicts between the hierarchical levels are implicated (Volberg & Hübner, 2004). These authors attributed the effect of conflicting incongruency on hemispheric asymmetry to an elaborated stimulus representation which might be necessary for resolving the response conflict induced by these hierarchical stimuli.

5. Selective and divided attention affects the temporal locus of hemispheric asymmetry differently, a phenomenon that we will discuss below.

A method that has repeatedly been applied to the investigation of hemispheric specialization is the recording of ERPs. The ERP technique offers measures of cortical activity with excellent temporal resolution, even if events do not require behavioral responses (Luck, 2005). Three groups of ERP components may be distinguishable on a relatively large scale:

1. Early components are related to sensory processing, with clearly modality-specific characteristics, and are often referred to as exogenous ERP components (P1, N1). However, it should be stressed that pure top-down mechanisms, such as the voluntary allocation of visual spatial attention, can modulate the amplitude of exogenous components (Hillyard, Teder-Sälejärvi, & Münte, 1998). In contrast to processes related to spatial attention, the allocation of voluntary feature-based visual attention modulates, in a more sustained manner, later parts of the ERP waveform at posterior and anterior sites (P2, e.g., Potts, 2004).

2. Late ERP components show only minimal modality-specific characteristics. Therefore, they are often referred to as endogenous components, and they are related to processes that are implicated in sensorimotor decisions (N2: Folstein & van Petten, 2008; P3: Kopp, 2008). Both endogenous ERP components should be subclassified into dissociable anterior and posterior components: The P3b component is a parietal positivity, peaking at approximately 400 ms after stimulus on-

set. It is larger to infrequent stimuli, particularly when these stimuli are targets (Picton, Lins, & Scherg, 1995). Instead, infrequent stimuli that are irrelevant to the task (distractors), but that are more salient than the targets, evoke the P3a (Friedman, Cycowicz, Gaeta, 2001). The P3a has its peak earlier than the P3b, and it has a more frontocentral scalp distribution. The anterior N2 (here denoted N2c; Kopp, Rist, & Mattler, 1996) has a mediofrontal scalp distribution, and peaks around 250-300 ms post-stimulus in tasks that utilize simple stimuli. Attention-related N2 components have, in the visual modality, a posterior scalp distribution (Folstein & van Petten, 2008).

3. The readiness potential is a slow negative potential that precedes spontaneous voluntary movements of the distal limbs (Kornhuber & Deecke, 1965). The later part of the RP is larger over the contralateral scalp of a moved hand, and it arises mainly from primary motor cortex (Lang et al., 1991). The lateralized portion of the readiness potential (LRP) can be measured in choice RT tasks in which a stimulus signals that a response should be made with one of two effectors, usually one of the hands (Coles, 1989; Rinkenauer et al., 2004). LRP recordings are made from two electrode sites (C3 and C4) located over the left and right hand areas of the motor cortex, respectively. Let the potentials recorded at the contralateral and ipsilateral sites at time $t$be denoted as Contralateral(t) and Ipsilateral(t) to the responding hand. The LRP at time $t$is then defined as LRP (t) = Average over hands [Contralateral (t) – Ipsilateral (t)]. The resulting LRP will be negative when the response is performed with the signaled hand, but it will be positive when the response is performed with the wrong hand.

There are several main findings from ERP studies of processing of hierarchical visual stimuli:

1. Selective vs. divided attention tasks led to a dissociation with regard to the P1 component of the ERP: The P1 component was not different for global versus local targets under conditions of divided attention. But under selective attention conditions, the P1 component was enlarged for global versus local attention (Heinze, Hinrichs, Scholz, Burchert, & Mangun, 1998). Similar results were obtained for the N1 component (Proverbio, Minniti, & Zani, 1998).

2. The posterior N2 component of the ERP showed the expected hemispheric asymmetries, i.e. a relatively larger amplitude over the left hemisphere for local targets and over the right hemisphere for global targets (Heinze & Münte, 1993; Heinze et al., 1998; Malinowski, Hübner, Keil, & Gruber, 2002; Volberg & Hübner, 2004; Yamaguchi, Yamagata, & Kobayashi, 2000; Yoshida, Yoshino, Takahashi, & Nomura, 2007). While one cannot assume that potentials over one hemisphere are necessarily generated in the underlying hemisphere, these data showed differential lateralization of local and global visual processing.

3. The LRP received relatively little consideration. In Experiment 1 of Miller & Navon's (2002) study, subjects responded to local shapes and ignored global shapes (selective attention). As revealed by the LRP, the irrelevant global shapes activated responses in the motor cortex. In Experiment 2, subjects responded to conjunctions of target shapes at local and global levels (divided attention), while withholding the response if

the target shape appeared at only one level (i.e. a go-nogo task). Global, but not local, target shapes activated responses. These LRP results substantiate global precedence. However, another LRP study (Ridderinkhof & van der Molen, 1995), in which no RT global precedence effect became apparent, revealed that the level effect varies as a function of the temporal advantage for the processing of information from either level: The individually faster (local or global) level interferes with the slower level, but it is immune to such interference from the slower level.

Together the ERP findings indicate that, at least under conditions of divided attention, early sensory inputs are not modulated to gate global versus local information differentially into the two hemispheres. Rather, later stages of processing that may be asymmetrically organized in the left and right hemispheres operate in parallel to process global and local aspects of hierarchical stimuli (c.f. the posterior N2 effect of the ERPs). This pattern of results supports models proposing that spatial frequency analysis is only asymmetric at higher stages of perceptual processing and not at the earliest stages of visual cortical analysis (Sergent, 1982; Hellige, 1993; Ivry & Robertson, 1998). The available LRP results show that the processing of information from the faster (usually, but not always, the global) level interferes with the slower level whenever the fast level activates the conflicting response in the motor cortex.

The present study aimed at an electrophysiological analysis of global precedence and hemispheric asymmetry. The study made use of an adaptation of the hierarchical letter paradigm (Navon, 1977) which was akin to Miller and Navon's (2002) which combined the demand to divide attention and to decide whether or not one has to respond (i.e, a go-nogo task). A set of four hierarchical stimuli like those shown in Figure 1 were presented. This set was produced by factorially combining two letter shapes (namely, E and H) at two hierarchical levels (local, global). Subjects had to respond to conjunctions of target shapes at local and global levels, while withholding the response when the target shape appeared at only the local or the global level, respectively, or when the target shape appeared at none of the levels. The presence of response conflicts can be evaluated by comparing cortical responses in response to global and local distractors, respectively, with cortical responses in response to standard distractors (cf. Figure 1). Specifically, the global – standard comparison allows to evaluate the interference effect induced by target compatibility at the global level, whereas the local – standard comparison allows to evaluate the interference effects induced by target compatibility at the local level. It is worth noting, however, that it is the target-incompatible level of these hierarchical stimuli which implies to withhold the response (i.e., the local level of the global distractor and the global level of the local distractor).

The global precedence hypothesis leads to the prediction of larger interference effects by global distractors in comparison to local distractors. It is not possible to analyze RT effects in this study because the distractors are presented in nogo trials. Yet, the experiment could provide information about the global precedence effect. First, ERPs offer measures of cortical activity with excel-

lent temporal resolution (Luck, 2005). Our group described ERP results that were obtained from non-hierarchical versions of this go-nogo task in two earlier publications (Kopp, Tabeling, Moschner, & Wessel, 2007; Kopp & Wessel, 2010). Specifically, an enhanced anterior N2 (N2c) and an enhanced anterior P3 (P3a) were observed when an easily discriminated attribute activated the go response, whereas a less easily discriminated attribute implied to withhold the response. Second, when the response has to be made with one hand, but in other parts of the experiment with the other hand, the LRP provides information whether level-specific target compatible information led to response activation. These nogo trials should provide a sensitive test for global and/or local response activation because in these nogo trials no response-related LRP is generated to obscure the level-specific preliminary response activation (Miller & Navon, 2002).

With regard to hemispheric asymmetry, the global distractor is expected to be preferably processed in the left hemisphere. This is because it is the local, target-incompatible information that drives the nogo decision. The correct decision requires an elaborated local representation (Volberg & Hübner, 2004) which is expected to be located within the left hemisphere (Sergent, 1982; Hellige, 1993; Ivry & Robertson, 1998). In contrast, the local distractor is expected to be preferably processed in the right hemisphere. Here, it is the global, target-incompatible information that drives the nogo decision. The correct decision requires an elaborated global representation (Volberg & Hübner, 2004) which is expected to be located within the right hemisphere (Sergent, 1982; Hellige, 1993; Ivry & Robertson, 1998).

Methods

Participants

Twenty-four volunteers participated (M = 22 years; range = 18-39 years; four males; twenty-two right-handed). All participants were un-medicated and neurologically unimpaired. All had normal or corrected-to-normal vision and normal hearing. All participants were students at the University of Technology at Braunschweig. They were compensated with course credits. A written consent statement was obtained from participants after the nature and objectives of the experiment were explained.

Stimuli

Navon figures (large, global letters made up of small, local letters) were created within a 4 $\times$ 7 matrix (Figure 1). Two different letters (E, H) were used to create the stimuli. There were four different stimuli: global shape “E” and local shape “E”, global shape “E” and local shape “H”, global shape “H” and local shape “E”, as well as global shape “H” and local shape “H”. The letters were displayed in black against white background. Stimuli (150 ms duration) and a preceding (red) fixation star (250 ms duration; 0.3˚ visual angle) were presented centrally. The visual angles subtended by the global and local letters were: 6.6˚ (global letter – vertical axis), 3.3˚ (global letter – horizontal axis), 0.8˚ (local letter – vertical axis), 0.6˚ (local letter – horizontal axis). Viewing distance was 125 cm. The stimuli were presented one at a time in the

center of a computer screen (FlexScan T766 19“(Eizo, Hakusan, Ishikawa, Japan); 1280 × 1024 pixels at 100 Hz presentation rate; 1150 ms inter-stimulus-interval). Stimulus presentation was controlled by the Presentation® software (Neurobehavioral Systems, Albany, CA) that was installed on an IBM- compatible personal computer.

Apparatus and Procedure

Participants were instructed that one stimulus was the target (denoted g+l+, i.e., the stimulus with the target-compatible global shape and with the target-compatible local shape; cf. Figure 1) throughout the experiment. In any given trial, one out of the four stimuli was presented and participants had to decide whether or not the current stimulus equaled the target. Participants pressed the space bar with their index finger on a standard computer keyboard when they recognized the target stimulus. Participants were instructed not to respond if the stimulus was recognized as one of the distractors. No feedback about response accuracy was provided.

There were three types of distractors, the global distractor, g+l–, the local distractor, g–l+, and the standard distractor, g–l–. Individual participants received different stimuli as the target stimulus, i.e. the global “E” / local “E”, the global “E” / local “H”, the global “H” / local “E”, or the global “H” / local “H”, respectively. Adequate counterbalancing (i.e., six participants received each of these types of stimuli as the target) yielded targets and distractors that were, on average, composed of physically identical stimuli (cf. Figure 1). Thus, comparisons between averaged ERPs in response to the various distractor types avoid physical stimulus confounds (Luck, 2005).

Each participant performed eight blocks of 144 trials each (8 × 144 = 1152 trials overall). Blocks were divided by short breaks (lasting two or three minutes). The four stimuli occurred with equal probabilities within each block (i.e., in 144 / 4 = 36 trials per block). The order of succession of stimuli was pseudorandom. Response hand (left, right) was alternated. The responding hand was maintained across four consecutive blocks. The order of succession of the responding hand was counterbalanced across participants. Within each level of response hand, each stimulus occurred in 144 (4 × 36) trials.

Participants were instructed that they would receive four different types of stimuli in rapid succession, and that one of these stimuli would be their target throughout a block of trials. They were informed about the randomness of the stimulus sequence, and they were asked to respond as fast as possible without committing errors. Participants received twenty-four practice trials in the run-up to the experiment. The target detection task that was performed on the practice stimuli was based on the number (one or two) and the spatial orientation (towards the left or towards the right) of green bars.

Recording

Continuous EEG was recorded by means of another IBM-compatible personal computer, a QuickAmps-72 amplifier (Brain Products, Gilching, Germany) and the BrainVisionRecorder® software (Brain Products, Gilching, Germany) from frontal (F7, F3, Fz, F4, F8), central (T7, C3, Cz, C4, T8), parietal (P7, P3, Pz, P4, P8), occipital (O1, O2),

and mastoid (M1 (TP9), M2 (TP10)) sites. Ag-AgCl EEG electrodes were used. They were mounted on an EasyCap (EasyCap, Herrsching-Breitbrunn, Germany). Electrode impedance was kept below 10 kΩ. All EEG electrodes were referenced to average reference. Participants were informed about the problem of non-cerebral artifacts and they were encouraged to reduce them (Picton et al., 2000). Ocular artifacts were monitored by means of bipolar pairs of electrodes positioned at the sub- and supraorbital ridges (vertical electrooculogram, vEOG) and at the external ocular canthi (horizontal electrooculogram, hEOG). The EEG and EOG channels were amplified with a bandpass of 0.01 to 30 Hz and digitized at 250 Hz.

Offline analysis was performed by means of the BrainVisionAnalyzer® software (Brain Products, Gilching, Germany). Semi-automated artifact rejection was performed before averaging to discard trials during which an eye movement or any other non-cerebral artifact occurred (maximum allowed voltage step per sampling point: 50 μV; maximum allowed amplitude difference: 200 μV; minimum allowed amplitude: -200 μV; maximum allowed amplitude: 200 μV; lowest allowed activity (max-min, interval length 100 ms): 0.5μV). Ocular correction included semi-automatic blink detection and the application of an established method for ocular artifact removal (Gratton, Coles, & Donchin, 1983).

The EEG was then divided into epochs of 1000 ms duration, starting 100 ms before the onset of stimuli. Error trials (misses, false alarms) were excluded from analysis (misses when the stimulus was a target, false alarms when the stimulus was a distractor). Next, the pre-stimulus baseline of 100 ms was subtracted from the sampling points. Deflections in the averaged EOG waveforms were small, which indicated good maintenance of fixation. No digital filtering was applied to the data.

Data analysis

Behavioral task performance was quantified in two ways: Firstly, the median of the response speed at each level of response hand was computed for each individual participant, and these median individual response times (RTs) were subjected to statistical analysis. Secondly, the accuracy of the behavioral responses was computed at each level of response hand for each individual participant. The percentage of hits was computed for the target stimuli (g+l+). Percentages of correct rejections were separately computed for each distractor type. Finally, the percentage of correct rejections was computed as an average across all three distractor types. These percentage values were arcsin transformed prior to statistical analysis.

Peak amplitudes of the P1 in response to the targets and to the distractors were measured at latency 88 ms with respect to the pre-stimulus baseline period at occipital electrodes (i.e., the peak latency of the P1 in the grand-average, cf. Figure 4; this and all following latencies were determined after inspection of the individual and group grand averages). Peak amplitudes of the N1 in response to the targets and to the distractors were measured at latency 160 ms (i.e., the peak latency of the N1 in the grand-average, cf. Figure 4) with respect to the pre-stimulus baseline period at occipital electrodes. Peak amplitudes of the P3b in response to the targets and to the distrac-

tors were measured at latency 432 ms (i.e., the peak latency of the P3b in the grand-average, cf. Figure 2) with respect to the pre-stimulus baseline period at electrode Pz at which the P3b was maximal. The analysis of the anterior P2, of the anterior and posterior N2 and of the P3a are described in detail in the Results. The analysis of the LRP followed the specifications that were described in the Introduction.

Performance measures and the ERP amplitude measures were subjected to repeated measures analyses of variance (ANOVAs) using the Greenhouse-Geisser correction. The results of the univariate tests are provided, using a format which gives the uncorrected degrees of freedom, and ε (Picton et al., 2000). A significance level of α = 0.01 was fixed.

Results

Behavioral data

Response speed and response accuracy are documented separately for left hand and right hand responses in Table 1. RT measures were analyzed by a one-way hand (left, right) ANOVA, F (1, 23) < 1, p = 0.85.[1] Participants performed the required classification at a near-perfect level, as revealed by the hit rates (both means $\geq$ 99.5%) and by the correct rejection rates (all means $\geq$ 98.8%). Another one-way ANOVA revealed that hand (left, right), F (1, 23) < 1, p = 0.51, did not affect hit rates. When the correct rejection rates of the various types of distractors were tested in a two-way stimulus category (global distractor, local distractor, standard distractor) $\times$ hand (left, right) ANOVA, the stimulus category main effect,F (2, 46) = 10.9, p = 0.001, ε = 0.73, but neither the hand main effect, F (1, 23) = 1.1, p = 0.30, nor the interaction between stimulus category and hand, F (2, 46) < 1, p = 0.77, ε = 0.99, proved significant. Simple contrasts revealed that the correct-rejection rates related to the local distractor were slightly lower than the correct rejection rate related to the global distractor, F (1, 23) = 11.4, p < 0.004, as well as to the standard distractor, F (1, 23) = 4.6, p < 0.05. These behavioral results show that there was a small, yet significant, decrease of correct rejections in response to the local distractors compared to the global and standard distractors, respectively. The finding of a selective increase of false alarms in response to local distractors is consistent with the conclusion that the availability of local information, wrongly implying a go decision, tended to exceed the availability of global information, correctly implying a nogo decision.

Global precedence

Stimulus-locked ERP

The left panel of Figure 2 plots grand-average ERPs at midline electrodes that were obtained in response to target stimuli as well as in response to global, local, and standard distractors. Target stimuli evoked a significantly larger P3b with parietal maximum (+7.4 μV peak amplitude at Pz) compared to the global (+3.6 μV peak amplitude at Pz), the local (+3.8 μV peak amplitude at Pz), or the standard distractor (+2.7 μV peak amplitude at Pz). The presence of a prominent target-P3b at Pz was confirmed by a two-way stimulus category (target, global distractor, local distractor, standard distractor) $\times$ hand (left, right) ANOVA, yielding a highly reliable stimulus category effect, F(3, 69) = 48.1, p < 0.001, ε = 0.60. Simple con-

Table 1: Response speed and response accuracy as a function of responding hand.

	left		right	
	M	*SD*	*M*	*SD*
RT (ms)	488	36	489	51
Hits	99.7	.6	99.5	.8
CR (g+l-)	99.3	1.0	99.1	1.3
CR (g-l+)	99.0	1.2	98.8	1.3
CR (g-l-)	100	.1	99.9	.2

Note. RT, response time; hits (in percent); CR, correct rejections (in percent). g+l- = global distractor; g-l+ = local distractor; g-l- = standard distractor.

trasts revealed that the target P3b was larger than any distractor P3b (target vs. global distractor: $F(1, 23) = 58.9$, $p < 0.001$; target vs. local distractor: $F(1, 23) = 45.4$, $p < 0.001$; target vs. standard distractor: $F\ (1, 23) = 71.4$, $p < 0.001$).

Difference waveforms at midline electrodes were computed as ERP indices of global precedence. Specifically, difference waves between global and standard distractor ERPs (see the left panel of Figure 2) and difference waves between local and standard distractor ERPs (see the left panel of Figure 2) were calculated (see the right panel of Figure 2). The statistical analysis of the differences waves relied on the calculation of mean amplitudes within 50 ms bins (time intervals) across the waveforms. Three-way stimulus category (global/standard distractor difference, local/standard distractor difference) $\times$ hand (left, right) $\times$ electrode site (Fz, Cz, Pz) ANOVAs yielded significant deviation of the difference waves from zero in the 200 (175-225) ms, 400 (375-425) ms, 450 (425-475) ms, 500 (475-525) ms, and 550 (525-575) ms bins (all F's $\geq$ 10.2, all p-values $\leq$ 0.004). The early positive deflection around 200 ms indicates a more prominent anterior P2 in response to the global and local distractors in comparison to the standard distractor, whereas the later positive deflection between 400 ms to 550 ms indicates a more prominent P3a in response to the global and local distractors in comparison to the standard distractor. The finding that no negative deviation of the difference waves from zero was discernible is consistent with the conclusion that the anterior N2 was equally prominent in response to global or local distractors in comparison to standard distractors. Importantly, stimulus category affected the difference waves solely in the 650 (625-675) ms, 700 (675-725) ms, and 750 (725-775) ms bins (all F-values $\geq$ 13.1, all p-values $\leq$ 0.001).[2] These ERP results show that the time course and the magnitude of the anterior P2 and the P3a were indistinguishable in response to the global and the local distractors, respectively.

Stimulus-locked LRP

As shown in Figure 3, there was a distinct negative dip in the stimulus-locked LRP (sLRP) in response to target stimuli approximately 350 ms after stimulus onset. To verify this LRP statistically, mean sLRP amplitude was computed during 50 ms bins, starting 50 ms and ending

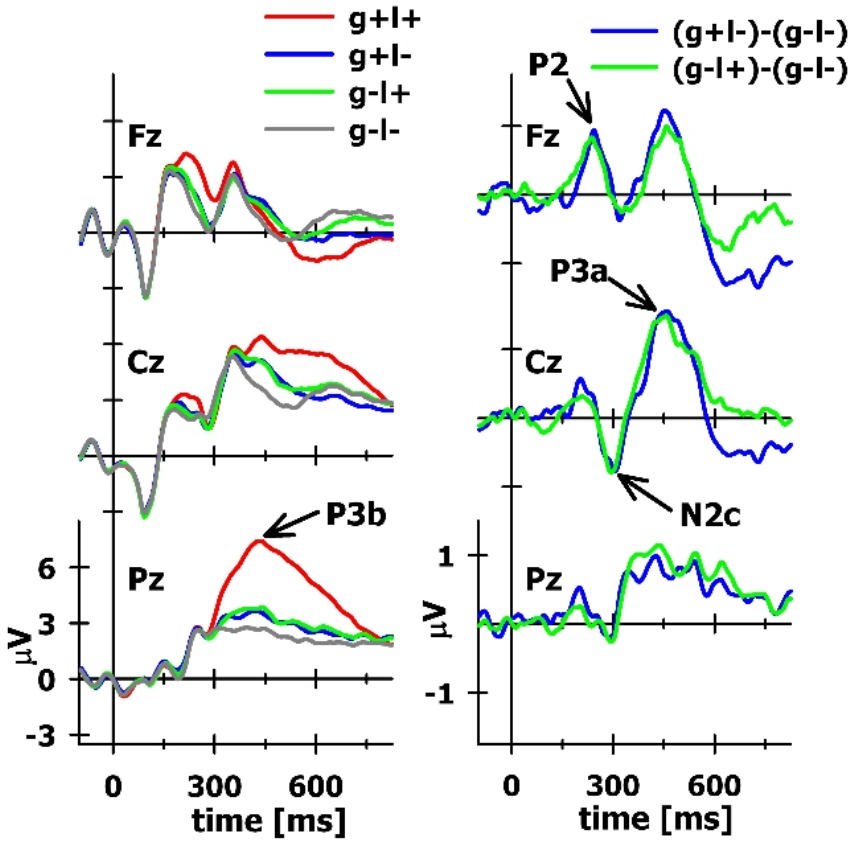

Figure 2: *Left panel. Stimulus-locked grand-average ERPs at midline electrodes that were obtained in response to targets (g+l+), global distractors (g+l–), local distractors (g–l+) and standard distractors (g–l–). Right panel. Difference waveforms at midline electrodes, i.e. difference waves between global and standard distractor ERPs ((g+l–)-(g–l–)), and difference waves between local and standard distractor ERPs ((g–l+)-(g–l–)).*

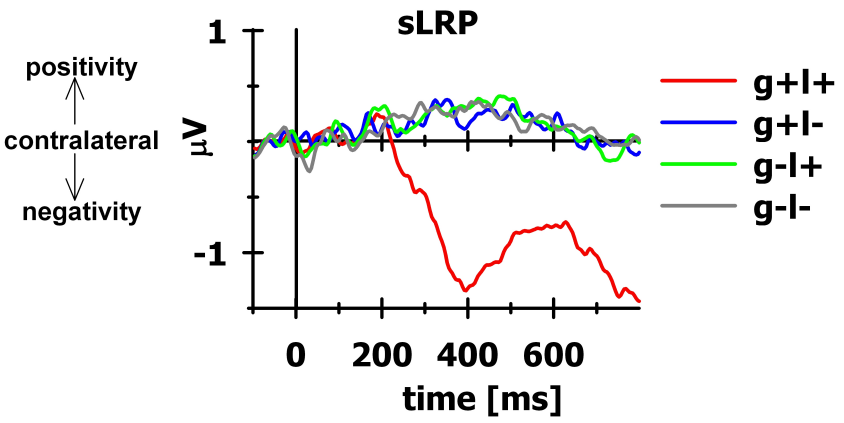

Figure 3: *Stimulus-locked LRPs (sLRP) that were obtained in response to targets (g+l+), global distractors (g+l–), local distractors (g–l+) and standard distractors (g–l–).*

800 ms after stimulus onset. The first bin in which this amplitude was significantly less than zero was the 350 ms bin, F (1, 23) = 19.9, p < 0.001. The sLRP waveform remained below zero in all later bins, without exception (F's $\geq$ 13.1, all p-values $\leq$ 0.001).

Next, stimulus-locked LRPs in response to the distractors were analyzed (see Figure 3). Inspection of Figure 3 reveals that distractors did not elicit noticeable negative dips. The statistical analysis of the LRPs relied on the calculation of mean amplitudes within 50 ms bins across the waveforms. One-way stimulus category (global distractor, local distractor, standard distractor) ANOVAs yielded positive deviation of the LRPs from zero in the 350 (325-375) ms, 400 (375-425) ms, 450 (425-475) ms, and 500 (475-525) ms bins. All other effects, and specifically all stimulus category effects, fell below significance (remaining intercept effects: F's $\leq$ 6.9, all p-values $\geq$ 0.015); all stimulus category effects: F's $\leq$ 1.1, all p-values $\geq$ 0.34). These LRP results suggest that none of the distractors was associated with noticeable response activation, as would be reflected by a negative dip in the LRP. Furthermore, the tonic positive deflection of the LRPs possibly indicates functional deactivation of the contralateral motor areas in the time bin between 350 ms and 500 ms.

Hemispheric asymmetry

Stimulus-locked ERP

Figure 4 plots grand-average ERPs at lateral frontal and occipitoparietal electrodes, separately for target stimuli as well as for global, local, and standard distractors. A three-way stimulus category (target, global distractor, local distractor, standard distractor) $\times$ hand (left, right) $\times$ hemisphere (left, right) ANOVA was performed on P1 and N1 peak amplitudes at

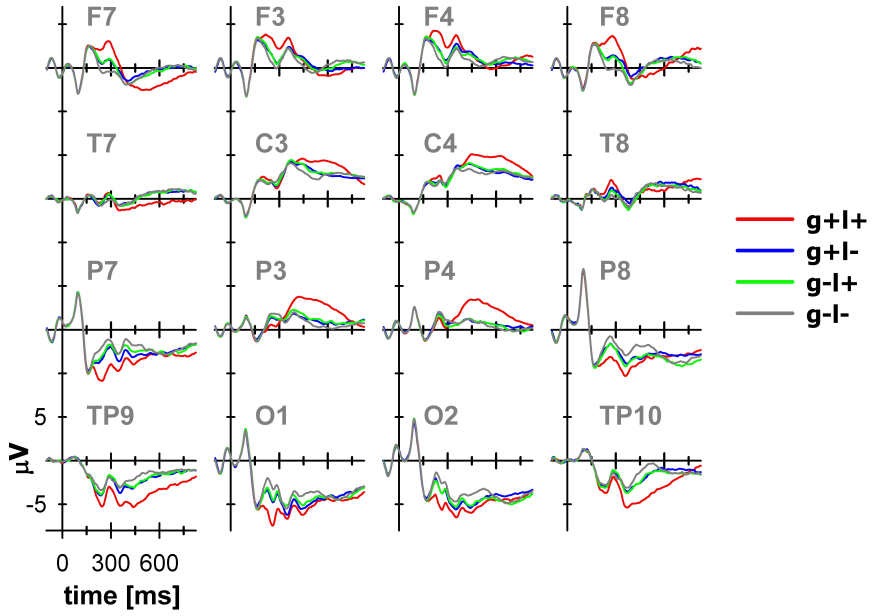

Figure 4: *Stimulus-locked grand-average ERPs at lateral electrodes that were obtained in response to targets (g+l+), global distractors (g+l–), local distractors (g–l+) and standard distractors (g–l–).*

occipital electrodes. With regard to the P1 amplitude, no main or interaction effect attained statistical significance (all F-values $\leq$ 4.4, all p-values $\geq$ 0.017). With regard to the N1 amplitude, no main or interaction effect attained statistical significance (all F-values $\leq$ 4.1, all p-values $\geq$ 0.055). Together these results indicate that early visual cortical processing was not affected by stimulus category, hemisphere or responding hand, nor by their interactions.

Two-way hand (left, right) $\times$ region (anterior, posterior) ANOVAs were performed on the double subtraction waveforms (cf. legend of Figure 5). The results on the intercept are of particular importance because they indicate bins during which a reliable deviation of the difference waveforms from zero was observed. A negative deflection in these difference waveforms occurred exclusively in the 350 ms bin, F (1, 23) = 9.4, p = 0.006.[3] A conventional four-way region (frontocentral, parietooccipital) $\times$ stimulus category (global distractor, local distractor) $\times$ hand (left, right) $\times$ hemisphere (left, right) ANOVA on the mean ERP amplitudes (posterior N2) in the 350 (325 – 375) ms bin revealed a significant main effect of region, F (1, 23) = 33.8, p < 0.001, and a significant interaction between stimulus category and hemisphere, F (1, 23) = 9.3, p < 0.01, while none of the remaining main effects or interaction effects reached statistical significance (all F-values $\leq$ 6.6, all p-values $\geq$ 0.017). Although the interaction between region, stimulus category and hemisphere failed to reach statistical significance, inspection of the difference waves suggested a parietal maximum of the stimulus category $\times$ hemisphere interaction. An additional three-way stimulus cate-

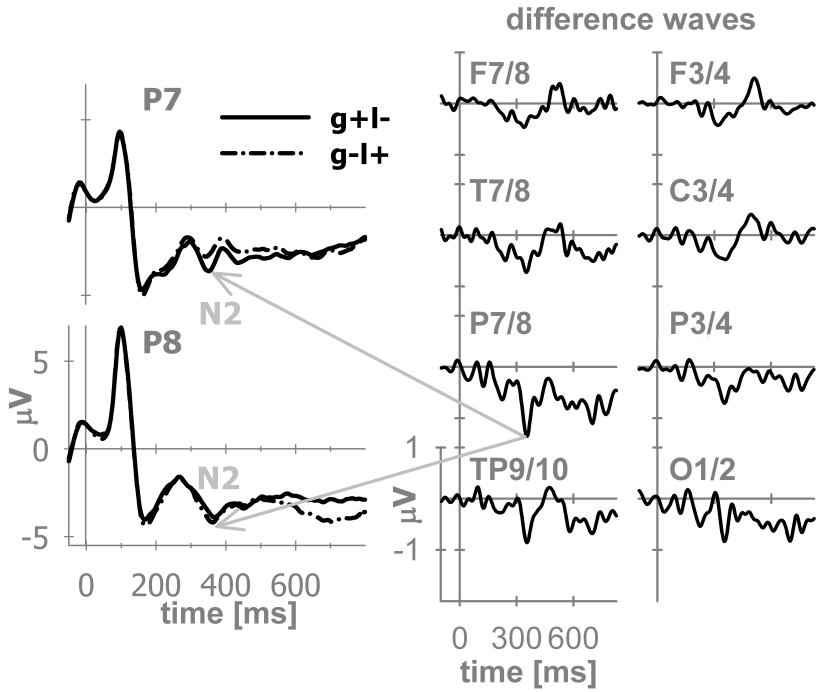

Figure 5: *Stimulus-locked double subtraction waveforms obtained at eight electrode pairs. Double subtraction waveforms were computed as ERP indices of hemispheric asymmetry. Specifically, hemispheric ERP differences were computed, i.e. ERP at left electrodes – ERP at homologous right electrodes (anterior region: F7 – F8, F3 – F4, C3 – C4, T7 – T8; posterior region: P7 – P8, P3 – P4, O1 – O2, TP9 – TP10), separately for global and local distractors. Next, the difference global distractors – local distractors of the hemispheric ERP differences was computed, a procedure which mainly tests for algebraic sign differences of hemispheric ERP differences. In particular, if the hemispheric differences are negative in case of the global distractor, whereas these are positive in case of the local distractor, the difference between a negative value and a positive value will yield a strongly negative value, and indicating a cross-over of hemispheric lateralization. Mean amplitudes of this measure were computed for 50 ms bins, starting 50 ms and ending 800 ms ms after stimulus onset. The inlet (left panels) shows the grand-average ERPs at parieto-lateral electrodes (P7, P8) that were obtained in response to global distractors (g+l–, solid lines) and local distractors (g–l+, dashed lines).*

gory (global distractor, local distractor) $\times$ hand (left, right) $\times$ hemisphere (left, right) ANOVA on the mean ERP amplitudes (posterior N2) at the lateral parietal electrodes (P7, P8) in the 350 (325 – 375) ms bin yielded a significant stimulus category $\times$ hemisphere interaction, F (1, 23) = 8.1, p < 0.007, while none of the remaining main effects or interaction effects reached statistical significance (all F-values $\leq$ 6.7, all p-values $\geq$ 0.016).

The stimulus category $\times$ hemisphere interaction for the amplitude of the posterior N2 can be easily identified in Figure 5. Inspection of the inlet reveals that the global distractor evoked a more negative ERP wave at P7 (over the left hemisphere) in the latency range of the posterior N2, whereas the local distractor elicited a slightly more negative ERP wave at P8 (over the right hemisphere) in the latency range of the posterior N2. While one cannot assume that potentials over one hemisphere are necessarily generated in the underlying hemisphere, this pattern of hemispheric lateralization seems to be consistent with the predicted hemispheric asymmetry. Specifically, as outlined in the introduction, the global distractor is expected to be preferably processed in the left hemisphere, whereas the local distractor is expected to be preferably processed in the right hemisphere.

Response-locked ERP

Figure 6 shows the scalp topography of the response-locked ERPs in response to target stimuli, separately for right- and left-hand responses. With regard to the lateralization of the ERPs, three observations are noteworthy: First, an anterior contralateral negativity occurred at electrodes C3 and C4 as well as F3 and F4. The anterior contralateral negativity at C3 and C4 gives rise to the response-locked LRP (rLRP) once the contralateral – ipsilateral difference is averaged over the two responding hands. As shown in Figure 7, there was a distinct negative deflection in the rLRP approximately 150 ms before the response. To verify this negative rLRP dip statistically, mean rLRP amplitude was computed during 50 ms bins, starting -450 (i.e., the -475 – -425 ms bin) ms before the response and ending +450 (i.e., the +425 – +475 ms bin) ms after the response. The first bin during which this amplitude was significantly less than zero was the -150 ms bin, F (1, 23) = 22.6, p < 0.001. The rLRP waveform remained below zero in all later bins (all F-values $\geq$ 26.5, all p-values $\leq$ 0.001), with two noteworthy exceptions: 1. There was a sharp positive peak in the rLRP waveform at the time of the response (see Figure 7), and the mean rLRP amplitude in the 0 ms bin did not differ statistically from zero, F (1, 23) = 6.9, p = 0.015. 2. There was a later positive peak in the rLRP waveform (see Figure 7), and the mean rLRP amplitude in the 100 ms bin and in the 150 ms bin did not differ statistically from zero (all F-values $\leq$ 2.8, all p-values $\geq$ 0.11).

Second, a contralateral positive peak emerged at posterior electrodes that peaked at the time of the response. Inspection of Figure 7 reveals that this contralateral positive peak had a parietocentral topography, in contrast to the frontocentral topography of the rLRP. One-way region (frontal, average of the F7/F8 and F3/F4 electrode pairs; parietal, average of the P7/P8 and P3/P4 electrode pairs, occipitotemporal, average of the O1/O2 and TP9/TP10 electrode pairs) ANOVAs were computed for mean amplitudes within 50 ms

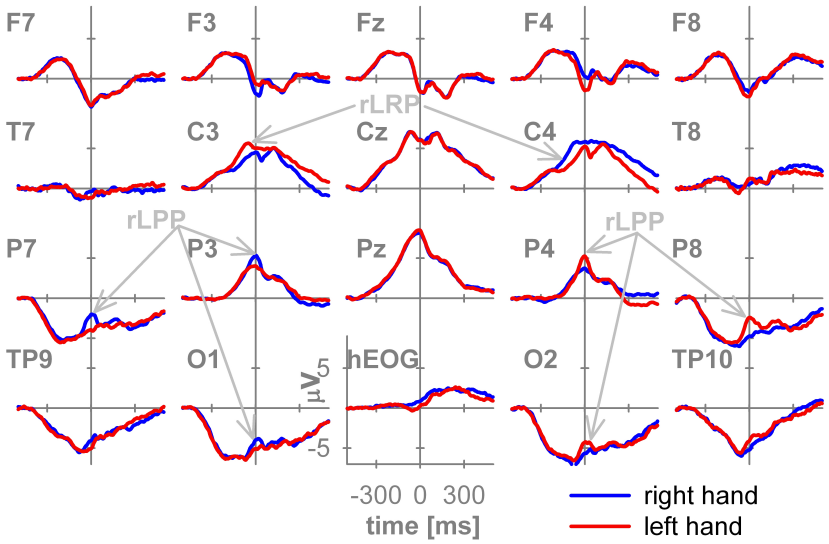

Figure 6: *Response-locked grand-average ERPs in response to targets, separately for left and right hand responses. rLRP: response-locked lateralized readiness potential; rLPP: response-locked lateralized posterior positivity; hEOG: horizontal electrooculogram.*

bins across the waveforms. Region affected the waveforms in the -100 ms and all later bins (all F-values $\geq$ 6.0, all p-values $\leq$ 0.005), with two exceptions (100 ms bin: F (2, 46) $<$ 1; 200 ms bin: F (2, 46) = 2.3, p = .12). The waveforms were positively deflected in the 0 ms (F (1, 23) = 32.6, p < .001) and 150 ms (F (1, 23) = 13.6, p < .002) bins, whereas starting with the 350 ms bin, a negative deflection of the waveforms became apparent (all F-values $\geq$ 17.1, all p-values $\leq$ 0.001).[4]

Discussion

The present data are inconsistent with the predictions that were derived from the global precedence hypothesis. Specifically, the amplitudes of the anterior N2 (N2c) and of the anterior P3 (P3a) did not differ between local and global distractors. In addition, the sLRP obtained in nogo trials did not indicate substantial preliminary response activation by local distractors or by global distractors. In contrast, the present data are consistent with the predictions that were derived from the hypothesis of hemispheric asymmetry. Specifically, the posterior N2 showed the expected pattern of hemispheric lateralization. In addition, we observed a new, response-locked lateralized posterior positivity (rLPP) that might provide a clue towards hemispheric interaction. We discuss issues related to the global precedence hypothesis and issues related to hemispheric asymmetry separately in the following paragraphs.

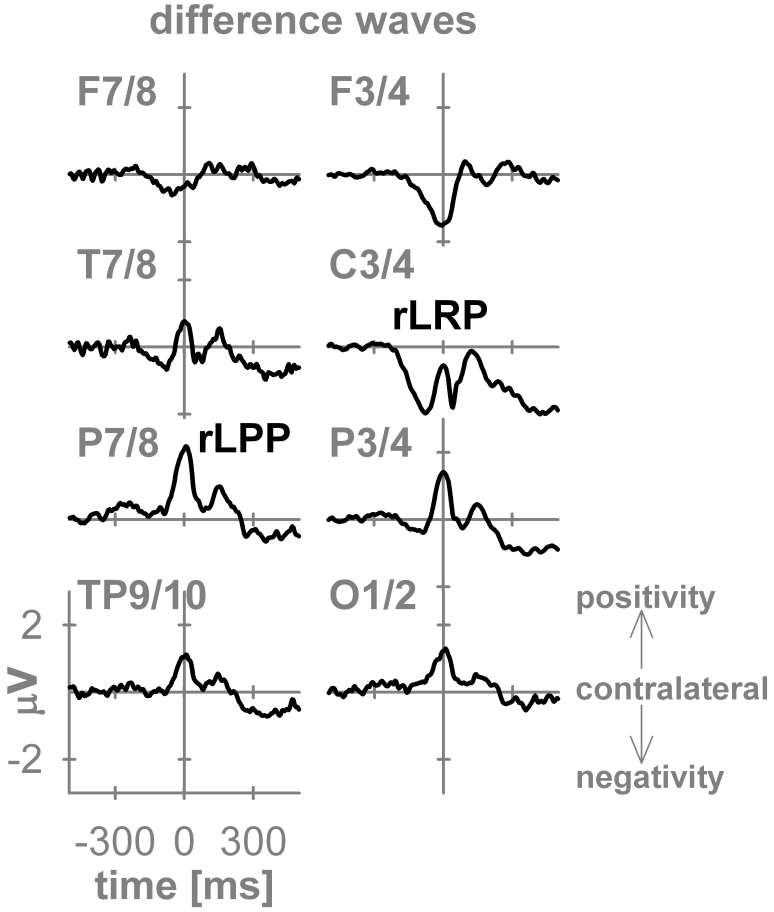

Figure 7: *Response-locked double subtraction waveforms obtained at eight electrode pairs. At C3/4, the resulting difference wave equals the rLRP. At posterior electrode pairs, a novel contralateral positive peak emerged (rLPP, response-locked lateralized posterior positivity). Note, that the rLRP at C3/4 and the rLPP seem to overlap.*

Global precedence

As outlined in the introduction, the global precedence hypothesis led to the prediction of larger interference effects by global distractors in comparison to local distractors. Specifically, an enhanced anterior N2 (N2c) and an enhanced anterior P3 (P3a) in response to global distractors compared to local distractors were expected. Furthermore, the sLRP obtained in these nogo trials provided a test for preliminary global and/or local response activation, with the expectation that global response activation should exceed local response activation. None of these predicted ERP (N2, P3, sLRP) effects showed up in the present experiment. Instead, our results indicate that preliminary response activation by global information equaled preliminary response activation by local information.

There are at least two possible reasons for the absence of a global precedence effect. 1. Global precedence may not be obtained when stimuli contain local, but not global, shapes at fixation. It has been argued that local shapes at fixation confound stimulus level with eccentricity (Miller & Navon, 2002; Navon, 1977). If local features at fixation were more easily discriminable than local shapes at other locations in the visual field or than global shapes, this discriminability advantage could counteract the typical speed advantage for global information. 2. Participants in Ridderinkhof & van der Molen's (1995) study performed a two-choice task. Participants in Miller & Navon's (2002) experiments had to solve left/right/nogo tasks, i.e. they chose between left hand response, right hand response and no response within each trial. Participants in our experiment chose between left hand response and no response as well as between right hand response and no response within different blocks of trials. These decisional discrepancies might also have contributed to the heterogeneity of the reported results (cf., Introduction).

We described ERP results in two earlier publications that were obtained from non-hierarchical versions of this go-nogo task. Color and shape were the stimulus attributes in our first study (Kopp et al., 2007). Stimulus color, but not stimulus shape, led to response preparation (as indicated by ERP measures) when color was easily discriminated. In contrast, color did no longer induce response preparation when the color discriminations were more difficult. In the second study (Kopp & Wessel, 2010), stimulus size, but not stimulus shape, led to response preparation when size could be easily discriminated. When size discriminations were more difficult, stimulus shape, but not stimulus size, led to response preparation. Thus, we reported electrophysiological evidence that response preparation can be carried out in parallel with stimulus recognition based on preliminary output from perceptual processes, before stimulus recognition is complete. In the present study, the sLRP findings indicate that preliminary response activation was not detectable in nogo trials.

Hemispheric asymmetry

Our results clearly support earlier ERP studies on hemispheric asymmetry. As in earlier divided attention paradigms (Heinze et al., 1998; Proverbio et al., 1998), early visual cortical processing, as indicated by the P1 and N1 ERP components, was not influenced by any of the experimental factors (stimulus cate-

gory, hemisphere or responding hand). Thus, at least under conditions of divided attention, early sensory inputs are not modulated to gate global versus local information differentially into the two hemispheres.

The posterior N2 component of the ERP (Folstein & van Petten, 2008) showed the expected hemispheric asymmetry, i.e. a relatively larger amplitude over the left hemisphere for global distractors and over the right hemisphere for local distractors. These data show differential lateralization of local and global visual processing (see also Heinze & Münte, 1993; Heinze et al., 1998; Malinowski et al., 2002; Volberg & Hübner, 2004; Yamaguchi et al., 2000; Yoshida et al., 2007). The hemispheric asymmetry of the posterior N2 appeared in a temporally and topographically distinct manner. Specifically, we observed asymmetrical N2 amplitudes in the latency range around 350 ms following stimulus onset, with parietal maximum.

These posterior N2 findings indicate that later stages of processing are asymmetrically organized in the left and right hemispheres and operate in parallel to process global and local aspects of hierarchical stimuli. This pattern of results supports models proposing that spatial frequency analysis is only asymmetric at higher stages of perceptual processing and not at the earliest stages of visual cortical analysis (Sergent, 1982; Hellige, 1993; Ivry & Robertson, 1998). There is, however, a caveat which should be mentioned here because verbal stimuli (hierarchical letters) produce more pronounced evidence for hemispheric specialization than do nonverbal (hierarchical figures) stimuli (Han et al., 1997, 2001). Therefore, a replication study, based on nonverbal stimuli, seems desirable. Furthermore, the use of multiple statistical tests demands caution in interpretation.

An unexpected, novel finding was the identification of the rLPP. The rLPP reflects response-locked, asymmetrical cortical activity, with a parietal topography. We have argued above that our (and others) ERP results indicate that each hemisphere performs its specialized processing, that this processing occurs in parallel, and that the results of this processing are simultaneously available. Thus, in this type of divided attention, hierarchical visual perception tasks, local and global information are concurrently available and are distinctively distributed across hemispheres.

Under these circumstances, efficient performance monitoring hinges upon interhemispheric interaction. Zaidel (1987) formulated the hypothesis of hemispheric monitoring: Although each hemisphere contains its own performance monitor, each hemisphere can also monitor the other. Thus, it becomes possible for one hemisphere to monitor the results of processing in the other hemisphere. To date, however, there is no empirical evidence to support Zaidel's hypothesis (Hochman & Eviatar, 2004, 2006). Hemispheric monitoring should be advantageous whenever elaborated stimulus representations are distributed across hemispheres. Therefore, it is an intriguing possibility that the rLPP indicates performance monitoring across hemispheres, albeit this assertion remains by nature somewhat speculative. If this interpretation of the rLPP is correct, our data suggest that hemispheric monitoring takes place at a relatively late stage of information processing. Specifically, hemispheric monitoring, as possibly indi-

cated by the rLPP, seems to be time-locked to the execution of the response.

Here, we presented evidence that the left and right hemisphere preferentially perform either local or global processing, respectively, and that this processing occurs in parallel. The results of this processing are simultaneously available in the present hierarchical visual perception task, without global precedence. The ERP findings indicated hemispheric specialization at a relatively late stage of processing. Furthermore, we suggest that this task provides an instance for investigating collaboration between hemispheres. Specifically, hemispheric monitoring, hitherto a purely theoretical construct, may become an empirically addressable characteristic of interhemispheric interaction.

Acknowledgements

We thank Jasmin Kizilirmak and Carolin Liebscher for their help in data acquisition and data analysis.

References

Banich, M.T. (1998). The missing link: The role of interhemispheric interaction in attentional processing. *Brain and Cognition, 36,* 128-157.

Banich, M.T., & Belger, A. (1990) Interhemispheric interaction: how do the hemispheres divide and conquer a task? *Cortex, 26,* 77-94.

Coles, M.G. (1989). Modern mind-brain reading: psychophysiology, physiology, and cognition. *Psychophysiology, 26,* 251-269.

Corballis, M.C. (1997). The genetics and evolution of handedness. *Psychological Review, 104,* 714-727.

Folstein, J.R., & van Petten, C. (2008). Influence of cognitive control and mismatch on the N2 component of the ERP: a review. *Psychophysiology, 45,* 152-170.

Friedman, D., Cycowicz, Y.M., & Gaeta, H. (2001). The novelty P3: an event-related brain potential (ERP) sign of the brain's evaluation of novelty. *Neuroscience and Biobehavioral Reviews,*25, 355-373.

Gratton, G., Coles, M.G., & Donchin, E. (1983). A new method for off-line removal of ocular artifact. *Electroencephalography and Clinical Neurophysiology, 55,* 468-484.

Han, S., Fan, S., Chen, L., & Zhuo, Y. (1997). On the different processing of wholes and parts: A psychophysiological analysis. *Journal of Cognitive Neuroscience, 9,* 687-698.

Han, S., He, X., Yund, E.W., & Woods, D.L. (2001). Attentional selection in the processing of hierarchical patterns: an ERP study. *Biological Psychology, 56,* 113-130.

Han, S., Weaver, J., Murray, S., Yund, E.W., & Woods, D.L. (2002). Hemispheric asymmetry in global/local processing: effects of stimulus position and spatial frequency. *Neuroimage, 17,* 1290-1299.

Heinze, H.J., Hinrichs, H., Scholz, M., Burchert, W., & Mangun, G.R. (1998). Neural mechanisms of global and local processing. A combined PET and ERP study. *Journal of Cognitive Neuroscience, 10,* 485-498.

Heinze, H.J., Matzke, M., Dorfmüller, G., & Smid, H.G. (1997). Flexibility in the structure of human information processing. *Advances in Neurology,*73, 359-375.

Heinze, H.J., & Münte, T.F. (1993). Electrophysiological correlates of hierarchical stimulus processing: dissociation between onset and later stages of global and local target processing. *Neuropsychologia, 31,* 841-852.

Hellige, J.B. (1993). Hemispheric asymmetry. What's right and what's left. Cambridge, MA: Harvard University Press.

Hillyard, S.A., Teder-Sälejärvi, W.A., & Münte, T.F. (1998). Temporal dynamics of early perceptual processing. *Current Opinion in Neurobiology, 8,* 202-210.

Hochman, E.Y., & Eviatar, Z. (2004). Does each hemisphere monitor the ongoing process in the contralateral one? *Brain and Cognition, 55,* 314-321.

Hochman, E.Y., & Eviatar, Z. (2006). Do the hemispheres watch each other? Evidence for a between-hemispheres performance monitoring. *Neuropsychology, 20,* 666-674.

Hugdahl, K., & Davidson, R.J. (2003). *The asymmetrical brain.* Cambridge, MA: MIT Press.

Ivry, R.B., & Robertson, L.C. (1998). *The two sides of perception.* Cambridge, MA: MIT Press.

Kopp, B. (2008). The P300 component of the event-related brain potential and Bayes' theorem. In M.K. Sun (Hg.), *Cognitive Sciences at the Leading Edge* (pp. 87-96). New York: Nova Science Publishers.

Kopp, B., Rist, F., & Mattler, U. (1996). N200 in the flanker task as a neurobehavioral tool for investigating executive control. *Psychophysiology, 33,* 282-294.

Kopp, B., Tabeling, S., Moschner, C., & Wessel, K. (2007). Temporal dynamics of selective attention and conflict resolution during cross-dimensional go-nogo decisions. *BMC Neuroscience 8:* 68.

Kopp, B., & Wessel, K. (2010). Event-related brain potentials and cognitive processes related to perceptual-motor information transmission. *Cognitive, Affective, and Behavioral Neuroscience, 10,* 316-327.

Kornhuber, H.H., & Deecke, L. (1965). Hirnpotentialänderungen bei Willkürbewegungen und passiven Bewegungen des Menschen: Bereitschaftspotential und reafferente Potentiale [Changes in the brain potential in voluntary and passive movements in man: readiness potential and reafferent potentials]. *Pflügers Archiv European Journal of Physiology,* 284,1-17.

Lang, W., Cheyne, D., Kristeva, R., Beisteiner, R., Lindinger, G., & Deecke, L. (1991). Three-dimensional localization of SMA activity preceding voluntary movement—A study of electric and magnetic fields in a patient with infarction of the right supplementary motor area. *Experimental Brain Research, 87,* 688–695.

Luck, S.J. (2005). *An Introduction To The Event-Related Potential Technique.* Cambridge, MA: MIT Press.

Lux, S., Marshall, J.C., Ritzl, A., Weiss, P.H., Pietrzyk, U., Shah, N.J., Zilles, K., & Fink, G.R. (2004). A functional magnetic resonance imaging study of local/global processing with stimulus presentation in the peripheral visual hemifields. *Neuroscience, 124,* 113-120.

Malinowski, P., Hübner, R., Keil, A., & Gruber, T. (2002). The influence of response competition on cerebral asymmetries for processing hierarchical stimuli revealed by ERP recordings. *Experimental Brain Research, 144,* 136-139.

Miller, J., & Navon, D. (2002). Global precedence and response activation: evidence from LRPs. *Quarterly Journal of Experimental Psychology A, 55,* 289-310.

Navon, D. (1977). Forest before trees: the precedence of global features in visual processing. *Cognitive Psychology, 9,* 353-383.

Picton, T.W., Bentin, S., Berg, P., Donchin, E., Hillyard, S.A., Johnson, R. Jr., Miller, G.A., Ritter, W., Ruchkin, D.S., Rugg, M.D., & Taylor, M.J. (2000). Guidelines for using human event-related potentials to study cognition: recording standards and publication criteria. *Psychophysiology, 37,* 127-152.

Picton, T.W., Lins, O.G., & Scherg, M. (1995). The recording and analysis of event-related potentials. In F. Boller, J. Grafman (Eds.), *Handbook of Neuropsychology, Vol. 10* (pp. 3-73). Amsterdam: Elsevier.

Potts, G.F. (2004). An ERP index of task relevance evaluation of visual stimuli. *Brain and Cognition, 56,* 5-13.

Proverbio, A.M., Minniti, A., & Zani, A. (1998). Electrophysiological evidence of a perceptual precedence of global vs. local visual information. *Cognitive Brain Besearch, 6,* 321-334.

Reinvang, I., Magnussen, S., & Greenlee, M.W. (2002). Hemispheric asymmetry in visual discrimination and memory: ERP evidence for the spatial frequency hypothesis. *Experimental Brain Research, 144,* 483-495.

Ridderinkhof, K.R., & van der Molen, M.W. (1995). When global information and local information collide: a brain potential analysis of the locus of interference effects. *Biological Psychology, 41,* 29-53.

Rinkenauer, G., Osman, A., Ulrich, R., Müller-Gethmann, H., & Mattes, S. (2004). On the locus of speed-accuracy trade-off in reaction time: inferences from the lateralized readiness potential. *Journal of Experimental Psychology: General, 133,* 261-282.

Robertson, L.C. (1995). Hemisphere specialization and cooperation in processing complex visual patterns. In F.L. Kitterle (Ed.), *Hemispheric communication. Mechanisms and models* (pp. 301-318). Hillsdale, NJ: Lawrence Erlbaum Associates.

Robertson, L.C., & Ivry, R.B. (2000). Hemispheric asymmetries: attention to visual and auditory primitives. *Current Directions in Psychological Science, 9,* 59-63.

Robertson, L.C., Lamb, M.R., & Knight, R.T. (1988). Effects of lesions of temporal-parietal junction on perceptual and attentional processing in humans. *Journal of Neuroscience, 8,* 3757-3769.

Sergent, J. (1982). The cerebral balance of power: confrontation or cooperation? *Journal of Experimental Psychology: Human Perception and Performance, 8,* 253-272.

van Kleeck, M.H. (1989). Hemispheric differences in global versus local processing of hierarchical visual stimuli by normal subjects: new data and a meta-analysis of previous studies. *Neuropsychologia, 27,* 1165-1178.

Volberg, G. & Hübner, R. (2004). On the role of response conflicts and stimulus position for hemispheric differences in global/local processing: an ERP study. *Neuropsychologia, 42,* 1805-1813.

Yamaguchi, S., Yamagata, S., & Kobayashi, S. (2000). Cerebral asymmetry of the top-downällocation of attention to global and local features. *Journal of Neuroscience, 20,* RC72:1-5.

Yoshida, T., Yoshino, A., Takahashi, Y., & Nomura, S. (2007) Comparison of hemispheric asymmetry in global and local information processing and interference in divided and selective attention using spatial frequency filters. *Experimental Brain Research, 181,* 519-529.

Yovel, G., Yovel, J., & Levy, I. (2001) Hemispheric asymmetries for global and local visual perception: effects of stimulus and task factors. *Journal of Experimental Psychology: Human Perception and Performance, 27,* 1369-1385.

Zaidel, E. (1987). Hemispheric monitoring. In D. Ottoson (Ed.), Duality and unity of the brain (pp. 247-281). Hampshire, UK: Macmillan.

Zaidel, E. (2001). Brain asymmetry. In N.J. Smelser, P.B. Baltes (Series Eds.), R.F. Thompson (Vol. Ed.), *International Encyclopedia of the Social and Behavioral Sciences: Vol. 2. Behavioral and Cognitive Neuroscience* (pp. 1321-1329). Amsterdam: Elsevier.

Zaidel, E., & Iacoboni, M. (2003). The parallel brain. Cambridge, MA: MIT Press.

Zaidel, E., Iacoboni, M., Zaidel, D. W., & Bogen, J. (2003). The callosal syndromes. In K. M. Heilman, E. Valenstein (Eds.), *Clinical Neuropsychology, 4th Edition* (pp. 347-403). New York: Oxford University Press.

Footnotes

[1]Half of the subjects responded to congruent targets and the other half responed to incongruent targets. However, RTs were not influenced by the congruency of the target stimulus (congruency main effect, F (1, 22) < 1, p = .71; interaction congruency $\times$ hand, F (1, 22) < 1, p = .88).

[2]The remaining effects were site main effects (250 (225-275) ms, 550 (525-575) ms, 600 (575-625), and 650 (625-675) ms (all F-values $\geq$ 6.9, all p-values $\leq$ 0.006), whereas all remaining main and interaction effects fell below significance.

[3]All remaining main and interaction effects fell below significance, with the exception of a region effect in the 600 (575-626) ms bin, F (1, 23) = 7.8, p = 0.01.

[4]These results remained by and large identical when the ERPs were re-referenced to the average of TP9 and TP10.

Abstract

K. Schneider (Aachen, Germany) – Neuroimaging in German Court Rooms
Steiner (1981), an Austrian philosopher of the 20th century, stated that a deep understanding of human life and nature should be the essential prerequisite for legislation and jurisdiction, and the foundation of all legal studies. Neuroscience, claiming to give new insights into human nature, leads to an outstanding current relevance of Steiner's conclusion: By targeting fundamentals of the human self-conception (e. g. free will), the rapidly growing field of cognitive neuroscience and neuroimaging in particular challenges the traditional way of thinking in many sciences, the humanities, and the law. The use of neuroimaging methods as evidence in legal proceedings is meanwhile a key part of scientific discussions, and also attracts attention of the legal practice. However, "lie detection", the most popular aspect of neuroimaging in court, is only one aspect of the possible legal/forensic applications of brain scans. Even more questionable is the attempt of "diagnosing criminals", thus the idea of revealing potentially dangerous behavior traits by means of a brain scan. These intentions are not only ethically alarming, but also raise legal questions. Though neuroscientific research will probably not completely change the fundamental principles of the (German) law system, there is an urgent need for discussion with special regard to legal regulation. The present paper is divided into two parts, of which the first one introduces neuroimaging studies on relevant legal and forensic questions, while the second gives a legal commentary on the implications of this research.

Keywords: Law and neuroscience, Neuroimaging, Lie detection, "Diagnosing criminals"

Neuroimaging in German Court Rooms

Karla Schneider, Department of Psychiatry, Psychotherapy and Psychosomatics, IRTG 1328, Pauwelsstr. 30, 52074 Aachen, Germany
karlaschneider@web.de

Introduction

"Is it possible to diagnose pedophilia with the help of brain scans?" A German law office posed this question to a researcher in the field of neuroscience at the beginning of 2008. One of their clients was found guilty of sexually abusing two adolescent girls and sentenced to prison. However, the court's decision was built on circumstantial evidence, and there was no clear proof for or against the offense. Hence, the lawyers, inspired by the media, were interested in the possibilities given by the new neuroscientific methods of brain scanning to have the court procedure revisited.

This short episode reveals not only the practical relevance of neuroscientific methods, in particular of functional magnetic resonance imaging (fMRI), but also the danger of these techniques as they are misleadingly thought to provide objective measurements of guilt and criminal behavior.

Developed for medical purposes to aid neurological diagnostic examinations, neuroimaging quickly attracted the interest of scientists because of its social applications. If it is possible to detect tumors and blood flow in the brain to diagnose pathological aberrations, why not try to brain-read the thoughts of healthy people, criminal offenders in particular?

The present paper will be divided into two parts: first introducing neuroscientific research on relevant forensic questions, followed by a legal commentary on the implications of this research.

The Neuroscientific Point of View

Introduction to neuroimaging

fMRI is the most popular neuroimaging technology because according to today's medical knowledge, its use is harmless. It is non-invasive, as it uses the level of blood oxygenation as a "brain-internal" contrast medium (the so called BOLD contrast - Blood Oxygenation Level-Dependent Contrast) (Jäncke 2005). The magnetic field strength, that is commonly used, is 1.5 or 3 Teslas.

The theory behind fMRI is that a working neuron needs more oxygen than a neuron at its "resting state". When neurons are activated, the level of oxygen in the brain region where they are located immediately drops. Unfortunately, today's technology cannot measure this "initial dip" of oxygen, but only the subsequent increase. For reasons that are not fully understood, the brain overcompensates for the decreasing amount of oxygen before it falls back to the null level of an inactive neuron (Goebel & Kriegeskorte 2005). These changes in blood-oxygen level lead to changes in the electromagnetic signal that can then be registered. This signal depends on the underlying substance, e.g. different types of tissue and the liquor, and therefore allows analyses of brain structure and/or the activity of the brain during a certain task.

While fMRI guarantees a relatively satisfying spatial resolution, it suffers from a time lag due to the fact that the increase of blood oxygen appears about two to three seconds after the onset of neural activity. This lag may be overcome by the use of multimodal imaging (e.g. one of the first trials by Gamer et al. 2007), i.e. by combining fMRI with another method such as electroencephalography (EEG), which is known to have poor spatial, but very good temporal resolution. Another conceivable possibility is combining polygraphy with neuroimaging.

Further neuroimaging methods are Positron Emission Tomography (PET) and Near-Infrared-Spectroscopy (NIRS), but so far these are rarely used in "forensic functional brain imaging" (Langleben & Dattilio 2008). Their practical disadvantage is that the need for nuclear tracers in PET and NIRS only allows for the study of activity relatively close to the surface of the cortex and not of deeper structures.

Research on "neuroscience-based" lie detection

Simultaneously with the rejection of polygraphic evidence In Germany by the "Bundesgerichtshof (BGH)" (German federal court) in 1998 (BGHSt 44, 308) (see also below), the interest of neuroscientists in neuroimaging-based "brain reading" was increasing. Kathy O'Craven and Nancy Kanwisher (O'Craven

& Kanwisher 2000), while investigating visual stimuli and their neural correlates, were among the first who stated that the dream of reading human thoughts might finally come true. From there, it did not take long before the first studies on detecting lies in the brain were published. Leading researchers in this field are Daniel D. Langleben (Langleben et al. 2005, 2006) and Christos Davatzikos (Davatzikos et al. 2005), both professors at the University of Pennsylvania. Davatzikos is also the scientific counselor for the commercial brain reading firm, No Lie MRI (www.noliemri.com; see also www.cephoscorp.com).

To conduct polygraphic lie detection examinations, there are basically two ways of testing available: the so called Guilty Knowledge Test (GKT) and the Control Question Test (CQT).

The GKT provides a kind of ”multiple choice” test, which consists of several items as potential answers to a given question (e.g. ”The color of the shoes of the victim was a) blue, b) red, c) brown, d) black.”). The theory behind the polygraphic GKT is, that the de-facto-offender would show increased reactions (namely electrodermal activity (EDA)) towards that stimulus, which pertains to the facts of the offense, while non-offenders would show the same physiological response towards each of the presented items. The problem with this test is that it only makes sense in such cases in which just the accused offender has crime-related knowledge, and thus has a prerequisite, which is hard to fulfill in times of widespread public media. Additionally, it remains unclear, whether a physiological response to a stimulus is really related to the offense or whether the item just evoked another memory, which is emotionally relevant to the interview person.

The CQT, which is more rarely used, is based on a set of questions, of whom two are offense-related, two are somehow emotionally relevant and at best evoke an insecurity about the correct answer (e.g. ”Did you ever steel something before the age of 18?”) and two are emotionally irrelevant (e.g. ”Are you sitting on a chair?”). The participant is asked to answer every question with ”No” (in rare cases with ”Yes”), no matter whether ”No” is true or false. The idea behind this test as a polygraphic examination is that someone who is familiar with the details of the offense will show the most pronounced reaction when denying knowledge of the crime, as seen when answering the offense-related questions. However, the CQT examination raised even more concerns than the GKT, as its questions have to be generated conjointly with every individual test person in every single case, which makes this method and its results very subjective and hardly comprehensible to neuroscientific lay people, including judges.

The results of both, GKT and CQT, are additionally questioned for relying significantly on the experience of the investigator. Aside from these two basic test variants there are some modifications and supplements which are still to some extent based on the principles of GKT and CQT.

The most widespread hypothesis behind neuroscientific lie detection studies is that a lie would take up more cognitive resources than telling the truth, since a lie would be a combination of inhibiting the true answer and creating the lie. Studies in the field are mostly based on polygraphic test concepts modeled after the GKT. However, there are a few ex-

ceptions dealing with a form of the CQT (Kozel et al. 2005).

Many studies apply a comparable and simple task, the denial of a playing card. In the study conducted by Langleben et al. (2005), participants received a $20 note and a playing card. During the scanner session, they were presented a sequence of playing cards and asked to deny the ownership of every presented card, even if it was the one that they had been given previously. Increased activation was found for the lie condition compared to truth condition, particularly in brain areas that are also related to behavioral inhibition (e.g. anterior cingulate gyrus (ACC); Agam et al. 2010; Hester et al. 2004). According to the authors, this data supports the hypothesis of a lying being a more complex cognitive act than truth telling (Langleben et al. 2005).

A similar task was chosen by Davatzikos et al. (2005) who confirmed a stronger activation of the ACC and lateral prefrontal areas for the Lie > Truth contrast. To set up more realistic scenarios, recent studies have used mock crime situations, in which none of the investigators, except a study coordinator, are informed about which of the participants is playing the role of the ”criminal” and which as the control person (Kozel et al. 2009). Though Kozel et al. (2009) could come up with a 100% sensitivity rate, the specificity of fMRI lie detection was low (33%). Moreover, the high sensitivity was the result of extensive analyses, which also influenced the selection of the final group of participants (see Table 1).

While most investigations choose to use fMRI for the detection of lies, there are a few exceptions of those who use PET (Abe et al. 2006), EEG (”brain fingerprinting”, P300-analysis, Mertens & Allen 2008) or NIRS (Tian et al. 2009), indicating a role for the lateral and medial prefrontal regions and for the ACC in deception.

Mock crimes are an attempt to better approximate reality. However, it is not only the complexity of the generated task, which needs to be discussed: Real-life settings display many grey areas between truth and lie and thus, it would be a key issue to find a way to distinguish between truth, conscious lies and false memories or related grey ”in-between” areas.

Thus, investigating activation of real and false memories was the aim of Markowitsch et al. (2000). According to their results, real memories evoke stronger responses in the limbic system, the right amygdala in particular, and thus in emotion-related areas.

The criticisms, which were brought forward against the use of ”forensic functional or structural neuroimaging”, were and are still manifold and predominantly address methodological aspects. Though studies on lie detection revealed comparable networks, which seem to be involved in the process of telling a lie, and could partly come up with impressive sensitivity values up to 100% in case of the Kozel study (Kozel et al. 2009), they are still standardized lab situations. Generating stimuli for the use in a neuroimaging study and evaluating the data require extensive analyses. More, the technology of the current methods with their relatively poor spatial and/or temporal resolution combined with the yet incomplete understanding of structure-function relations of higher cognitive functions in the human brain do not allow for making statements about the meaning of the brain activation of individuals,

Table 1: Examples of studies on lie detection

Study	Method	Participants	Task	Results
Markowitsch et al. 2000	fMRI	Healthy volunteers	Generating a real life situation and a comparable false story and remembering both during the scanner session	Real Memories > False Memories. Stronger right amygdala activation
Spence et al. 2001	fMRI	Healthy volunteers	Lying about real life situations	Lie > Truth: Stronger activation of ventro-lateral and anterior cingulate regions
Langleben et al. 2002	fMRI	Healthy volunteers	Denying ownership of a playing card (variant of the Guilty Knowledge Test)	Lie > Truth: Stronger activation of left anterior cingulate, right superior frontal gyrus, prefrontal to dorsal premotor cortex, anterior parietal cortex and inferior intraparietal sulcus
Langleben et al. 2005	fMRI	Healthy volunteers	Denying ownership of a playing card (variant of the Guilty Knowledge Test)	Lie > Truth: Stronger activation of the parietal cortex, insula, medial and lateral prefrontal cortex, anterior cingulate cortex
Davatzikos et al. 2005	fMRI	Healthy volunteers	Denying ownership of a playing card (variant of the Guilty Knowledge Test)	Lie > Truth: Stronger activation of the parietal cortex, insula, medial and lateral prefrontal cortex, anterior cingulate cortex
Abe et al. 2006	PET	Healthy volunteers	Telling the truth and lying about experienced and unexperienced events	Lie: Lateral and medial prefrontal cortex; Pretending not to know: ACC
Gamer et al. 2007	fMRI and polygraphy	Healthy volunteers	Denying ownership of a playing card (variant of the Guilty Knowledge Test)	Lie > Truth: Stronger activation of the cerebellum, right inferior frontal cortex, inferior motor cortex
Mertens & Allen 2008	EEG	Healthy volunteers	Virtual reality crime scenario	
Tian et al. 2009	NIRS	Healthy volunteers	Mock crime	Lie > Truth: PFC
Kozel et al. 2009	fMRI	Healthy volunteers	Mock crime (variant of the Control Question Test)	Lie > Truth: Stronger activation of orbitofrontal cortex, dorsolateral cortex, anterior cingulate cortex

especially not in real-life settings. Additionally, the identified regions (e.g. ACC) are not functionally and/or structurally specific to the act of a lie, as they are also associated with working memory (e.g. Broome et al. 2010), self-concept (e.g. Rameson et al. 2010) and further higher cognitive abilities. Also, regions as the ACC and amygdala consist of structurally and functionally differing subunits, an often underestimated aspect. With the help of fMRI and the other common methods of neuroimaging, it is currently not possible to exactly determine, which part of a certain brain region plays a role in which task (Axer et al. 2010).

More, the groups of participants in the studies are usually small (around 20 per study, only nine in the final sensitivity analysis of the Kozel study, Kozel et al. 2009) and at the same time very homogeneous comprising of healthy Caucasian students in their twenties with an above average IQ, who join the studies voluntarily. But these samples are far away from the forensic reality (Schneider et al. 2006), where the mean levels of education and IQ are significantly below these participant samples and also the variety of age and ethnicity is much broader. While the understanding of the brain and neuroimaging technologies is still in its infancies, there is even more a lack of knowledge to which extent these factors might influence the results of a brain scan.

"Diagnosing Criminals"

While the interest in neuroscience-based lie detection has decreased slightly in the past two to three years, there has been a growing interest in analyzing brain structure and function of criminal offenders and paraphiliacs, and in the neural correlates underlying moral behavior (Greene 2006) (for an overview of current studies see Tables 2 and 3).

The idea of linking physical traits to criminal or moral/immoral behavior traits is not new. In the mid 19th century, Cesare Lombroso, an Italian physician and psychiatrist often regarded as the "father" of criminology, along with his student Raffaele Garofalo and the followers of phrenology tried to link certain physical traits to criminal behavior. While Lombroso was mainly interested in the shape of the face, the idea behind phrenology was to analyze bumps on the skull: special areas of the brain were assumed to be responsible for certain behavioral traits. If a bump over an area was found, this area and its function were said to be pronounced (Meier 2006) and would potentially indicate a certain aspect or character.

Modern desires to investigate the brains of psychopaths or other criminal offenders have been criticized as a revival of these ideas and have been referred to as "modern Lombrosionism" (Tondorf 2008; Baskin et al. 2007) or "modern phrenology". Though it is not controversial that certain brain structures are dedicated to certain brain functions such as Broca's Area for language processing, exactly locating higher cognitive functions is currently impossible due to the exceeding individual variability of brain shapes, insufficient accuracy of contemporary methods and because of conceptual ambiguities. Only a few studies are discussing issues of the use of complex terms as "lie" (Langleben et al. 2005) or "morality" (Moll et al. 2002) and likewise, there is no standardized diagnosis of psychopathy. The lack of clear definitions of what to investigate makes the results of studies questionable and hardly comparable across studies (Bennet & Hacker

Table 2: Study examples on neuroscience and criminal behavior.

Study	**Methods**	**Group**	**Results**
Criminals/ Psychopathy and related topics			
Soderstrom et al. 2000	SPECT	Non-psychotic violent offenders	Reduced regional cerebral blood flow (rCBF) in the right angular gyrus, in the right medial temporal gyrus, bilateral hippocampus and left frontal white matter Increased rCBF in the parietal associative cortex bilaterally
Lindberg et al. 2005	EEG	Murderer with antisocial personality disorder	Reduced alpha-, but bilaterally increased theta- and delta-waves in arousal EEG, in occipital regions in particular. Altered brain maturation? Altered day arousal
Deeley et al. 2006	fMRI	Psychopathic criminal offenders (PCL-R-Score > 25)	Reduced and even increasing activation of the fusiform face area and extrastriatal cortex during viewing of (fearful) facial stimuli
Schiltz et al. 2007	fMRI	Pedophiles	Reduced right-sided amygdala volume. Reduced white matter in the right amygdala, the hippocampus bilaterally, septal regions and the substantia innominata. Increase of the right temporal pole
Anckarsäter et al. 2007	SPECT	Violent offenders	Frontotemporal hypoactivation
Müller et al. 2008	Structural MRI	Psychopathic criminal offenders (PCL-R score > 28)	Increase of gray matter in frontal and temporal regions, in the right superior temporal gyrus in particular
Tiihonen et al. 2008	MRI (Voxel-based morphometry)	Criminal offenders with antisocial personality disorder (PCL-R score > 30)	Atrophic gray matter in the postcentral gyrus, frontopolar and orbitofrontal cortex, which was positively correlated with the PCL-R score. Increased white matter in the right cerebellum. Bilaterally increased white matter in the occipital and parietal lobe and in the left cerebellum. Within the offender group no correlation between increased gray and white matter and the PCL scores, substance abuse, the use of psychotropic pharmaceuticals and global IQ

Table 3: Study examples on neuroscience and criminal behavior.

Study	Methods	Group	Results
Moral Brain			
Moll et al.2001	fMRI	Healthy participants	Moral > Morally Irrelevant: Fronto-polar cortex, medial frontal gyrus, right anterior temporal cortex, lenticular nucleus, cerebellum
Moll et al.2002	fMRI	Healthy participants	Moral judgments: Medial orbitofrontal cortex, temporal pole, STS. Emotional, but non-moral judgments: Left amygdala, lingual gyri, lateral orbital gyrus
de Oliveira-Souza et al. 2008	Structural MRI	Psychopaths (PCL:SV-Score 17.8 3.8)	Decreased gray matter in the prefrontal cortex, orbito-frontal cortex (laterally and left medial), superior temporal sulcus, medial anterior insula and left anterior temporal cortex. Significant correlation between reduced gray matter and antisocial behavior

2003).

Most of the forensic studies refer to individuals with antisocial personality disorder or even psychopathic traits, which is a common group among convicted felons. (Schneider et al. 2006). The studies reveal alterations and dysfunctions of prefrontal and parietal regions and parts of the limbic system such as the amygdala (see Weber et al. 2008 for review).

Another focus is shedding light on the neural correlates of the basic ability to distinguish between right and wrong. Moll, de Oliveira-Souza and colleagues began investigating the neural substrates of moral decision making in healthy people (Moll et al. 2001). They followed up with structural MRI studies on psychopathic brains, concluding that there are distinctive deviances in regions that are associated with morally-desirable behavior, in particular the ventro-medial prefrontal areas (de Oliveira-Souza et al. 2008).

While moral studies reveal a functional network of certain brain areas including the ventro-medial prefrontal cortex, the anterior cingulate and posterior cingulate cortex, parietal areas and the precuneus, these regions are not specific to moral reasoning and also found in studies concerning self-referential cognition (Rameson et al. 2010) and the resting state (Mason et al. 2007). Additionally, studies on moral decision making mostly lack a clear definition of the term ”morality” (Bennett & Hacker 2003).

The Legal Point of View

History of Lie Detection in Germany

Lie detection is, and always has been, at best, skeptically considered in German jurisdiction. However, the ”Bundesgerichtshof (BGH)” (German federal court) and the ”Bundesverfassungsgericht (BVerfG)” (German constitutional court) have three pertinent decisions regarding the validity of lie detectors currently in court.

In 1954, the BGH (BGHSt 5, 332) interpreted the use of polygraphic lie detection as an offense against human dignity (Art. 1 I

”German Grundgesetz” - GG). Polygraphy was regarded as an illegal intrusion into the subconscious mind. In 1981, the BVerfG (BVerfG NStZ 1981, 446) still agreed with the ruling of it being an offense against the principles of fundamental law - though not against human dignity but against personal rights (Art. 2 I, 1 I GG) - in 1998, the BGH (BGHSt 44, 308) denied any transgression of fundamental legal principles. However, polygraphy was not accepted as legal evidence either. On the contrary, after reviewing four expert reports the BGH stated the infeasibility of the use of the polygraphic lie detector in court. As a result, even today the lie detector has not made its way into the German law system.

Discussing Neuroscience

As pointed out by the BGH in 1954 (BGHSt 5, 332), the use of polygraphs as lie detectors in courtrooms may only be justified following the rules of law and not primarily by scientific evidence. Emanating from that, during that decision the BGH analyzes the meaning of polygraphy according to the legal guideline of human dignity.

Like polygraphy or forensic DNA analysis, neuroscience challenges fundamental principles of law such as human dignity, rights of personality and principles of the law of evidence (Spranger 2009, Beck 2007). Its in part intrusive methods require detailed discussions on potential applications and the need for regulations. Likewise the BGH in 1954 for the polygraphy with regard to neuroscience Schauer (2010) points to the questionable confusion of normative terms as guilt and responsibility and descriptive standards of statistics and psychological evaluations: What works for science needs not work for law and vice versa, as both disciplines are following differing standards. Thus, the decision about admissibility of evidence in courtrooms must not only be based on scientific principles such as statistical values and the construct validity of paradigms, but also has to take legal standards into account. More even, to avoid a kind of ”neural fallacy” one has to consider that it is outside of the function of a descriptive science such as neuroscience to determine whether the prerequisites of the criteria of law principles are fulfilled. In order to ensure a reasonable way of dealing with the new neuroimaging methods one has to thoroughly pay attention to which (legal) goals can be addressed by scientific studies and to consider what can be derived from their results (Brown & Murphy 2010; Greely & Illes 2007).

Conclusion

Though there are some promising and impressive developments in the field of neuroscience (Axer et al. 2010; Kozel et al. 2009; Haynes et al. 2007), the current neuroimaging technology does not allow for conclusions about the higher cognitive functions of a single person in a way that makes it suitable as evidence in court (Spranger 2009; Beck 2006). However, the rapidly growing technology exposes the need for regulations in order to guarantee a standardized handling of neuroimaging and a thorough consideration of its impacts for society, also taking its potential suggestive effects into account (McCabe & Castel 2008). To allow for exact definitions of research objectives and the implications of the results, an intensified discussion between lawyers and neuroscientists is highly desirable.

Acknowledgements

The project was supported by the Andrea-von-Braun-Stiftung and written during funding by the German Research Foundation ("Deutsche Forschungsgemeinschaft, DFG", IRTG 1328).

References

Abe, N, Suzuki, M., Tsukiura, T., Mori, E., Yamaguchi, K., Itoh, M. & Fujii, T. (2006) Dissociable roles of prefrontal and anterior cingulated cortices in deception. *Cerebral Cortex, 16,* 192 - 199

Agam, Y, Joseph, RM, Barton, JJ & Manoach, DS (2010) Reduced cognitive control of response inhibition by the anterior cingulate cortex in autism spectrum disorders. *Neuroimage, 52,* 336 - 347

Anckarsäter H, Piechnik S, Tullberg M, Ziegelitz, D., Sörman, M., Bjellvi, J., Karlsson, E., Fernandez, NV, Wikkelso, C. & Forsman, A. (2007) Persistent regional frontotemporal hypoactivity in violent offenders at follow-up. *Psychiatry Research, 156*, 87 - 90

Axer, M., Amunts, K., Grässel, D, Palm, C., Dammers, J., Axer, H., Pietrzyk, U., Zilles, K. (2010) A novel approach to the human connectome: Ultra-high resolution mapping of fiber tracts in the human brain. *Neuroimage, 51*, 1091 - 1101

Baskin, J.H., Edersheim, J.G. & Price, B.H. (2007) Is a picture worth a thousand words? Neuroimaging in the Courtroom. *American Journal of Law & Medicine, 33*, 239 - 269

Beck, S. (2006) Unterstützung der Strafermittlung durch die Neurowissenschaften. *Juristische Rundschau, 4*, 146 - 149

Bennett MR & Hacker PMS (Eds.) (2003) Philosophical Foundations of Neuroscience. Malden / Oxford / Victoria, Blackwell

BGHSt *5*, 333

BGHSt *44*, 308

Broome, M.R., Fusar-Poli, P., Matthiasson P. et al. (2010) Neural correlates of visuospatial working memory in the 'at-risk mental state'. *Psychological Medicine, 40*, 1987 - 1999

Brown, T. & Murphy, E. (2010) Through a scanner darkly: functional neuroimaging as evidence of a criminal defendant's past mental states. *Stanford Law Reviews, 62*, 1119 - 1208

BVerfG NStZ 1981, *446*

Chadwick, M.J., Hassabis, D., Weiskopf, N. & Maguire, E.A. (2010) Decoding individual episodic memory traces in the human hippocampus. *Current Biology, 20*, 1 - 4

Davatzikos, C., Ruparel, K. & Fan, Y. et al. (2005) Classifying spatial patterns of brain activity with machine learning methods: Application to lie detection. *NeuroImage, 28*, 663 - 668

Deeley Q, Daly E, Surguladze S, Tunstall, N., Mezey, G., Beer, D., Ambikapathy, A., Robertson, D., Giampietro, V., Brammer, M.J., Clarke, A., Dowsett, J., Fahy, T., Phillips, M.L. & Murphy, D.G. (2006) Facial emotion processing in criminal psychopathy. Preliminary functional magnetic resonance

imaging study. *British Journal of Psychiatry, 189*, 533 - 539

de Oliveira-Souza, R., Hare, R.D. & Bramati, I.E. (2008) Psychopathy as a disorder of the moral bra Fronto-temporo-limbic grey matter reductions demonstrated by voxel-based morphometry. *Neuroimage, 40*, 1202 - 1213

Gamer, M., Bauermann T., Stoeter P. & Vossel G. (2007) Covariations among fMRI, skin conductance, and behavioral data during processing of concealed information. *Human Brain Mapping, 28*, 1287 - 1301

Goebel, R. & Kriegeskorte, N. (2005) Funktionelle Magnetresonanztomographie. In Walter, *Funktionelle Bildgebung in Psychiatrie und Psychotherapie*. Stuttgart, p. 26

Greely, H.T. & Illes, J. (2007) Neuroscience-based lie detection: The urgent need for regulation. *American Journal of Law and Medicine, 33*, 377 - 431

Greene, J. (2006) From neural 'is' to moral 'ought': what are the moral implications of neuroscientific moral psychology?. *Nature Reviews Neuroscience, 4*, 847 - 850

Haynes, J.D., Sakai, K., Rees, G, Gilbert, S., Frith, C. & Passingham, R.E. (2007) Reading hidden intentions in the human brain. *Current Biology, 17*, 323 - 328

Hester, R., Fassbender, C. & Garavan H. (2004) Individual differences in error processing: a review and reanalysis of three event-related fMRI studies using the GO / NOGO task. *Cerebral Cortex, 14*, 986- 994

Jäncke, L. (2005) *Methoden der Bildgebung in der Psychologie und den kognitiven Neurowissenschaften*, 1. Auflage, Stuttgart, pp. 80 - 81

Kozel, F.A., Johnson, K.A. & Grenesko, E.L. et al. (2009) Functional MRI Detection of deception after committing a mock sabotage crime. *Journal of Forensic Science, 54*, 220 - 231

Langleben, D.D. & Dattilio, F.M. (2008) Commentary: The future of forensic functional brain imaging. *Journal of the American Academy of Psychiatry and Law, 36*, 502 - 504

Langleben, D.D., Loughead, J.W., Bilker, W.B., Ruparel, K., Childress A.R., Busch S.I. & Gur, R.C. (2005) Telling truth from lie in individual subjects with fast event-related fMRI. *Human Brain Mapping, 26*, 262 - 272

Langleben, D.D., Schroeder, L., Maldjian, J.A., Gur, R.C., McDonald, S., Ragland, J.D., O'Brien, C.P. & Childress, A.R. (2006) Brain activity during simulated deception: An event-related functional magnetic resonance study. *NeuroImage, 15*, 727-732

Lindberg, N., Tani, P., Virkunnen, M., Porkka-Heiskanen, T., Appelberg, B., Naukkarinen, H & Salmi, T. (2005), Quantitative electroencephalographic measures in homicidal men with antisocial personality disorder. *Psychiatry Research, 136*, 7 - 15

Mason, M.F., Norton, M.I., Van Horn, J.D., Wegner, D.M., Grafton, S.T. & Macrae, C.N. (2007) Wandering minds: The default network and stimulus-independent thought. *Science, 315*, 393 - 395

McCabe, D.P. & Castel, A.D. (2008) Seeing is believing: the effect of brain images on judgments of scientific reasoning. *Cognition, 107*, 343 - 352

Meier, B., *Kriminologie*, 3. Auflage, München 2007

Mertens, R. & Allen, J.J. (2008) The role of psychophysiology in forensic assessments: deception detection, ERPs, and virtual reality mock crime scenarios. *Psychophysiology, 45*, 286 - 298

Moll, J., Esslinger, P.J. & de Oliveira-Souza, R. (2001) Frontopolar and anterior temporal cortex activation in a moral judgment task - Preliminary functional MRI results in healthy subjects. *Arquivos De Neuro-Psiquiatria, 59*, 657 - 664

Moll, J., de Oliveira-Souza, R., Bramati, I.E. & Grafman, J. (2002) Functional networks in emotional moral and nonmoral social judgments. *Neuroimage, 16*, 696 - 703

Moll, J., Zahn, R., de Oliveira-Souza, R., Krueger, F. & Grafman, J. (2005) The neural basis of human moral cognition. *Nature Reviews Neuroscience, 6*, 799 - 809

Müller, J.L., Gänssbauer, S., Sommer, M., Döhnel, K., Weber, T., Schmidt-Wilcke, T. & Hajak, G. (2008) Gray matter changes in right superior temporal gyrus in criminal psychopaths. Evidence from voxel-based morphometry. *Psychiatry Research, 163*, 213 - 222.

Müller, J.L., Sommer, M., Wagner, V., Lange, K., Taschler, H., Röder, C.H., Schuierer, G., Klein, H.E. & Hajak, G. (2003) Abnormalities in emotion processing within cortical and subcortical regions in criminal psychopaths: evidence from a functional magnetic resonance imaging study using pictures with emotional content. *Biological Psychiatry, 54*, 152 - 162

O'Craven, K. & Kanwisher, N. (2000) Mental imagery of faces and places activates corresponding stimulus-specific brain regions. *Journal of Cognitive Neuroscience, 12*, 1013 - 1023

Rameson, LT, Satpute, AB & Lieberman, MD (2010) The neural correlates of implicit and explicit self-relevant processing. *Neuroimage, 50*, 701 - 708

Schauer, F. (2010) Neuroscience, lie-detection, and the law. *Trends in Cognitive Science, 14*, 101 - 103

Schiltz, K., Witzel, J., Northoff, G., Zierhut, K., Gubka, U., Fellmann, H., Kaufmann, J., Tempelmann, C., Wiebking, C. & Bogerts, B. (2007) Brain Pathology in Pedophilic Offenders. *Archive of General Psychiatry, 64*, 737 - 746

Schneider, P.M. (2007) Scientific standards for studies in forensic genetics. *Forensic Science International, 165*, 238 - 243

Soderstrom, H., Tullberg, M., Wikkelsö, C., Ekholm, S. & Forsman, A. (2000) Reduced regional cerebral blood flow in non-psychotic violent offenders. *Psychiatry Research, 98*, 29 - 41

Spranger, T.M. (2009) Der Einsatz neurowissenschaftlicher Instrumente im Lichte der Grundrechtsordnung. *Juristen Zeitung, 21*, 1033 - 1040

Steiner, R. (1981) *Ursprung und Ziel des Menschen*. Rudolf Steiner Verlag, Dornach/Schweiz

Tian, F., Sharma, V., Kozel, F.A. & Liu, H (2009) Functional near-infrared spectroscopy to investigate hemodynamic responses to depetion in the prefrontal cortex. *Brain Research, 1303*, 120 - 130

Tiihonen, J., Rossi, R., Laakso, M.P., Hodgins, S., Testa, C., Perez, J., Repo-Tiihonen, E., Vaurio, O., Soininen, H., Aronen, H.J., Könönen, M., Thompson, P.M . & Frisoni, G.B. (2008), Brain anatomy of persistent violent offenders: More rather than less. *Psychiatry Research, 163*, 201 - 212

Tondorf, G. (2008) Der neue Lombrosionismus. In Rode/Kammeier/Leipert, *Paradigmenwechsel im Strafverfahren*, Berlin (pp.19)

von Schönfeld C.E., Schneider, F., Schröder, T., Widmann, B., Botthoff, U. & Driessen, M. (2006) Prevalence of psychiatric disorders, psychopathology, and the need for treatment in female and male prisoners. *Nervenarzt, 77*, 830 - 841

Weber, S., Habel, U., Amunts, K. & Schneider, F. (2008) Structural brain abnormalities in psychopaths - a review. *Behavioral Sciences & the Law, 26*, 7 - 28

Abstract

T. Sauer (Giessen, Germany – Time-Frequency Analysis, Wavelets and Why Things (Can) Go Wrong

Wavelets are an increasingly popular tool in time–frequency–analysis that helps, among others, to detect time localized frequency components in a signal. Because of that, they are frequently used in the analysis of biosignals or of technical systems. However, the underlying mathematical theory that makes things work so beautifully is based on some nontrivial assumptions whose violation makes the tool useless and creates information that leads to misinterpretation of the signal content. This article gives a brief overview over the background of the wavelet transform in continuous theory and digital practice and highlights some of the difficulties that can arise if the transform are applied inappropriately.

Keywords: Wavelets, Fourier transform, Gabor transform, numerical computations

Time-Frequency Analysis, Wavelets and Why Things (Can) Go Wrong

Tomas Sauer, Lehrstuhl für Numerische Mathematik, JLU Giessen,
Heinrich–Buff–Ring 44, D–35392 Gießen,
Germany
Tomas.Sauer@math.uni-giessen.de

Introduction

Nowadays, the *wavelet transform* has become quite a standard tool for *time–frequency analysis* that allows for signal processing in terms of resolution of time *and* frequency.

There is a simple musical analogy that helps us to understand the meaning of that sentence. The classical and well–known *Fourier transform* decomposes a signal into its frequency components and is ideally suited for the analysis of a single tone played by a musical instrument where the tone is rewritten as a superposition of its *partial tones* which, in our music analogy, appear with frequencies that are multiples of the frequency of the tone itself, (Helmholtz, 1885). The spectrum gives us information on the nature and "color" of the tone but it lacks any time information. This makes perfect sense as the tone is a periodic function and any time information only affects the *phase* of the signal which is mostly irrelevant. The situation changes as soon as, instead of a single tone, a melody is considered, that is, a sequence of different tones of different duration. Perceiving the melody is a task where the Fourier transform fails completely: all that it is able to figure out is which tone had contributed which percentage to the melody. Though this may be statistically interesting, it

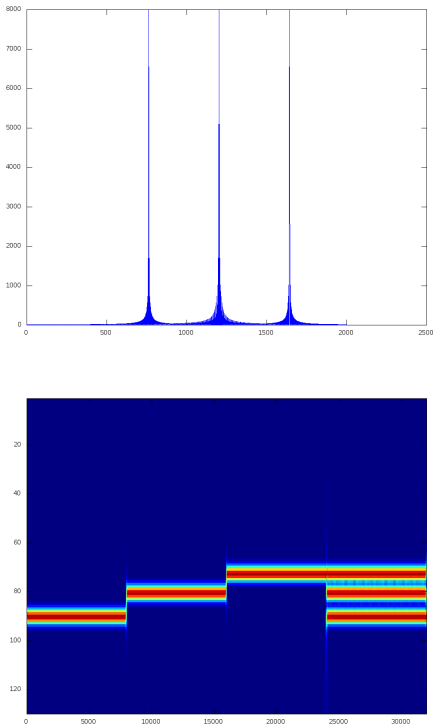

Figure 1: *The spectrum* (above) *and the "wavelet scalogram"* (below) *of the three tones and the chord.*

gives no information about the melody. This is the point where *time–frequency analysis* enters the scene, trying to figure out whether some frequencies or frequency components appear *locally* in time. Let us rush ahead a bit and consider a very simple example where a pure sine is played, followed by its pure third and fifth and, finally, the full chord. As can be seen in Figure 1 the spectrum is a purely "statistical" evaluation of the frequencies that occur in the course of the "melody" while the scalogram shows the "melody" in some almost musical notation. Note, however, that reality would not be that simple as practically any realistic signal is composed of various partial

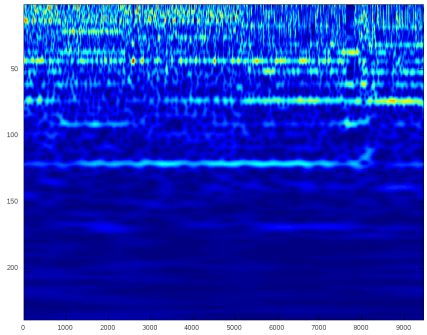

Figure 2: *A snippet from some real musical recording. The appearance of overtones makes things a lot more complicated even if some piece of the melody could be guessed.*

tones and not a pure sine as here. Look at Figure 2 for a small example. We will return to Figure 1 several times in this paper as the two pictures show even more effects that typically appear in numerical signal processing.

The idea of time–frequency precedes that of wavelets, the *windowed Fourier transform* being the oldest and most straightforward approach, followed, for example, by the Gabor transform, cf. (Gabor, 1946). A good source of information in width and depth about time–frequency analysis is the excellent book by Mallat (Mallat, 1999), a very easygoing introduction on a journalist level can be found in (Hubbard, 1996).

In general, no perfect localization in time and frequency is possible as is stated in the famous *Heisenberg uncertainty principle*. Again, we can express this in a musical analogy: it is impossible to play a jig on the bass pedals of an organ, no matter how fast your feet are. To explain and understand this effect, just keep in mind that in order to be audible a tone should

have at least one oscillation which takes a time that is reciprocal to its frequency. If the tone is played in more rapid sequence than this time permits, it is not the tone any more, it needs partial tones of much higher frequency to obtain the "truncation" effect. Hence, its better localization in time (the rapid playing) destroys its localization if frequency (the pure tone). Why this is mentioned? It has the simple but fundamental consequence that there is no perfect version of time–frequency analysis and therefore any attempt to perform such a detection of time local frequency components must have its advantages and drawbacks that require choosing and, if necessary, adapting the method to a specific task. This paper will focus on the wavelet transform and how it can be used as a time localized bandpass filter, i.e., how to localize certain frequency components in time and then remove them from the signal. This requires an *analysis step* that transforms the signal into it scalogram, some sort of time dependent spectrum, and a *synthesis step* which reconstructs the original signal from the possibly modified scalogram. All this is, by nature, mathematical and any reasonable and understandable presentation of the material requests an appropriate amount of formulas and formalism. I will try to be as precise as possible, but will always sacrifice details (as important and crucial as they may be) for the sake of explaining the ideas and concepts.

There is also a *discrete wavelet transformation*, based on the concepts of *multiresolution analysis (MRA)* and filterbanks, cf. (Cavaretta, Dahmen, & Micchelli, 1991; Daubechies, 1992; Mallat, 1999; Strang & Nguyen, 1996; Vetterli & Kovačević, 1995). This is wonderful theory with plenty of applications, for example in the JPEG2000 standard, but this is not what we are interested in here. This paper deals with discrete aspects of the *continuous wavelet transform* that result from the very simple fact that all numerical computations are of a discrete nature.

Basics

In this section, we will review some of the basics of Fourier transform and time–frequency analysis, aiming not so much for completeness or details and definitely not for proofs of these concepts, but for the hidden catches in the mathematics that often are missing in engineering or biosignal processing literature.

In most of signal processing, signals are modeled as real valued L_2–functions, that is, functions f whose *energy integral*

$$\|f\|_2 := \int_{\mathbb{R}} |f(t)|^2 \, dt \tag{1}$$

is finite. In fact, this finiteness of the *energy norm* $\|\cdot\|_2$ is what defines a *square integrable* or L_2–function. With the hair–splitting precision mathematicians are often accused of, it has to be mentioned that this is an integral in the *Lebesgue sense* (thus the letter "L") and that such function are not really pointwise objects as they can be altered on a set of measure zero. All definitions and basic properties can be found in any reasonable book on analysis, with analysis to be understood in some contrast to good old calculus. Fortunately, the subtle points to be taken care of in Lebesgue integrals do not really matter – at least usually. Keep in mind, however, that very simple objects like constants, polynomials or oscillations like sine and cosine do *not* belong to the class L_2.

The use of the letter "t" in (1) already indicates what type of signals we have in mind, namely real valued time series like music recordings or biosignals like the channels of an EEG. All these realistic signals are finite – not finite, however, because of their nature, but because we only record and analyze finite chunks of data from a larger context: neither does the brain activity of the test person end with the experiment, at least not always, nor is the studio turned into eternal silence once the recording of a piece of music is finished. Theoretically, finite signals are great as for such signals the only way to reach infinite energy is the very unrealistic case of a singularity occurring, but since our signals are not finite by nature, only finite by measurement, we have to be prepared to face unwanted artifacts.

Fourier and windows

The *Fourier transform* of a signal will be defined here as

$$\widehat{f}(\xi) = \int_{\mathbb{R}} f(t)\, e^{-i\xi t}\, dt, \qquad \xi \in \mathbb{R}.$$

The function $\widehat{f}$ is called the *spectrum* of the function f, contains essentially the same energy, $\left\|\widehat{f}\right\|_2 = \sqrt{2\pi}\,\|f\|_2$ (the factor $\sqrt{2\pi}$ is due to an ubiquitous normalization issue of the Fourier transform which can and usually will cause serious trouble in careless applications of software libraries) and provides full information about f as there exists the *inversion formula*

$$f = \widehat{f}^{\vee}, \qquad g^{\vee}(t) := \frac{1}{2\pi}\int_{\mathbb{R}} g(\xi)\, e^{i\xi t}\, d\xi. \quad (2)$$

So all is well that ends well? No, not really. Mathematics are usually correct, but they are only correct within a certain framework that has to be understood and interpreted properly! All the above results are L_2–statements and only hold true in the "world" of L_2 functions. Particularly that means:

1. Equation (2) does not hold true in *pointwise* sense, it can be violated on a set of measure zero which may even include all points where the integral can really be computed – explicitly or numerically.
2. The theory already excludes a lot of "interesting" functions like constants (which usually do not even have a Fourier transform) or periodic functions. In fact, even the Fourier transform for signals of finite energy is even more tricky as it is obtained by a completion argument and not directly.
3. Periodic functions have to be handled by means of *Fourier series* which are trigonometric polynomials and their associated spectrum is not a function defined on the continuum $\mathbb{R}$ but a sequence defined on the integers $\mathbb{Z}$. There is a whole theory of such groups and dual groups, the basis of modern Harmonic Analysis, a nice introduction to which can be found in (Katznelson, 1976).
4. Things are significantly easier when *finitely supported* signals are considered, and after all any opera starts and ends sometime (but first the fat lady has to sing). Nevertheless, usually these finite signals will eventually be embedded into signals defined on all of $\mathbb{R}$, as handling fixed beginning and end also creates difficulties.

The Fourier transform computes "only", or, more euphemistically, "precisely", the frequency content of the signal, and the *complex*

number $\widehat{f}(\xi)$ describes the amplitude and the phase of the respective frequency content simultaneously.

The simplest way to pass from the Fourier transform to some elementary form of time–frequency analysis is by means of *windowing*. Instead for transforming the entire function f, the spectrum is computed only for a part of it. This task can be performed, for example, by *convolving* f with a *window function* w whose compact support (the region where the function is nonzero) is centered around the origin. The latter is by no means necessary for the theory to work, but coincides better with the general intuition. The windowed part of f is then obtained by multiplying f with a u–shifted window,

$$f_{w,u}(t) = f(t)\, w\,(t-u)\,,$$

simply "cutting off" all information on f outside the window. If, for example, w "lives" only on $[-1,1]$, then $f_{w,x}$ considers only the values $f(t)$ for $t \in [x-1, x+1]$, which is the window around t. The Fourier transform of the windowed function, also known as the *short time Fourier transform*, is

$$\begin{aligned} \widehat{f}_{w,x}(\xi) &= \left(f(\cdot)\, w\,(\cdot + t)\right)^{\wedge}(\xi) && (3)\\ &= \widehat{f}(\xi) * \left(e^{i\xi\cdot}\widehat{w}\right)(\xi) && (4)\end{aligned}$$

with the *convolution*

$$(f * g)\,(t) := \int_{\mathbb{R}} f(s)\, g(t-s)\, ds.$$

In terms of signal processing, convolutions are often identified with filtering, cf. (Hamming, 1989), so that this again is a well known operation: the spectrum (not the signal itself!) is filtered by a modulated and phase shifted Fourier transform of the window function w. This operation does not come for free as it introduces windowing artifacts, known as the *leaking effect*, see again (Hamming, 1989), that lead to a "distorted" spectrum that has to be interpreted with care.

But back to (3). This formula defines the short time Fourier transform of f around x as

$$\widehat{f}\,(x,\xi) := \left(f(\cdot)\, w(\cdot - x)\right)^{\wedge}(\xi) \qquad (5)$$

and has *two* parameters, $x, \xi \in \mathbb{R}$, corresponding to the "positions" x in time and ξ in frequency. Back to our musical analogy, the short time Fourier transform computes the spectrum, i.e., the frequency content over a limited time of our musical record, maybe a bar or a single tone, depending on the size of the window. It should be clear that this window has to be small enough to distinguish between different tone and that we will not get a precise resolution of frequency whenever the window covers the transition between two tones.

Time, frequency, and Heisenberg

In *time–frequency analysis* we consider a more general analysis tool, namely an integral by means of so called *time–frequency atoms* $\phi_{u,\xi}$, indexed by *time parameter* u and a *frequency parameter* ξ. Formally,

$$T_\phi f\,(u,\xi) = \int_{\mathbb{R}} f(t)\, \phi_{u,\xi}(t)\, dt. \qquad (6)$$

In the example of our short time Fourier transform, also referred to as *Gabor transform*, the time–frequency atoms were the modulated window functions

$$\phi_{u,\xi}(t) = e^{-i\xi t}\, w\,(t-u)\,, \qquad (7)$$

where the *window* w is a real–valued symmetric funtion, i.e. $w(t) = w(-t)$, and the $e^{-i\xi t}$ term is responsible for the close relationship to

the Fourier transform. The Fourier transform itself is given in the context of time–frequency atoms by

$$\phi_{u,\xi}(t) = e^{-i\xi t}, \qquad \text{i.e.,} \qquad w \equiv 1,$$

and thus simply ignores the time component u. After all, Fourier analysis is frequency analysis in its purest form. An obvious advantage of the Gabor transform or of any type of windowed Fourier transform is that the frequency part of the transformation is really a frequency and not some parameter *somehow related* to frequency as the scale parameter in the wavelet transform will be; this can become a very important point, for example in audio applications.

A fundamental property of a time–frequency atom is its ability to localize the information in time *and* frequency. To quantify this and to clarify what we are actually talking about, we define the *localization* of a function f in time and frequency as

$$\mu(f) := \frac{1}{\|f\|_2^2} \int_{\mathbb{R}} t\ |f(t)|^2\ dt \tag{8}$$

$$\widehat{\mu}(f) := \frac{1}{2\pi\|f\|_2^2} \int_{\mathbb{R}} \xi\ \left|\widehat{f}(\xi)\right|^2\ d\xi, \tag{9}$$

and the associated *variations* as

$$\sigma^2(f) := \frac{1}{\|f\|_2^2} \int_{\mathbb{R}} (t-\mu(f))^2\ |f(t)|^2\ dt,$$

$$\widehat{\sigma}^2(f) := \frac{1}{2\pi\|f\|_2^2} \int_{\mathbb{R}} (\xi-\widehat{\mu}(f))^2\ \left|\widehat{f}(\xi)\right|^2\ d\xi.$$

The idea behind the concept of localization is more intuitive than it may seem from equation (8): if, for example, f "lives" only on the interval $[t-\varepsilon, t+\varepsilon]$ for some $\varepsilon > 0$, then $|\mu(f) - t| \le \varepsilon$, i.e., $\mu(f) \sim t$ and $\sigma(f) \le \varepsilon$. Therefore, we say that f is *perfectly localized in time* if $\sigma(f) = 0$ and *perfectly localized in frequency* if $\widehat{\sigma}(f) = 0$. Unfortunately there is no perfect localization as the *Heisenberg uncertainty principle* states that

$$\sigma^2(f)\,\widehat{\sigma}^2(f) \ge \frac{1}{4} \tag{10}$$

for any function f so that the *simultaneous* localization in time and frequency always hits a lower bound. The "Heisenberg optimal" functions are the particular short time Fourier atoms

$$\phi(t) = a\, e^{-i\xi t}\, e^{b(t-u)^2}, \tag{11}$$

with the window functions $e^{b(t-u)^2}$ and the "tuning parameters" $a, b \in \mathbb{C}$, $\xi, u \in \mathbb{R}$. These windows are no more finitely supported but decay exponentially for $t \to \infty$ provided that b lies in the left half plane, which is perfectly OK in theoretical terms but requires some care if the function is considered numerically and has to be truncated in order to have finite computations.

The time–frequency localization of a function f or an atom ϕ can be visualized by the *Heisenberg boxes*

$$H(f) = [\mu(f)-\sigma(f), \mu(f)+\sigma(f)] \times [\widehat{\mu}(f)-\widehat{\sigma}(f), \widehat{\mu}(f)+\widehat{\sigma}(f)]$$

in the *time–frequency plane* $\mathbb{R}^2 \ni (t, \xi)$. If $f = \phi_{u,\xi}$ is a time–frequency atom, we simply write $H(u, \xi)$. The Heisenberg boxes for the Gabor atoms (7), for example, are usually rectangles around (u, ξ) with sides $\sigma(w)$ and $\widehat{\sigma}(w)$. It should be intuitively clear that the time–frequency resolution of time–frequency atoms is related to the area of the Heisenberg boxes and that a system $\{\phi_{u,\xi} : (u, \xi) \in \Gamma\}$ can capture the time frequency content of an analyzed function f only if the associated Heisenberg boxes cover the time–frequency region of interest and the more these boxes overlap, the higher the redundancy between the atoms will

be. Here the index set Γ can be $\mathbb{R}^2$ or an infinite or finite subset of $\mathbb{R}^2$ – in practical applications it will definitely be the latter. If we know *all* values of the Gabor transform of a function f, we can even reconstruct this function by means of the "averaged inverse Fourier transform"

$$\frac{1}{2\pi \|w\|_2^2} \int_{\mathbb{R}} \int_{\mathbb{R}} \widehat{f}(u,\xi)\, e^{i\xi t} \overline{w(t-u)}\, d\xi\, du. \quad (12)$$

Again, this identity only holds true in the weak sense of L_2 functions and not necessarily for any $t \in \mathbb{R}$. Nevertheless, the existence of inverse transforms fulfills an important purpose: it shows that the transform, in this case the Gabor transform preserves all the information about the underlying function since the function can be reconstructed from the values of the transformation. Whether the the function can be reconstructed from a discrete or even finite subset of transformation values and how such a subset should be constructed, is another issue.

Wavelets

Another family of time–frequency transforms is given by the *wavelet transform*. Here the atoms $\psi_{u,s}$, $u, s \in \mathbb{R}$, are of the form

$$\phi_{u,s}(t) := \frac{1}{\sqrt{s}} \psi\left(\frac{t-u}{s}\right), \quad (13)$$

where the function ψ is called the *wavelet* and the word "frequency" has to be understood in a more generous sense as $1/u$ for the *scale parameter* u. To be precise, $1/u$ is not **the** frequency, but related to it. The *wavelet transform* of a function f is defined as

$$W_\psi f(u,s) := \int_{\mathbb{R}} f(t)\, \frac{1}{\sqrt{s}} \overline{\psi\left(\frac{t-u}{s}\right)}\, dt. \quad (14)$$

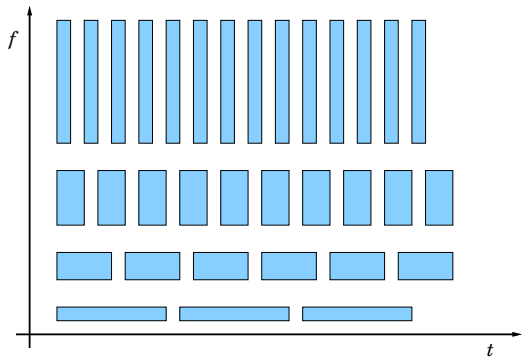

Figure 3: *The Heisenberg boxes of a wavelet; this is, of course, only schematic, but at least the area of the boxes is all the same as it should be.*

The time–frequency boxes for wavelets

$$H(u,s) = [u - s\,\sigma(\psi), u + s\,\sigma(\psi)] \times \left[\frac{\widehat{\mu}(\psi)}{s} - \frac{\widehat{\sigma}(\psi)}{s}, \frac{\widehat{\mu}(\psi)}{s} + \frac{\widehat{\sigma}(\psi)}{s}\right]$$

are of a different type than those above as they change their shape according to the scale parameter s. If s increases, that is, if the "frequency" $1/s$ is lowered, the box stretches in time direction and narrows is "frequency" direction, indicating an improved frequency resolution for the price of reduced time resolution, see Figure 3. In our musical analogy, a low tone takes some time to sound (it should at least perform one full period to be perceivable as a tone, which is a periodic event), hence cannot be located very well in time and therefore precise measurements are not necessary. Instead, the wavelet has a good capacity to discriminate between different frequencies there. After all, the low tones are denser in frequency than the high ones.

Things turn around if s decreases: in "high frequencies" the discrimination between frequencies deteriorates (what remains constant is the *relative error* in determining them) but

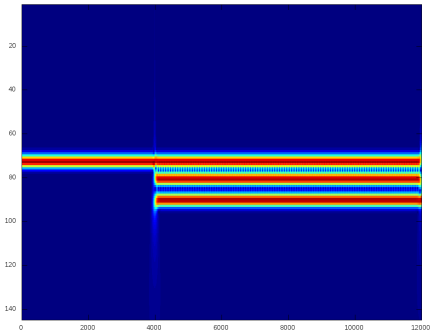

Figure 4: *Zoom into the wavelet transform of the "chord" signal*

the time resolution improves. In summary one could say:

> The Gabor transform focuses on *absolute* precision in the localization of time and frequency while the wavelet transform cares for *relative* precision.

Funny enough, the *area* of the Heisenberg boxes remains constant in both cases, it is $4\sigma^2(w)\,\widehat{\sigma}^2(w)$ in the case of the Gabor transform and $4\sigma^2(\psi)\widehat{\sigma}^2(\psi)$ in the case of wavelets; both values have to be at least 1 by means of (10).

This effect of "relative precision" can actually be seen in our simple example of Figure 1. If one carefully looks at the chord on the right hand side of the image, there is a blur between the two "high" frequencies while the two lower parts of the chord are better separated. Figure 4 shows a "zoom" to this effect and indeed it should become even clearer that there is this blur or leakage between the "frequency bands". This is due to the decay of *frequency resolution* for higher scales, and in order to avoid artifacts or, even worse, misinterpretations of signals, it is of extreme importance to carefully choose the frequencies or scales for which the wavelet transform is computed. This can also mean to "trim" or "tune" the wavelet such that it provides sufficient frequency resolution in the "band of interest". In terms of Heisenberg boxes this means that the wavelet has to provide "sufficiently flat" boxes.

Also wavelets admit an inversion formula, namely

$$f = M_\psi W_\psi f \tag{15}$$

with the "inversion formula"

$$\frac{1}{C_\psi}\int_{\mathbb{R}}\int_{\mathbb{R}} g(u,s)\frac{1}{\sqrt{s}}\psi\left(\frac{t-u}{s}\right)\,du\,\frac{ds}{s^2}. \tag{16}$$

We denote this expression by $M_\psi g$ and thus obtain the *inversion operator* which is defined for functions g of two variables, but obviously the existence of the double integral is again an issue by itself.

It is illustrative to look at the proof as some of the formulas and ideas will become important later. If we fix the scale s and consider the wavelet transform as a function in u, we can follow a good engineering tradition and take its Fourier transform which yields

$$\left(W_\psi f(\cdot,s)\right)^\wedge(\xi) = \sqrt{s}\,\widehat{f}(\xi)\,\widehat{\psi}\,(s\xi)\,. \tag{17}$$

In the proof, one takes the u–integral from (16), uses the classical Perceval identity

$$\int_{\mathbb{R}} f(t)g(t)\,dt = \frac{1}{2\pi}\int_{\mathbb{R}}\widehat{f}(\xi)\widehat{g}(\xi)\,d\xi$$

and substitutes (17). Applying the s–integral to all that stuff and doing a few relatively simple manipulations like change of variables, we can express the double integral as a product of an inverse Fourier transform of $\widehat{f}$ and the integral

$$\int_{\mathbb{R}}\frac{\left|\widehat{\psi}\right|^2}{|\xi|}\,d\xi =: C_\psi, \tag{18}$$

which determines the value of the "magic" constant C_ψ in (15) and completes the proof. Did we forget something? Indeed! In order to have a well–defined expression, the constant should be finite, which is the famous *admissibility condition* for wavelets. Sometimes a function is even called a wavelet only if the expression in (18) is finite – which makes perfect sense as any function of that type must satisfy $\int \psi = 0$, that is, it has the same amount of "mass" above and below the x–axis, which is a "wave–like" behavior. Again it is time for a few remarks:

1. The wavelet transform (14) can be computed even if the underlying wavelet is *not* admissible, in other words, even if the wavelet is not a wavelet. In fact, one of the most popular wavelets, the so–called *Morlet wavelet*, see (Mallat, 1999) is not admissible but nevertheless used for analysis purposes.

2. If the wavelet is admissible, then the wavelet transform captures the full information on the function; after all, that is what invertibility of the transform means. However, an admissible wavelet always "kills" constants so that constants can always be lost during a wavelet transform. This is perfectly in accordance with the "laws" of L_2 as the only square integrable constant function is the zero function. In practical applications, however, only a *finite* piece of the function is transformed and there shifts by constants could very well matter – at least in part.

3. In general, modification by constants of a finitely supported function only affect that part of the wavelet transform where the overlap between the constant function and the wavelet takes place only in a non-relevant part of the wavelet. In other words, such effects only show on the boundary of the wavelet transform.

Even if wavelets can be almost completely "custom designed" with the only requirement being the very mild admissibility condition (18), there are only three "classical" wavelets that cover most of the known applications:

The Haar wavelet is the simplest case of a wavelet and defined as

$$\psi(t) = \begin{cases} 1, & t \in [-1, 0), \\ -1, & t \in (0, 1], \\ 0, & \text{otherwise}, \end{cases} \tag{19}$$

hence, it is *compactly supported*. It provides excellent time localization but since its Fourier transform is the difference of two modulated copies of the function $\xi := \frac{\sin \pi\xi}{\pi\xi}$, the Fourier transform decays very slowly leading to quite poor frequency localization.

The Mexican hat wavelet is defined as

$$\psi(t) = \left(1 - t^2\right) e^{-t^2/2} = -\frac{d^2}{dt^2} e^{-t^2/2} \tag{20}$$

and decays exponentially for $|t| \to \infty$, which means still very good time localization even if the function is no more compactly supported. It almost coincides with its Fourier transform $\widehat{\psi}(\xi) = \xi\, e^{-\xi^2/2}$ and therefore offers good time **and** frequency localization.

The Morlet wavelet or "Morlet's Gaussian wavelet" is the "complex brother" of the Mexican hat and uses a complex modula-

tion of the form

$$\psi(t) = e^{ia\omega t}e^{-bt^2/2}, \qquad \omega,\, a,\, b \in \mathbb{R}_+, \tag{21}$$

instead of the polynomial component. Strictly speaking, the definition from (21) does not even satisfy the admissibility condition, but this can be easily solved by adding a suitable correction term, cf. (Mallat, 1999). The decay parameters a, b allows to "tune" the wavelet to a certain *central frequency*, cf. (Mallat, 1999). Loosely speaking, this means, we can use it to determine the frequency or scale range where the Heisenberg boxes are approximately squares, where time are frequency are resolved equally well.

Mexican hat and Morlet wavelet are not some miraculous inventions of pure genius' inspiration. Instead, they result from almost systematic constructions of wavelets emerging of the *time–frequency optimal* frequency atoms in (11) which admit equality in the Heisenberg uncertainty equation (10). Also the "differentiation trick" that leads to the Mexican hat wavelet is based on a very simple idea: by means of partial integration it is very easy to see that

$$\int_{\mathbb{R}} f(t)\psi(t)\,dt = 0$$

if f is a linear function of the form $f(t) = at + b$. The technical term for that property is to say that ψ has *two vanishing moments* – one vanishing moment would mean $\int \psi = 0$, so the Mexican hat "over-satisfies" this requirement by another polynomial, $f(t) = t$. In general, the wavelet is said to have n *vanishing moments* if it "kills" all polynomials of degree $< n$, that is, if

$$\int_{\mathbb{R}} t^k\,\psi(t)\,dt = 0, \qquad k = 0, \ldots, n-1. \tag{22}$$

Vanishing moments are crucial for the good approximation of smooth functions (functions that have a lot of derivatives) and for the detection of jumps and discontinuities. In fact, we now know how to construct wavelets with an arbitrary number of vanishing moments, namely, as derivatives of a function ϕ that has to satisfy some mild conditions: $\psi = \frac{d^k}{dt^k}\phi$ *automatically* has k vanishing moments.

Customizing wavelets

One great advantage of wavelets is that the can be customized to a given application. Since the wavelet transform (14) essentiallly measures the correlation between the signal and shifted and dilated (i.e., "frequency modulated") versions of the wavelet function, wavelet coefficients will be particularly large in modulus whenever the signal contains a strong "wavelet–like" piece. This can be made use of, for example in the analysis of EEG data where often the detection of spindle–like features is desired. But how to design?

The simplest way is to choose a function ϕ such that

$$\int_{\mathbb{R}} \frac{|\phi(t)|^2}{|t|} < \infty$$

and to use ϕ as the Fourier transform $\widehat{\psi}$ of the wavelet. We will see later when we consider the numerical realization that this is perfectly sufficient, that indeed the wavelet itself will not even be needed for a fast computation of the transform. The disadvantage is that it is not so easy to control the shape of the wavelet just by means of its Fourier transform.

A slightly more sophisticated approach is to adapt ψ as a linear combination

$$\psi = \sum_{j=1}^{N} a_j\,\psi_j, \qquad a_j \in \mathbb{C},\, \psi_j \in \Psi,$$

where the wavelets ψ_j are chosen from a (possibly infinite) *dictionary* Ψ of wavelet functions or as scaled versions of the original wavelet. Under some mild conditions on Ψ the admissibility of the resulting wavelet function ψ can be easily assured. The coefficients a_j can then be determined by "tuning" the wavelet ψ against, for example, a given feature function, that is, by solving an optimization problem where the coefficients are chosen to minimize the deviation from the feature function or some variance in the wavelet transformed signal. A method that includes the dictionary selection into the optimization by means of a so–called *greedy algorithm* is the computation of a *Karhunen–Loève basis* as described in (Mallat, 1999).

However, usually wavelet dictionaries are more popular in the context of MRA–based wavelet analysis, see (Rubinstein, Zibulevsky, & Elad, 2010) for a recent application with relevant references, which is not the topic of this paper.

Wavelets as regularity detectors

In addition to time–frequency decompositions, wavelet also perform well as an *analysis tool*, cf. (Holschneider, 1995), since the are able to detect *singularities* of a function via the decay of the wavelet coefficients. This is, by the way, perfectly in accordance with the Fourier spectrum as well: no function can have infinitely high frequency content, $\widehat{f}(\xi)$ has to tend to zero as $|\xi|$ tends to infinity, a fact passed around as the *Riemann–Lebesgue–Lemma* at mathematical campfires. Even more interesting, the rate in which the Fourier transform tends to zero is closely related to the smoothness of the transformed function, where smoothness has to be seen in

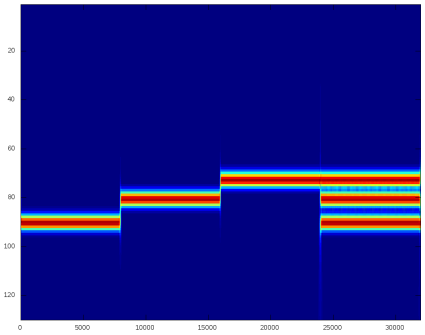

Figure 5: *The scalogram from Figure 1. This time focus on the vertical lines at the transition between different tones in our "melody".*

the sense of differentiability again. The same happens – no surprise – with wavelets: if the scale tends to zero, i.e., the frequency tends to infinity, then the wavelet coefficients decay, but they do so *locally*! This means that in principle, i.e. up to some technical conditions,

$$|W_\psi f\,(x,s)| \sim s^\alpha \qquad \text{for } s \to 0 \qquad (23)$$

if the function f is α times differentiable *at* x. The quite tricky details needed for a precise and quantitative formulation of this statement can be found in the books by Holschneider (Holschneider, 1995) and Mallat (Mallat, 1999), but do not expect things to be very simple or easy to understand. Nevertheless, the phenomenon is easy to *recognize* in our chord example which nicely illustrates also that phenomenon. Indeed, if we look at Figure 1, we see that at every transition there is a thin but clearly visible vertical line. This line shows wavelet coefficients that slowly fade to background color, hence decay, but very slowly. On the other hand, they exactly belong to the positions where the frequency of the sine tones changes, i.e., where the first derivative has a

discontinuity even if the signal is continuous there. Thus, wavelets can do *local* singularity detection but it is not hard to imagine that this becomes more tricky for non–artificial signals since eventually one has to read *asymptotic* decay off a *finite* signal.

Wavelets vs. Fourier

The difference between Fourier and wavelet transform can nicely be illustrated by yet another musical phenomenon which is known as *beats*, cf. (Benade, 1960; Helmholtz, 1885) and is often used for the tuning of musical instruments. Mathematically, it is just an immediate consequence of the simple trigonometric identity

$$\sin x + \sin y = 2 \sin \frac{x+y}{2} \cos \frac{x-y}{2}, \qquad (24)$$

which says that two pure sine tones with close frequencies mix into a sine with the *average* frequency whose amplitude rises and falls like the cosine of the *difference* frequency. If, for example, we take a 440 Hz sine tone and apply to it a 2 Hz amplitude modulation, then what we would perceive is “beating” sound of 440 Hz. The Fourier analysis, however, would detect two tones of 438 Hz and 442 Hz, respectively, and indeed this is what the computed Fourier transform on the left of Figure 6 shows. In plot resolution, and that makes it even worse, it looks almost like single, blurred peak of 440 Hz, and it is very hard to decide whether this computation really shows two peaks or a numerical artifact. The wavelet transform, on the other hand, represents the signal as it is perceived, namely as a frequency band with periodic amplitude modulation. Even the frequency can be determined quite accurately from the maximal entries in the spectrogram, but of course, the picture shows a rather blurred frequency, by far less sharp than the peaks in the Fourier transform.

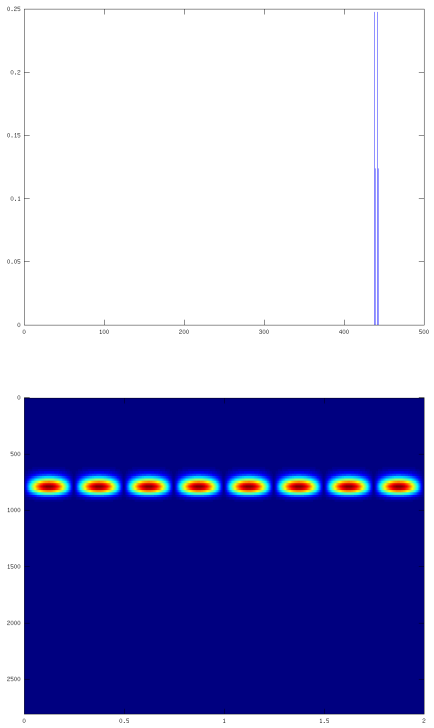

Figure 6: *Fourier and wavelet analysis of the beat phenomenon. The original signal is a 440 Hz sine tone of two seconds with a 2 Hz amplitude modulation. The plots show the Fourier transform* (above) *and the Morlet wavelet spectrogram* (below).

The beat phenomenon can also be observed in the Gabor transform, at least as long as the frequency resolution, that is, the length of the analyzing window is chosen relatively small. The more the size of the window and thus the frequency resolution of its Fourier transform approaches the frequency resolution of the original signal, the more the Gabor transform behaves “Fourier like” with separated frequencies. For small windows,

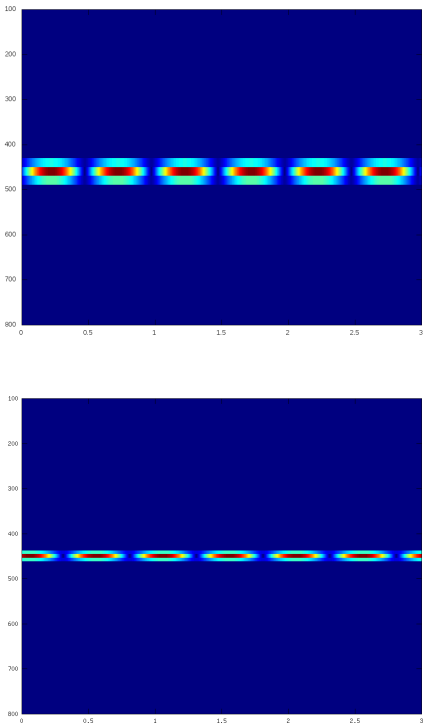

Figure 7: *The Gabor transfor with a small (∼ 5% of the frequency resolution) and mid–sized (∼ 12 % frequency resolution window. The beat effect is slightly less with the latter, but also the phase of the beat is shifted.*

on the other hand, beats are displayed as a single modulated frequency, see Figure 7 and Figure 8.

Keep in mind, however, that there is no "right" or "wrong" here as we simply look at the left or right hand side of the trigonometric identity (24). Both decompositions are valid representations of the original signal and both require proper interpretation to be understood in the right sense.

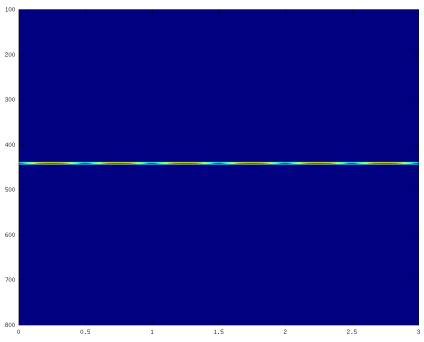

Figure 8: *At a window size of half the frequency resolution the signal looks essentially like two separated frequencies.*

The finite world

As mentioned before, finite measurement or recording is unavoidable in reality. After all, also the available resources, time, storage and patience for example, are only finite. On the other hand, the integral in the wavelet transform (14) is an *infinite* one. Now, suppose that the wavelet ψ "lives" on the interval $[-T, T]$, then, to compute $W_\psi f(s,t)$, we need to know f on the interval $[t - sT, t + sT]$. If t is now close to the beginning or the end of the measurement of f, then this interval will exceed the region where we know f and hence we will have to fill in "phantom values" for f at these locations where we do not know the function. Usually, these values are either set to zero or taken from a periodic wrapping of f. Whatever we do, there are values of s and t where we cannot trust the wavelet transform as it is based on values of f that are not known but are entirely based on pure guesswork. And also note that this region grows if the scale grows! Depending on the support of the wavelet, there is only a U–shaped region of the scalogram of certain

size (the size depending on the support of the wavelet) where the results of the transform can be trusted. It can even happen, if the support of the wavelet is large and the considered frequency range to low, that **all** of the scalogram is contaminated by overlap artifacts. The value of such a transform is easy to guess.

The discrete world

In practical signal processing one is not dealing with continuous functions, but with *discrete* data. Usually, our favorite piece of music is stored in a time–sampled fashion on a CD, EEG or other biosignal information are also available as *time discrete signals* only. Such signals are *sequences* or functions on $\mathbb{Z}$, the set of integers. Here $\mathbb{Z}$ takes the same role as $\mathbb{R}$ in the preceding chapters on time–continuous signals: even if realistic signals are usually of a finite nature, they will be embedded into this infinite domain which helps to avoid fiddling with boundary effects. The Fourier transform of a sequence f is the *trigonometric series*

$$\widehat{f}(\xi) = \sum_{k\in\mathbb{Z}} f(k) e^{ik\xi}, \tag{25}$$

a 2π–periodic function. Note the (almost) perfect analogy with the inverse Fourier transform (2) as the summation takes the role of "discrete integration"; in fact, the integral symbol $\int$ is only a "stylized" and "smoothed" version of the summation symbol $\sum$. The interchange of transform and inverse comes from the fact that usually, the *Fourier coefficients* of a 2π–periodic function g are

$$\widehat{g}(k) = \frac{1}{2\pi}\int_0^{2\pi} g(t)\, e^{-ikt}\, dt, \qquad k\in\mathbb{Z}, \tag{26}$$

but after all Fourier transform and its inverse are only distinguished by a complex conjugation of the exponential term and this is obviously exchangable. Nevertheless, (25) is not yet the *discrete Fourier transform (DFT)*! The DFT is the vector obtained by sampling the trigonometric series uniformly on $[0, 2\pi]$:

$$\widehat{f}_n := \left[\widehat{f}\left(\frac{2k\pi}{n}\right) \,:\, k = 0,\ldots,n-1\right]. \tag{27}$$

However, there remains the question of how to choose the 'sampling rate n. This is simple if f is a finite signal, i.e., if it can be described after an appropriate shift as $f = [f(j) \,:\, j = 0,\ldots,n-1]$. Then the DFT is simply a transformation that converts vectors of length n into vectors of length n. And exactly this is – once more up to normalization – what is done in a most efficient way by the FFT, the *fast Fourier transform*. For the sake of maximal confusion, we also write $\widehat{f}\in\mathbb{R}^n$ for the DFT of a vector $f\in\mathbb{R}^n$.

But whatever the DFT is - it is **not** the sampled version of the Fourier transform, hence no discrete spectrum, of the time–continuous function f whose discrete samples we claim to consider. Here is an example. Suppose that the discrete f is obtained by sampling a time continuous signal f_* at equidistant points $t_k = t_0 + kh$, $k = 0,\ldots,n-1$ with some *sampling distance* or *reciprocal sampling rate* $h > 0$:

$$f(k) = f_*(t_k). \tag{28}$$

Then the DFT is the vector

$$\left[\sum_{j=0}^{n-1} f(t_j)\, e^{2ijk\pi/n} \,:\, k = 0,\ldots,n-1\right] \tag{29}$$

which has no obvious connection to the spectrum of f. To understand what happens here,

it is useful to consider, for some function φ, the *quasi interpolant*

$$f_\varphi(t) = \sum_{k=0}^{n-1} f(k)\,\varphi\left(t/h - k\right), \qquad (30)$$

which is now a function again that, ideally, represents or at least approximates f, hence can be considered a "substitute" based on the discrete sampling information only. For example, if φ is the so–called *hat function*, then f_φ is the piecewise linear function connecting the discrete values. Now, we can consider the Fourier transform of f_φ and find that for the equidistant frequencies $\xi_k := \frac{2k\pi}{nh}$ we get

$$\widehat{f_\varphi}\left(\xi_k\right) = h\,\widehat{\varphi}\left(\frac{2k\pi}{n}\right)\,\widehat{f}(k), \qquad k = 0, \ldots, n. \qquad (31)$$

Here we finally find samples of a "real" Fourier transform, however, we take that of f_φ and we have to re–weight the spectrum with samples of $\widehat{\varphi}$ from the interval $[0, 2\pi)$. It's remark time again:

1. The frequency for the sampling of the Fourier transform are taken from $\left[0, \frac{2\pi}{h}\right)$, so the higher the sampling rate $1/h$, the larger the *frequency range*. The *frequency resolution*, however, depends on the number of samples, n. The more points we have, the larger the number of different frequencies and the smaller the (relative) distance between them.

2. Negative values of ξ play no role in what we do here. We always tacitly assumed the signal to be real which means that its Fourier transform is symmetric.

3. The choice of φ clearly affects the spectrum. "Natural" candidates would be piecewise constant or linear functions or general cardinal spline quasi–interpolants (Schoenberg, 1973) – whatever this is. They correspond to a stronger a stronger damping of high frequency content as they provide smoother and smoother approximants. In some sense, the choice must be made according to an underlying model from which type of function the discrete data f is supposed to be sampled.

4. Another choice would be

$$\varphi(t) = t = \frac{\sin \pi t}{\pi t}.$$

The resulting function *interpolates* the data f, i.e., $f_\varphi\left(t_k\right) = f(k)$, and if f is sampled from a band–limited function (a function whose Fourier transform is 0 whenever the frequency satisfies $|\xi| \geq T$ for some T) and h is smaller than a so–called *Nyquist rate*, then we are even guaranteed that f_φ is *identical* with this function. This is the famous *Shannon sampling theorem*, cf. (Shannon, 1948), that rediscovered a result by Whittaker (Whittaker, 1915) and put it into the context of signal processing. In fact, this sounds even more perfect since normally all records of data, for example audio or EEG date, are indeed bandlimited due to their acquisition method where at one place or another a low–pass filter is involved.

5. This sounds like the perfect solution, in particular as $\widehat{\varphi}$ is identically 1 for the values in (31), so all of a sudden $\widehat{f}$ can be directly interpreted as samples of a Fourier transform. So why bother at all? Simply because Heisenberg objects: being

band limited, the underlying function cannot have finite support and so the finitely many samples always miss some part of the function, hence causing artifacts.

6. But it is even worse! Though the function is an *interpolant* and thus perfectly approximates *at* the sampling points, it is a very poor *approximant* when considered *away from* these points due to the rather slow decay of that function. That means that the value at some point is still significantly affected even by rather far–away samples, in particular the missing samples that have been left out due to the finiteness of the signal. So the theoretically perfect method can be numerically very questionable.

Nevertheless, we can quite *efficiently* compute samples of the spectrum of a function from samples of the function, provided that the *global* difference between the function f_* and f_φ is not too large. But the quality of this approximation, i.e., the size of this distance, will definitely be affected by the choice of φ which therefore may be worth some thinking. All this is far from new and well–known, cf. (Schüßler, 1992), but rarely mentioned.

Summary

What was the point of this section? There are clearly a lot of techniques and methods to work with Fourier and wavelet transform and to perform time–frequency analysis but their strict validity depends on quite a few assumption that are hard or even impossible to check or provide in reality. Consequently, the results of numerical computations should always be taken with a certain amount of care. And it may pay off to invest some though about models for the underlying functions from which the samples are taken. Otherwise the price to be payed is usually an overestimation of the high–frequency content of the signal.

Fast wavelet and inverse transforms

We now turn to the practical numerical computation of wavelet transforms. To that end, we assume that the function f_* is only known by samples as in (28), the normal situation in most practical applications. Usually the sampling points are prescribed by technological side conditions and cannot be varied according to our needs.

The naive way to compute the wavelet transform would be to evaluate the integral from (14) by means of a *quadrature formula*, cf. (Gautschi, 1997), of the form

$$W_\psi f(u,s) \sim \sum_{k=0}^{n-1} f\left(t_k\right) \frac{1}{\sqrt{s}} \overline{\psi\left(\frac{t_k-u}{s}\right)} w_k, \tag{32}$$

with appropriate *weights* w_k, usually from the most popular family of so–called *Newton–Cotes formulas*, including the famous rectangular and trapezoidal rules. If we want to keep the spirit of the FFT and compute n time samples u_j, $j = 0, \ldots, n-1$, per scale s, the computational effort of this computation is $O\left(n^2\right)$. The numerical quality of the quadrature depends on the sampling distance h (encoded in the t_k) and the way how the weights w_k are chosen, which is usually related to the (assumed) smoothness of the underlying f_*. "Better" quadrature techniques, like Gaussian quadrature rules, are not available here, as they require a particular

non–uniform choice of the sampling points. In addition, it is not even clear whether an "improved", higher order quadrature formula will really be of advantage as such formulas' full power only occurs in connection with very smooth signals. There is also the tempting idea of interpreting the wavelet as a weight function and encode it into suitably adapted values w_k, but since the admissibility condition requires at least one vanishing moment, such quadrature would be built on an indefinite inner product and hence act without any theoretical background or justification. That does not mean it would not work, it simply means that it cannot be guaranteed to work, at least not in the "standard" environment.

FFT – the basis of everything

We have already defined the DFT of a vector of length n in (27) as an operation that transform the vector f into another vector $\widehat{f}$ of the same length n. Since this operation is linear, it can in fact be written as a matrix–vector multiplication $\widehat{f} = V_n f$ where the matrix V_n is a well–understood object with a rich and useful structure. What interests us here, however, is the cost of computing $\widehat{f}$, that is, the number of elementary computational operations that have to be performed. Since for every entry of $\widehat{f}$ we have to take an inner product between a row of V_n and f, the cost of such a matrix–vector multiplication appears to be n times the n multiplications and $n-1$ additions that are needed for such an inner product, leading to a total of $2n^2 - n$ operations. To make our lives easier, we introduce the "O notation". Let $F(n)$ be any function measuring the cost of an operation, then we say that F is a $O\left(G(n)\right)$ if there exists a constant $C > 0$ such that

$$\lim_{n\to\infty} \frac{F(n)}{G(n)} = C.$$

In our example of matrix–vector multiplication above, the cost is $O\left(n^2\right)$ and the constant is a modest 2, and it seems as if there is no cheaper way to multiply a matrix and a vector and so we are stuck with a complexity of $O\left(n^2\right)$ for the DFT. There is some truth in the above statement as the cost of the multiplication of a *general* $n \times n$ matrix with an n vector is indeed $O\left(n^2\right)$, but it is not true for the DFT matrix. If its structure, which we praised so highly before, is exploited in a proper way, then the DFT and hence this multiplication can be computed with $O\left(n \log n\right)$ operations (and still a very modest constant C). This extremely simple method, (re)discovered by Cooley and Tukey (Cooley, 1990, 1987; Cooley & Tukey, 1965), is the basis of almost any fast algorithm from the multiplication of particularly structured matrices, so–called Toeplitz matrices, to the fast multiplication of large integers by means of the Schoenhage–Strassen method (Gathen & Gerhard, 1999). Nevertheless, in order to really emphasize and earn the first "F" in an **F**FT, lots of implementation details have to be taken into account, cf. (Loan, 1992), but fortunately there exist very good and performant libraries, be it open source ones like `FFTW` or nVidia's `CUDA` library that even makes use of the graphics card to perform the computations.

What makes the FFT such a universal accelerator of computations is the fact that *convolutions* appear quite frequently in scientific computations, even in our wavelet transform. In the continuous case, the convolution $f * g$ of

two functions f, g yields the new function

$$\begin{aligned}(f * g)(t) &= \int_{\mathbb{R}} f(s)\, g(t-s)\, ds \\ &= \int_{\mathbb{R}} f(t-s)\, g(s)\, ds.\end{aligned}$$

Again, it is easy to see that a naive computation of such a convolution for n discrete samples of f and g has a complexity of $O\left(n^2\right)$. If, on the other hand, we use the fact that the Fourier transform of a convolution is

$$(f * g)^{\wedge}(\xi) = \widehat{f}(\xi)\, \widehat{g}(\xi),$$

we can compute the convolution as well by means of a Fourier transform, pointwise multiplication of these transformed values and finally an inverse transform which, costs us $2O\left(n \log n\right)$ for the transforms and $O(n)$ for the multiplication, summing up to a total cost of $O\left(n \log n\right)$ operations. Very convincing, isn't it, and that is indeed the way things work in this as banal as powerful principle:

> *Whenever there is a convolution, use FFT and multiplication instead.*

The magic word here is "in principle" as again we thoughtlessly mixed the continuous and the discrete universe. The DFT of sampled data is still not a sampled Fourier transform, regardless of whether we use fast or slow means of computation and the truth is as follows: If f, g are two vectors of length n, then the componentwise product of their DFTs indeed makes sense, namely

$$\widehat{f}(k)\, \widehat{g}(k) = (f *_n g)^{\wedge}(k),$$

where

$$(f *_n g)(k) := \sum_{j \in \mathbb{Z}/n\mathbb{Z}} f_j\, g_{k-j}.$$

The slight but fundamental difference lies in the convolution which has to be understood as a *periodic* summation where any index $k - j$ that is outside the admissible region $\{0, \ldots, n-1\}$ is "wrapped" into an admissible one by adding a proper multiple of n. In other words: Whenever an FFT is computed, it assumes the input vectors f, g to be *periodic*. If the are not, for example when a sound signal is not sampled according to its frequency, there will be artifacts tainting the result of the DFT. There are plenty of techniques in signal processing, zero padding for example, but nothing can fully compensate the fact that, by its very nature, the DFT is tied to the periodic convolution. So handle with care.

The fast wavelet transform

A faster and more efficient way to compute the wavelet transform makes use of the FFT. The key is a discretized version of (17) in which we once more replace f_* by f_φ and obtain by (31) that, for $k = 0, \ldots, n-1$,

$$\begin{aligned}&\left(W_\psi f_\varphi(\cdot, s)\right)^{\wedge}(\xi_k) \\ &\quad = \sqrt{s} h\, \widehat{\varphi}\left(\frac{2k\pi}{n}\right) \widehat{f}(k)\, \widehat{\psi}(s\xi_k), \quad (33)\end{aligned}$$

to which we can apply a fast *inverse* Fourier transform to compute the vector

$$\left[W_\psi f_\varphi(t_k, s) \;:\; k = 0, \ldots, n-1\right]$$

of n samples of the wavelet transform at the same points as the original function was sampled. Since the complexity of the FFT and its inverse is a cheap $O\left(n \log n\right)$ and since all the operations in (33) are $O(n)$, including the sampling of $\widehat{\varphi}$ (which needs only be done once, independent of the scale) and of $\widehat{\psi}$, the total

computational effort of the fast wavelet transform (FWT) is still $O(n \log n)$ and thus significantly better than in the case of quadrature.

In (33) a sampling of $\widehat{\psi}$ with different sampling rates, depending on the scale is required – which is, by the way, essentially the only scale–dependency in this formula. This sampling is very easy if the Fourier transform of the wavelet is explicitly known, like in the case of our three examples before, and it even suggests that designing a wavelet is easier in the Fourier domain. If the wavelet is only given in time domain, the values $\widehat{\psi}(s\xi_k)$ can nevertheless be computed efficiently from a set of samples $\psi(st_k)$ by yet another application of the FFT. This, however, requires a little bit of attention since the locations ξ_k from (31) depend on the sampling frequency and the number of samples which have to be chosen properly.

It should be said that an implementation of the FWT in a system like `Matlab` or its higly recommendable free open source clone `octave` (Eaton, 2008) requires a little bit of care to correctly apply the `fft` and `ifft` commands and handle all the needed normalizations correctly. There exists a stable implementation by our Scientific Computing group in Gießen that has been successfully applied to various time–frequency tasks meanwhile. There exist other implementations of the continuous wavelet transform that are based on resampling the function data or on computing the wavelet transform integral (14) by means of a more or less sophisticated quadrature formula. My experience on such implementations is not very good, they are significantly slower and any resampling of the function data must almost necessarily lead to artifacts unless more information is present on the nature of the sampled function.

So far, one important question is left unanswered: how to choose the frequencies. The FWT computes each frequency separately, so the frequencies (scales) can be chosen deliberately. Taking into account the structure of the Heisenberg boxes for wavelets, the most reasonable choice for the frequencies or, more precisely, scales, is to select the m scales under consideration as

$$s_j = s_0\,\sigma^j, \quad j = 0, \ldots, m-1, \qquad \sigma > 1, \tag{34}$$

where σ is a parameter that should be smaller than the size $\widehat{\sigma}(\psi)$ of the Heisenberg boxes to avoid gaps in frequency. Such a type of interval scaling is once more perfectly compatible with music, where, in a tempered scale a semitone step corresponds to multiplication of the frequencies by the factor $2^{1/12}$. The closer σ is chosen to 1 the larger the effort to compute the wavelet transform for given frequency band becomes since $m = \log_\sigma \frac{s_m}{s_0}$. The larger σ is chosen, on the other hand, the worse the *absolute* frequency resolution becomes for high frequencies. Hence, an appropriate choice of the parameters s_0, σ and m is fundamental in applications and depends on the wavelet function, the frequency band to be considered as well as the accuracy one aims for. Anyway, the total computational complexity of the FWT for m scales from n samples is $O(m\,n \log n)$.

The fast inverse transform

For the inverse transform, we accelerate the computation of (15) by noting that the "inner integral" over u is yet another convolution and can thus be computed in terms of the FFT: with $g_*(t,u) = W_\psi f(t,u)$, known from $g(k) = \widehat{g}(t_k)$,

$k = 0, \ldots, n-1$, we get as before that

$$\begin{aligned} \widehat{h}(k,s) &:= \left(\int_{\mathbb{R}} g_\varphi(u)\, \psi\left(\frac{\cdot - u}{s} \right) du \right)^\wedge (\xi_k) \\ &= \sqrt{s}\, h\, \left(g\left(\cdot, u\right) \right)^\wedge (k)\, \widehat{\psi}\left(s\xi_k\right), \quad (35) \end{aligned}$$

for $k = 0, \ldots, n-1$. For any $j = 0, \ldots, m-1$, we can then compute the vectors

$$\left[h\left(k, s_j\right) \,:\, k = 0, \ldots, n-1 \right]$$

by means of an inverse FFT and from that approximate

$$f\left(t_k\right) = \int_{\mathbb{R}} h\left(k,s\right) \frac{ds}{s^2} \sim \sum_{j=0}^{s-1} h\left(k, s_j\right)\, w_j \quad (36)$$

with weights w_j of a quadrature formula for the integral $\int \frac{ds}{s^2}$ with respect to the knots s_j. Specifically, if we set $s_j = s_0 \sigma^j$ and use the rectangular rule, then

$$\begin{aligned} w_j &= \int_{s_j}^{s_{j+1}} s^{-2}\, ds \\ &= -\frac{1}{3} s_0^{-3} \left(\sigma^{-3j-3} - \sigma^{-3j} \right) \\ &= \frac{s_j^{-3}}{3} \left(1 - \sigma^{-3} \right), \end{aligned}$$

hence, in vectorized form,

$$\begin{aligned} &\left[f\left(t_k\right) \,:\, k \right] \\ &\sim \frac{1-\sigma^{-3}}{3} \sum_{j=0}^{m-1} s_j^{-3} \left[h\left(k, s_j\right) \,:\, k \right]. \quad (37) \end{aligned}$$

Again, this operation has a total computational cost of $O\left(m\, n \log n\right)$, just like the FWT and once more a working implementation has to carefully take into account some more details like how to correctly apply an FFT routine, but the principle of the IFWT should be clear from the above exposition.

To some surprise, after reconsidering (33) the question arises why and whether such a complicated method with all this quadrature stuff in it will appear. The simple observation is that (33) can be rewritten as

$$\widehat{f}(k) = \frac{\left(W_\psi f_\varphi\left(\cdot, s\right)\right)^\wedge \left(\xi_k\right)}{\sqrt{s} h \widehat{\varphi}\left(2k\pi/n\right)\, \widehat{\psi}\left(s\xi_k\right)}, \quad (38)$$

so that $\widehat{f}$ can be reconstructed *from a single scale* s provided that $\widehat{\psi}\left(s\xi_k\right) \neq 0$ for $k = 0, \ldots, n-1$ which will usually work for $k \neq 0$, at least for the Mexican hat (20) and the (modified) Morlet wavelet – the Fourier transform of the (non–admissible) expression from (21) even has no zero at all. Numerically, there are two immediate arguments in favor of the inversion rule (37):

1. For small values of k, i.e., for low frequencies, the denominator in (38) will always be small; after all, $\widehat{\psi}$ should be continuous as ψ should be at least integrable, and $\widehat{\psi}(0) = 0$, so that any errors made in a preceding wavelet transform will be amplified and the low frequency content $\widehat{f}(k)$ will not be very trustworthy. Practically, this means, that f could be modified by a more or less random constant term. This effect can be mildened by reconstructing $\widehat{f}$ from a very large value of s, i.e., from a rather low frequency content, but then the corresponding Heisenberg box tells us that we use information with very poor time localization, loosing the benefits of time–frequency analysis.

2. Since the first step, (35) uses only multiplications and since $\widehat{\psi}$ decays to $\pm\infty$, hence is bounded, it already saves us the worries about divisions by zero or almost zero. Moreover, (37) is an *averaging* process which we can hope to milden some random error made in the computation or manipulation of the wavelet transform.

Numerically, the decision is clear, but there is a more substantial theoretical catch why the inverse transform should never use a formula like (38), since we are inverting something that actually cannot even be inverted in general. To get some idea what goes on there and to study the phenomenon without the influence of numerical effects, we return to the case of continuous transform

Invertibility and loss of information

If the wavelet is admissible, the process of wavelet transform (14) followed by its inversion (15) is an identity – as it should be. In terms of (14) and (16), this means that $M_\psi W_\psi = I$, that is, M_ψ is a *left inverse* of W_ψ. The converse, $W_\psi M_\psi = I$, does **not** hold true, however, as not any function in two variables is a wavelet transform. Intuitively, this appears reasonable since we cannot expect one dimensional curves to generate a two dimensional set of transforms: while the function f depends on only one variable t, the wavelet transform $W_\psi f$ has *two* variables, u and s, and it appears at least strange (though this is not impossible as the concept of so–called space filling curves, also known as *Peano curves*, cf. (Gelbaum & Olmstedt, 1964), shows) that a univariate curve should be the same as a bivariate "surface". Intuition, however, can be misleading, so we need a more sensible argument.

The key to a *proof* of this observation is (17). If s and s' are two scales, then it follows that

$$\begin{aligned} & W_\psi f\,(u,s') \\ &= \sqrt{\frac{s'}{s}} \left(\frac{\widehat{\psi}\,(s'\cdot)}{\widehat{\psi}(s\cdot)} \left(W_\psi f(\cdot,s)\right)^\wedge(\cdot) \right)^\vee (u). \end{aligned}$$

In other words: if we know *one* scale of the wavelet transform, we know *all of them* (at least if the Fourier transform of the wavelet does not have "nasty zeros"). On the other hand, any bivariate function $g(u,s)$ that does not satisfy the *compatibility condition*

$$\frac{\left(g(\cdot,s)\right)^\wedge(\xi)}{\left(g\,(\cdot,s')\right)^\wedge(\xi)} = \sqrt{\frac{s}{s'}}\,\frac{\widehat{\psi}\,(s\xi)}{\widehat{\psi}\,(s'\xi)} \qquad (39)$$

cannot be a wavelet transform, even if the inverse wavelet transform applied to this function is still well–defined and thus can be computed, at least numerically.

So what happens now, if we compute inverse transforms with our beautiful numerical algorithm? Suppose that $g(u,s)$ is a given function of two variables, maybe obtained from modifying a wavelet transform with some sort of time localized band pass filter. If we re–transform our inverse wavelet transform, we obtain a function $\widetilde{g} = W_\psi M_\psi g$ which now is a wavelet transform and hence satisfies the compatibility condition (39). To understand the relationship between g and $\widetilde{g}$ we apply the inverse transform to the difference, yielding

$$\begin{aligned} M_\psi\,(g-\widetilde{g}) &= M_\psi g - M_\psi W_\psi M_\psi g \\ &= M_\psi g - M_\psi g = 0, \end{aligned}$$

since $M_\psi W_\psi = I$. As simple as this computation appears and in fact is, it tells us what goes on in the inverse transform for which g and $\widetilde{g}$ are indistinguishable. Now, for any g there always exists such a *compatible* $\widetilde{g}$ with $g = \widetilde{g}$ if and only if g is compatible. All functions g that lead to the same compatible $\widetilde{g}$ are undistinguishable for the inverse transform, they form what is called an *equivalence class* and $\widetilde{g}$ is the *compatible representer* of this equivalence class. Clearly, each two different compatible functions belong to differ-

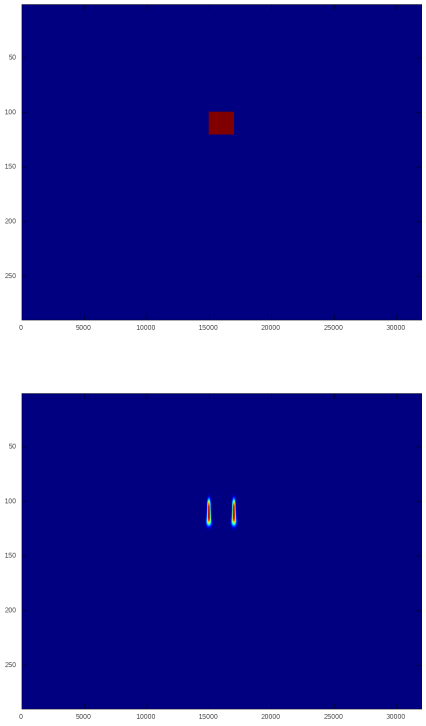

Figure 9: *A test signal* (above) *and its* $W_\psi W_\psi^{-1}$ *transform* (below). *Obviously not an identity.*

ent equivalence or, as one might say it, define a class of their own. And now it is clear what happens: the inverse wavelet transform always computes the inverse transform of the unique compatible representer in the equivalence class.

Let us consider this effect by means of an example. To that end, we define a completely localized signal by means of its wavelet transform as in Figure 9 and then transform this wavelet transform back and forward again. It is not hard to see that this is not really an identity. While the support remains similar, the "inner" information vanishes. To say it in the terminology from above, the left hand side of Figure 9 shows *one* element from the equivalence class

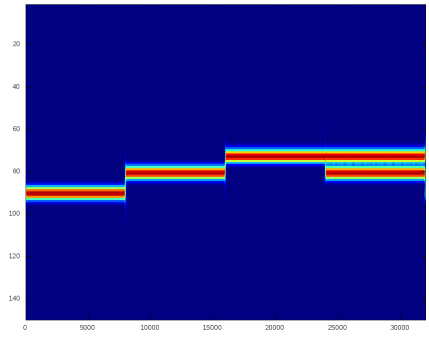

Figure 10: *The truncated melody*

while the right hand side shows *the* representer of this class defined by $W_\psi W_\psi^{-1}$.

The second example is using the "melody" from Fig 1, where we remove the lowest tone from the "chord" at the end. As the scalogram shows, the result is almost perfect, however, a plot of the signal and of the error would show that the modified signal is scaled differently. This is no surprise! The wavelet transform is an *isometry*, i.e., preserves energy, and any content we remove, be it on the function or on the transform side, reduces the energy on the other side as well. Hence, the resulting signal must have lower energy content which is *distributed equally* over the whole signal by the inverse wavelet transform. And even this is understandable from a brief but slightly careful look at the inversion formula (15) which contains an *averaging process* over all scales.

Finiteness and the loss of information

In (22) we introduced the concept of vanishing moments of a wavelet and sold it as something desirable, which it is, at least in principle. Actually, the regularity estimation in (23) works only if the number of vanishing moments of ψ ex-

ceeds α. Hence, to detect corners (i.e. singularities in the first derivative), the wavelet has to have at least two vanishing moments – another good reason for the nature of the mexican hat wavelet. On the other hand, a wavelet with a certain number of vanishing moments destroys a certain polynomial content of the signal. This is irrelevant in the sense of L_2–functions since the only polynomial in L_2 is the zero function, while for *finite* signals the effect of loss of constants, or more precisely *loss of kernel* can be quite dramatic in reality. Consider a noisy parabola, i.e. a quadratic function that is modulated by some random noise, see

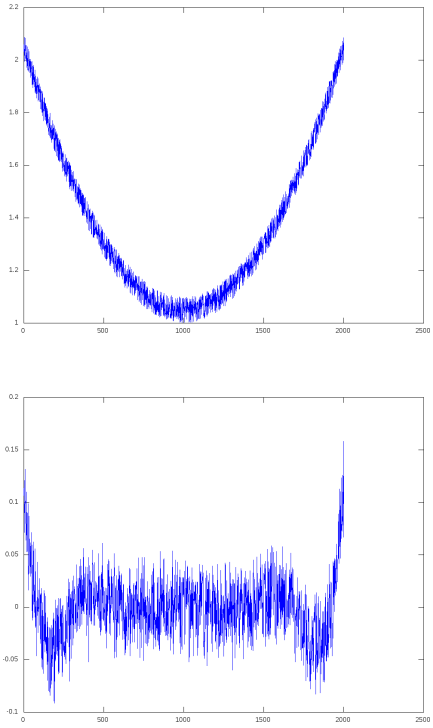

Figure 11: *A toy signal* (above) *and what an identity makes of it* (below). *The noisy parabola is simply transformed and then put into the inverse transform. The result is not really perfectly similar to the original signal.*

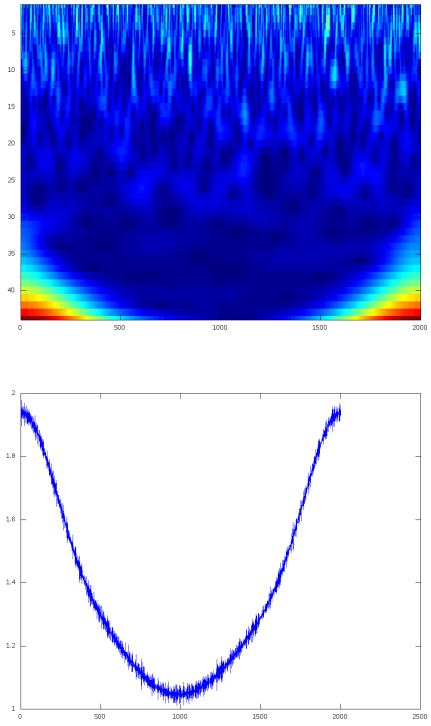

Figure 12: *The wavelet transform of* ***both*** *signals from Figure 11* (above). *Except the "artifact" part outside the U–shaped interior region, it contains no low frequency information which is due to the fact that the parabola is "killed" by the vanishing moments of the underlying wavelet, in this case he morlet wavelet. This image also shows how noise appears in wavelet transforms: as quite random peaks in the high frequency part. The "reconstruction signal"* $f - W_\psi^{-1} W_\psi f$ (below) *consists of the "lost parabola" from Figure 11 plus some high frequency noise that was beyond the frequency band of the original signal.*

Figure 11. The explanation can be found in the wavelet transform depicted in Figure 12 where it is visible that the parabola content is essentially removed by the vanishing moments of the wavelet. Nevertheless, such effects can quite easily be compensated when doing the time

local bandpass filters in the following section. Starting with a signal f, one first computes the information loss

$$\Delta_\psi f := \left(I - W_\psi^{-1} W_\psi\right) f, \qquad (40)$$

then performs manipulations on the wavelet transform $W_\psi f$, leading to function g, say, and then uses a back transformation of the form $\Delta_\psi f + W_\psi^{-1} g$.

But again keep in mind that according to theory Δ_ψ should be zero, the occurence of such errors is a pure *finiteness artifact* which can be as nasty as it is unavoidable in reality or whenever an infinite theory (on the real line $\mathbb{R}$) is applied to finite data.

Time local bandpass filters

Probably one of the most appealing applications of time frequency analysis and a numerical inverse wavelet transform is the implementation of time localized bandpass filters. Again, the musical analogy helps to understand the basic idea of this concept. Suppose that in our piece of music a wrong key has been played and this needs to be corrected. In other words, for some relatively short period of time, the frequency content needs to be modified. This can be done by "cutting out" some frequencies and "filling in" some others. Of course, we cannot expect the resulting scalogram to satisfy the compatibility condition (39) and hence, the result is not a valid wavelet transform, so that the resulting signal will not be only the inverse wavelet transform of the *compatible representer* of the equivalence class. How bad is that? Not so bad normally, as the following reasoning shows.

Suppose we have done a local modification, i.e., we replaced $g = W_\psi f$ by $g + h$ where the correction function h is zero everywhere except a small square of side length δ around u^* and s^* which leads to (41).

Since the "-let" of a good wavelet verbalizes the fact that the function $\psi(x)$ decays (rapidly) for $x \to \pm\infty$, we can assume that also ψ only "lives" on a bounded interval in the sense that outside that intervall, say $[-T, T]$, ψ is at least neglectable. Hence, the integral above is only relevant for those values of t such that $t - u \in s[-T, T]$ or

$$t \in [u^* - Ts - \delta, u^* + Ts + \delta]$$

an interval around u^* of essential width $2Ts$. Hence, if s is a small scale, hence corresponds to a high frequency, then the modification essentially remains located around u^* while for large values of s, i.e., low frequencies, the modification leaks out as might be expected. However, the s^{-2}–weighting of the integral in (41) "dampens" the effect and the wider the spread is, the larger the damping is – one more good reason to use this averaging formula for inversion. So essentially the modification remains at least local in time. A similar argument applied to the Fourier transform of the inverse transform in the same way as in the proof of the inverse formula, cf. (Daubechies, 1992; Mallat, 1999), also can be used to reason for localization in frequency. A more precise and mathematically relevant formulation of this phenomenon clearly has to take into account and will depend on the rate of decay of the wavelet ψ and other parameters.

What did we find here? There was no assumption made on the correction term h, in particular we did not require compatibility, and nevertheless the inverse wavelet transform modified f mainly locally around the

$$M_\psi\,(g+h)\,(t) = f(t) + \frac{1}{C_\psi}\int_{u^*-\delta}^{u^*+\delta}\int_{s^*-\delta}^{s^*+\delta} h(u,s)\frac{1}{\sqrt{s}}\psi\left(\frac{t-u}{s}\right)\,du\,\frac{ds}{s^2}. \tag{41}$$

time–frequency region where the wavelet transform was modified. This makes "scalogram surgery" quite a useful tool – at least heuristically.

It should, however, be emphasized once more that this is entirely a "locality" argument. Just look at Figure 9 to realize that both transforms show a signal that is local in time and frequency, but still quite a bit different.

Summary

In general, time–frequency analysis, be it Gabor or wavelet style, is a useful tool for biosignal processing that definitely extends the possibilities of the Fourier transform. The price to be payed is a significantly higher complexity – each single scale costs about as much as a Fourier transform – and some mathematical intricacies that should be understood, at least intuitively, to avoid certain pitfalls. Those pitfalls and their mathematical explanations were the goal of this paper. It is not necessary any more to advertise the wavelet transform or the Gabor transform as they are powerful tools, but it seems appropriate to show the limitations of these tools and to clarify how the results obtained by these tools have to be interpreted properly. The nice side effect is that music, a very popular sort of signals, can be used for explanations that are more intuitive than the application of the methods to biosignals like, for example, EEG data.

It would be tempting to make some remarks about existing wavelet toolboxes, but I want to avoid it. First, such statements can only be momentary snapshots and may change with the next release of the software. Second, an more important, most commercial systems do not offer insight into the precise implementation of the toolboxes so that the quality and correctness of the results simply can only be believed or not and everything else would mostly be speculation. This even starts with such elementary questions as whether the Morlet wavelet is used with our without the correction term, i.e., whether it is a wavelet at all, and extends to points like handling of resampling or padding issues. There are choices to be made and these choices affect the result.

The same holds for many of the papers where wavelets are applied to some problem, for example from physiology as, for example, in (Samar, Bopardikar, Raghuveer, & Swartz, 1999). Normally, such papers only give a definition of the wavelet transform like in (14) and a set of colored pictures from which conclusions are drawn, and not even (Klein, Sauer, Jedynak, & Skrandies, 2006) is an exception there. It is seldom even mentioned how and by which software these transforms were computed and those pictures were generated, so that it is mostly impossible to make any statements about these results and it would be unfair to judge the results based on such speculations.

References

Benade, A. H. (1960). *Horns, strings, and harmony*. Anchor Books. (Dover reprint 1992)

Cavaretta, A. S., Dahmen, W., & Micchelli, C. A. (1991). *Stationary subdivision* (Vol. 93 (453)). Amer. Math. Soc.

Cooley, J. W. (1987). The re–discovery of the Fast Fourier Transform. *Mikrochimica Acta*, *3*, 33–45.

Cooley, J. W. (1990). How the FFT gained acceptance. In S. G. Nash (Ed.), *A history of scientific computing* (pp. 133–140). ACM–Press and Addison–Wesley.

Cooley, J. W., & Tukey, J. W. (1965). An algorithm for machine calculation of complex Fourier series. *Math. Comp.*, *19*, 297–301.

Daubechies, I. (1992). *Ten lectures on wavelets* (Vol. 61). SIAM.

Eaton, J. W. (2008). *Gnu Octave manual*. Network Theory Ltd.

Gabor, D. (1946). Theory of communication. *J. IEEE*, *93*, 429–457.

Gathen, J. v. z., & Gerhard, J. (1999). *Modern computer algebra*. Cambridge University Press.

Gautschi, W. (1997). *Numerical analysis. an introduction*. Birkhäuser.

Gelbaum, B. R., & Olmstedt, J. M. H. (1964). *Counterexamples in analysis*. Holden–Day. (Dover reprint 2003)

Hamming, R. W. (1989). *Digital filters*. Prentice–Hall. (Republished by Dover Publications, 1998)

Helmholtz, H. (1885). *On the sensations of tone*. Longmans & Co. (Translated by A. J. Ellis, Dover reprint 1954)

Holschneider, M. (1995). *Wavelets: an analysis tool*. Clarendon Press, Oxford.

Hubbard, B. B. (1996). *The world according to wavelets*. A.K. Peters.

Katznelson, Y. (1976). *An introduction to harmonic analysis* (2. ed.). Dover Publications.

Klein, A., Sauer, T., Jedynak, A., & Skrandies, W. (2006). Conventional and wavelet coherence applied to human electrophysiological data. *IEEE Transactions on Biosignal Processing*, *53*, 266–272.

Loan, C. van. (1992). *Computational frameworks for the Fast Fourier Transform*. SIAM.

Mallat, S. (1999). *A wavelet tour of signal processing* (2. ed.). Academic Press.

Rubinstein, R., Zibulevsky, M., & Elad, M. (2010). Double sparsity: Learning sparse dictionaries for sparse signal approximation. *IEEE Trans. Sig. Proc.*, *58*, 1553–1564.

Samar, V. J., Bopardikar, A., Raghuveer, M. K., & Swartz, K. (1999). Wavelet analysis of neuroelectric waveforms: A conceptual tutorial. *Brain and Language*, *66*, 7–60.

Schoenberg, I. J. (1973). *Cardinal spline interpolation* (Vol. 12). SIAM.

Schüßler, H. W. (1992). *Digitale Signalverarbeitung* (3. ed.). Springer.

Shannon, C. E. (1948). A mathematical theory of communication. *Bell System Tech. J.*, *27*, 379–423.

Strang, G., & Nguyen, T. (1996). *Wavelets and filter banks*. Wellesley–Cambridge Press.

Vetterli, M., & Kovačević, J. (1995). *Wavelets and subband coding*. Prentice Hall.

Whittaker, E. T. (1915). On the functions which

are represented by the expansions of the interpolation–theory. *Edinb. R. S. Proc.*, *35*, 181–194.

Abstracts of the 19thGerman EEG/EP Mapping Meeting, Giessen, October 15 - 17, 2010

The monofractal signature of EEG microstates reveals rapid dynamics of resting-state networks. J. Britz (1,2), D. van de Ville (3,4), C. M. Michel (1,2,5), *(1) Department of Fundamental Neuroscience, University of Geneva, Geneva, Switzerland (2) EEG Brain Mapping Core, Biomedical Imaging Center (CIBM), Geneva, Switzerland, (3) Department of Radiology and Medical Informatics, University of Geneva, Geneva, Switzerland (4) Institute of Bioengineering, Ecole Polytechnique Fédérale de Lausanne, Switzerland, (5) Department of Neurology, University of Geneva Medical School, Switzerland*

Resting-state functional connectivity studies with fMRI show that the brain is intrinsically organized into large-scale functional networks (RSNs) for which the hemodynamic signature is stable for about 10 s. Spatial analyses EEG topography at rest also show discrete epochs of stable global brain states (so-called microstates), but they remain quasi-stationary for only about 100 ms. In order to test the relationship between the rapidly fluctuating EEG-defined microstates and the slowly oscillating fMRI-defined resting states, we recorded the EEG from 64 channels in the scanner while subjects were at rest with their eyes closed. Conventional EEG-microstate analysis determined the typical four EEG topographies that dominated across all subjects. The convolution of the time course of these maps with the hemodynamic response function allowed to fit a linear model to the fMRI BOLD responses and revealed four distinct distributed networks. These RSNs have previously been attribute to auditory processing, visual processing, attention reorientation, and subjective interoceptive autonomic processing. Surprisingly, the convolution with the HRF did not remove any information-carrying signal from the microstate sequence. The microstate sequences showed the same relative temporal behavior before and after convolution with the HRF, i.e. at temporal scales that are two orders of magnitude apart, which suggests that their time course is scale-free. We deployed powerful wavelet-based fractal analysis that allowed determining scale-free behavior. We found strong evidence that microstate sequences are scale-free over 6 dyadic scales covering the 256ms 16s range. The degree of long-range dependency was maintained when shuffling the local microstate labels but became indistinguishable from white noise when equalizing microstate durations, which indicates that temporal dynamics are their key characteristic. Taken together, the four typical EEG microstates seem to represent the neurophysiological correlate of four RSNs and their monofractal characteristics show that they are fluctuating much more rapidly than fMRI alone suggests.

Topographic EEG signatures of fMRI resting state networks. K. Jann (1), M. Kottlow (1), T. Dierks (1), C. Boesch (2), T. Koenig (1), *(1) Department of Psychiatric Neurophysiology, University Hospital of Psychiatry, University of Bern, Bern, Switzerland, (2) Department of Clinical Research (AMSM), Inselspital*

and University of Bern, Bern, Switzerland
The temporal fluctuations of fMRI Resting State Networks (RSNs) have been demonstrated to be correlated to the spectral fluctuations in several EEG frequency bands. However, there is no study accounting for the topographic distribution of EEG oscillations. In this study we explored the topography of spectral fluctuations associated to ten common RSNs. Therefore we recorded simultaneous EEG-fMRI in 20 healthy young subjects. We present topographic maps (covariance and t-maps) for all RSNs displaying their specific spatial EEG spectra in the standard EEG frequency bands.

It's a face - Continuous face integration in combined EEG/fMRI. M. Kottlow, K. Jann, T. Dierks, T. Koenig, *Department of Psychiatric Neurophysiology, University Hospital of Psychiatry, University of Bern, Switzerland*
Humans tend to automatically bind facial components into a face gestalt, making face perception a natural example for the analysis of feature binding. It is assumed that face processing involves specific brain regions including the fusiform face area and that binding depends on the synchronization of EEG frequencies in the gamma range. Here we integrated these findings by correlating gamma synchronization with BOLD responses. We presented unpredictably moving elements of a schematic face, which during some periods continuously produced a complete facial percept, representing analytic and holistic face processing. During holistic processing, the complete upright face is integrated to a face gestalt, while during analytic processing the spatial order of a face is disturbed and the face has to be composed part-by-part. As hypothesized, we found increased gamma phase synchronization during holistic face processing. BOLD responses with emphasis on the right fusiform face area were similar during both conditions. Finally, the standard boxcar predictors for each condition were modulated with gamma synchronization revealing a holistic face network comprising face perception regions, and an analytic network including parietal and prefrontal areas but not the fusiform gyrus. The precuneus was present in both networks. Thus, although the FFA is involved in both analytic and holistic binding, the modulation with gamma oscillations suggests different roles depending on the condition. The precuneus in contrasts seems to be involved in binding processes in general. Hence, the combination of BOLD responses and gamma phase synchronization may help to decode the functions of brain areas within networks.

EEG-BOLD coupling and brain development. R. Lüchinger, *Department of Child and Adolescent Psychiatry University Zurich, Zurich, Switzerland*
The development of the human brain is characterized by profound structural and functional reorganization. Using EEG, brain maturation has been studied since decades. The resting EEG is typically characterized by oscillations of different frequencies and amplitudes, reflecting ongoing neuronal activity. During development the EEG frequency composition changes dramatically. In recent years coregistering EEG and fMRI has allowed for linking electrophysiological scalp-recorded activity more directly to underlying cortical and subcortical regions without assumptions regarding source distribution. While the exact physiological relationship between EEG and the fMRI

blood oxygen-level dependency (BOLD) signal is still under debate, these studies have shown that EEG amplitude is functionally coupled to distinct brain regions and networks. However, in the emerging field of simultaneous EEG-fMRI research, little is known about the development of EEG-BOLD coupling. Both EEG and fMRI are sensitive for maturational changes, but capture partly different neuronal signals, witch presumably indicate different aspects of brain development. We aim to characterize changing and sustaining features of EEG-BOLD coupling pattern in the developmental course.

EEG-fMRI investigation of gamma oscillations. C. Mulert, *Psychiatry Neuroimaging Branch (PNB), Department of Psychiatry / NeuroImage Nord (NIN) UKE Hamburg, Germany*

Neuronal oscillations in the gamma-band frequency range have attracted much interest during the last few years because they were suggested to play an important role in the linking of neurons into cell assemblies that code information in the brain. Experimental data obtained both in animals and in humans suggest that gamma-band oscillations are involved in perception and cognition. In addition, disturbed gamma oscillations might be related fundamental pathophysiological aspects of schizophrenia. This talk will focus on recent results using single trial coupling of the gamma-band response (GBR) and the Blood Oxygenation Level Dependent (BOLD) signal. Furthermore, data of disturbed GBR in patients with schizophrenia and unaffected siblings will be presented and discussed with regards to implications for the understanding of disturbed brain mechanisms in schizophrenia.

Exploring the functional role of intrinsic brain states by simultaneous EEG-fMRI. P. Ritter, *Abteilung für Neurologie, Charite, University Medicine Berlin, Germany*

Functional magnetic resonance imaging (fMRI) measures neuronal activity not directly but relies on associated blood oxygenation changes. Electroencephalography (EEG) in contrast assesses neuroelectric population activity. We use simultaneous EEG-fMRI in order to investigate the relation between ongoing EEG signatures such as the alpha rhythm and the fMRI signal. We show that ongoing EEG dynamics influence not only the intrinsic ('resting state') fMRI signal but also determine fMRI response properties to visual stimulation.

Simultaneous EEG-fMRI. D. Brandeis, *Department of Child and Adolescent Psychiatry, University of Zürich, Zürich, Switzerland, Center for Integrative Human Physiology, University of Zürich, Zürich, Switzerland, Department of Child and Adolescent Psychiatry and Psychotherapy, Central Institute of Mental Health, Mannheim, Germany*

The symposium contributions cover the wide range of current applications of simultaneous EEG - fMRI recordings. Recent work has increasingly moved away from just concentrating on the advantage of combining high spatial and temporal resolution. One trend is to focus on the spontaneous dynamics of the background or resting state, and their interactions with stimulation and factors affecting the nature of the coupling between EEG and BOLD signals. Another recent trend is to focus on how the dynamics of spontaneous or event-related trial - to trial fluctuations of oscillatory activity interact with the dynamics of perception and cognition, and understand clinical and

genetic variations. The dynamics of the resting state are typically characterized by correlated BOLD fluctuations or by EEG power fluctuations, but both Britz and Jann show that specific EEG microstates or topographies more closely correspond to the BOLD fluctuations. Resting state studies the first part address how variations of the "backgroundresting state defined by the EEG affect the BOLD response to visual stimulation is addressed by Ritter et al, and how development affects the coupling between resting state EEG and BOLD is presented by Lüchinger.

The dynamics of gamma oscillation and their BOLD correlates are addressed in two contributions. Mulert focuses on event-related gamma oscillations in schizophrenia and discusses clinical alterations and familiality, while Kottlow demonstrates that gamma synchronization identifies those elements of the BOLD network involved binding coherent percepts during holistic face perception. In conclusion, these contributions illustrate how EEG-fMRI has progressed from focusing on mutual validation and on understanding epileptform activity to clarify basic physiological, cognitive and clinical aspects of brain function.

Spontaneous brain activity and EEG microstates. A novel EEG/fMRI analysis approach to explore resting-state networks. F. Musso, J. Brinkmeyer, *LVR-Klinikum Düsseldorf, Kliniken der Heinrich-Heine Universität Düsseldorf, Düsseldorf, Germany*

The brain is active even in the absence of explicit input or output as demonstrated from electrophysiological as well as imaging studies. Using a combined approach we measured spontaneous fluctuations in the blood oxygen level dependent (BOLD) signal along with electroencephalography (EEG) in eleven healthy subjects during relaxed wakefulness (eyes closed). In contrast to other studies which used the EEG frequency information to guide the functional MRI (fMRI) analysis, we opted for transient EEG events, which identify and quantify brain electric microstates as time epochs with quasi-stable field topography. We then used this microstate information as regressors for the BOLD fluctuations. Single trial EEGs were segmented with a specific module of the LORETA (low resolution electromagnetic tomography) software package in which microstates are represented as normalized vectors constituted by scalp electric potentials, i.e., the related 3-dimensional distribution of cortical current density in the brain. Using the occurrence and the duration of each microstate, we modeled the hemodynamic response function (HRF) which revealed BOLD activation in all subjects. The BOLD activation patterns resembled well known resting-state networks (RSNs) such as the default mode network. Furthermore we cross validated the data performing a BOLD independent component analysis (ICA) and computing the correlation between each ICs and the EEG microstates across all subjects. This study shows for the first time that the information contained within EEG microstates on a millisecond timescale is able to elicit BOLD activation patterns consistent with well known RSNs, opening new avenues for multimodal imaging data processing.

EEG source analysis improves interpretation of fMRI results obtained during EEG-fMRI of epileptiform discharges. M. Siniatchkin (1), A. Galka (1), R. Boor (2), F. Moeller (1), J. Moehring (1), L. Elshof (1), K. Groen-

ing (1), S. Wolff (1), L. Hamid (1), U. Stephani (1,2), *(1) Klinik für Neuropädiatrie, Universität Kiel, (2) Norddeutsches Epilepsiezentrum für Kinder und Jugendliche, Raisdorf*

Simultane Aufnahmen von EEG und funktionellem MRT ist eine neue Methode, die zur Charakterisierung hämodynamischer Veränderungen im Gehirn, die im Zusammenhang mit epileptiformen Entladungen auftreten, benutzt werden kann. Diese Methode wurde erfolgreich angewandt sowohl zur Beschreibung der epileptogenen Zone und der Propagationswege der epileptischen Aktivität bei fokalen Epilepsien als auch zur Darstellung epileptischer neuronaler Netzwerke bei verschiedenen Epilepsie-Syndromen. Aufgrund der niedrigen zeitlichen Auflösung von fMRT und dem Problem der statistischen Schwelle für multiple Vergleiche bei Multivoxelanalysen, zeigt fMRT häufig eine ausgedehnte und komplexe Aktivierung, die in vielen Fällen nur schwer interpretierbar ist. Diese Studie illustriert an einer Reihe von Beispielen, wie eine EEG-Quellenanalyse (LAURA-Verfahren, implementiert in Cartool, Genf) hilft, fMRT-Ergebnisse zu interpretieren. 260 Kinder im Alter von 3 Monaten bis 18 Jahren mit fokalen und generalisierten Epilepsien wurden mittels EEG-fMRT untersucht. Bei fokalen Epilepsien konnte die EEG-Quellenanalyse bei 60% der Patienten die Gehirnregionen der initialen epileptischen Aktivität (Generatoren) von den Gehirnregionen der Propagation trennen. Bei Patienten mit Continuous Spikes and Waves during Slow Sleep (CSWS) zeigte die Quellenanalyse, dass das für dieses epileptische Syndrom typische Netzwerk (eine bilaterale Aktivierung in einer perisylvischen Gehirnregion und im anterioren Cingulum) die propagierende epileptische Aktivität darstellt. Bei Absence-Epilepsie scheint die EEG-Quelle im medialen präfrontalen Kortex das Netzwerk zu dominieren, andere Quellen (frontaler und parietaler Kortex sowie Thalamus) sind eng mit der primären Quelle verbunden (kohärente Quellen). Ohne die Quellenanalyse lässt sich die Hierarchie und Aktivierungsreihenfolge von unterschiedlichen Gehirnregionen bei Absencen kaum erklären. Damit scheint die Kombination von EEG-Quellenanalyse und fMRT komplimentäre Informationen zu liefern, die komplexe neuronale Netzwerke bei Epilepsien präzise beschreiben können.

Ghost Sources due to Spherical Head Models: Do they exist? M. Wagner, M. Fuchs, J. Kastner, R. Tech, *Compumedics Neuroscan, Hamburg, Germany*

It is generally acknowledged, that in EEG source localization, the use of a spherical head model (as opposed to a realistically shaped head model) introduces errors in the computed source locations. But can the choice of head model also influence the more general characteristics of a dipole solution, such as the number of assumed sources? Single- and multi-dipole data sets for sources of random locations and orientations were created using a three-layer realistic boundary element method (BEM) head model. Noise was added. These data were then subjected to single- and multi-dipole analyses, assuming a realistic head model in one case and a spherical head model in the other case. Different strategies for determining the number of active sources were employed and compared in both cases. Strategies explored involved the ability of a dipole configuration to explain the signal part of the data, as well as the shapes of the

dipoles' confidence ellipsoids. The number of dipoles required to explain a given data point tended to be larger in the spherical head model case than in the realistic head model case or the simulated ground truth. Such additional sources do not account for features in the data but for inadequacies of the head model used.

Cortical generators following noxiuos laser stimulation as identified by source analysis from subdural grid recordings in humans. U. Baumgärtner, S. Ohara, R.-D. Treede, F. Lenz, *Lehrstuhl für Neurophysiologie, Medizinische Fakultät Mannheim der Universität Heidelberg, Mannheim, Deutschland; Department of Neurosurgery, Johns Hopkins University, Baltimore, MD, USA*

The role of the primary somatosensory (S1) cortex in nociceptive processing has been under debate for a couple of years (Apkarian et al. 2005, Eur J Pain 9: 463-84). Dipole source analyses of laser evoked potentials (LEP) from surface EEG or MEG recordings as well as single channel analysis of LEP obtained from subdural recordings in epilepsy patients support the view that S1 contributes in a relevant manner to the perception of pain. In combining LEP recordings from subdural grids with dipole source analysis we now aimed to localize the early generators more precisely. Noxious infrared laser stimuli were applied to the hand dorsum of two patients that underwent neurophysiological evaluation prior to epilepsy surgery. Subjects were awake and had to count the stimuli. LEP recordings were obtained from an 8 x 8 electrode grid (64 channels) which was implanted in the subdural space over the frontal lobe and covered the central sulcus as well as the sylvian fissure. After averaging the peri-stimulus segments (500ms pre, up to 1000 ms post stimulus, digitized at 1 kHz) and matching of the CT and MRI coordinate systems of the patients, dipole source analysis was performed (BESA®). The global field power yielded two major peaks (at 140 ms and at approx. 230 ms), during which we performed the initial fit procedure with regional sources. In both subjects, similar sources with a radial orientation and peak activity at approximately 140 ms were identified within S1 cortex in parallel with a source in the suprasylvian region. In one of the subjects, the early radial S1 source was followed by activity of a tangential source 60-70 ms later at almost the same position. The radial LEP sources were found to be at or slightly posterior to the individual central sulcus and the localization of the N20 source as obtained from analysis of median nerve SEP (as neurophysiologic marker for area 3b). Hence, we conclude that the LEP generator in this cortical region is localized most likely in Brodmann area 1, where nociceptive neurons have been identified in monkey (cf. Kenshalo and Isensee 1983, J Neurophysiol 50: 1479-96).

This study was supported by NIH (NS 38493 to FAL) and DFG (Tr236/13-4)

Cerebral processing of itch: EEG and MEG studies. H. Mochizuki, *Lehrstuhl für Neurophysiologie, Medizinische Fakultät Mannheim der Universität Heidelberg, Mannheim, Deutschland*

Itch is an unpleasant sensation with the desire to scratch. Previous studies using PET and fMRI identified brain regions activated by itch stimuli, such as the somatosensory cortex, cingulate cortex, insula, parietal cortex, frontal cortex, basal ganglia and cerebellum. However, temporal information of itch stimulus-

related neural activity in these regions is still unclear. Recently, the methodology to induce itch sensation by applying electrical stimulus to the skin with a certain condition (pulse duration > 2 ms, frequency > 50 Hz) through electrodes was developed (electrical induced itch). In a preliminary study, we confirmed that it is possible to measure brain responses associated with the electrical induced itch using EEG and also found that the electrical induced itch is associated with C-fibers. In the present study, we compared brain responses between itch and pain by collecting MEG data from 10 healthy volunteers. Itch sensation was evoked by stimulating the C-fibers using the electrode discussed earlier while C-fiber pain was evoked by laser. The dipoles associated with itch stimulus- and pain stimulus-related magnetic responses were mainly located in the contralateral and ipsilateral secondary somatosensory cortex / insula (SII/insula) and parietal cortex. The peak latency in contralateral SII/insula was significantly shorter than that in ipislateral one in itch and pain stimulus conditions. The location of dipole in SII/insula was not significantly different between itch and pain. The peak latency in the parietal cortex was significantly longer than that in the contralateral SII/insula only in pain stimulus condition. Interestingly, in the parietal cortex, the location of the dipole related to itch stimulus was significantly more medial than that related to pain stimulus. This finding suggests that there may be some difference in processing in the parietal cortex between itch and pain.

Delay-dependent changes in oscillatory delta, theta and alpha activity during recognition. B. Mathes (1,2), J. Bagdasaryan (1), J. Schmiedt (1), C. Pantelis (3), C. Basar-Eroglu (1,2), *(1) University of Bremen, Institute of Psychology and Cognition Research, Bremen, Germany, (2) Centre for Cognitive Science, Cognium, Bremen, Germany, (3) Melbourne Neuropsychiatry Centre, Department of Psychiatry, The University of Melbourne and Melbourne Health, Melbourne, Australia*
Changes in the oscillatory EEG activity during recognition were assessed using a delay-dependent working memory task. Twelve subjects classifying stimuli as matching or non-matching during the recognition phase with at least 90% correct were measured. Oscillatory activity was investigated in the delta, theta and alpha range. A late positive delta component occurred later for recognition of non-matching than matching trials, which might reflect prolonged searching. For the theta activity a long-range integrated network of occipital, parietal and frontal sites was identified. This network was modulated by stimulus type (matching versus non-matching) and delay. While for short delays recognition of matching stimuli relied on posterior theta activity, frontal theta activity was crucial for recognition after long delays. This might indicate switching between perceptual and cognitive strategies. Similar results were found for alpha activity. However, alpha networks might be additionally involved in increasing early sensory processing demands for matching the stimulus to the fading memory during longer delays. Taken together, these findings demonstrate that working memory relies on multiple oscillatory networks of different frequencies, which serve different functions necessary for recognition and are modulated in their timing and regional specificity depending on task demands.

Relationships between evoked potentials,

spontaneous EEG and intelligence measures. M. Schier, C. Stough, *FLSS, Swinburne University of Technology, Melbourne, Australia*

In our study we recorded and examined the relationship between evoked, spontaneous EEG, and a measure of intelligence. With evoked potentials, the string length is effectively the length of a piece of string laid over the normalised evoked response curve, and captures information about excursions of the evoked response trace, such that a larger string length effectively means more changes or greater differences between positive and negative changes. This has been previously correlated with intelligence. With spontaneous activity, a series of measures based around statistical moments (and also known as the Hjorth parameters activity, mobility & complexity) can be derived. Of these, the complexity makes a measure of rapidity of changes. This has been previously correlated with string length. As previous studies have demonstrated a relationship between string length (an evoked measure) and intelligence, and string length and complexity (a spontaneous measure), the missing connection is between complexity and intelligence. This study is a 3-way comparison of spontaneous, evoked and intelligence measures, using the auditory evoked potential. The initial results are the first to show relationships between these three measures and will be reported on in this presentation. The future benefits of the results of this study may save time and simplify recording parameters for analysing brain electrical activity.

Rapid information processing revealed by electrical brain activity mapping. W. Skrandies, *Institute of Physiology, Justus-Liebig University, D-35392 Giessen, Germany*

Human perception, thinking, and spontaneous movement or reaction to stimuli occurs in the split-second range. Electrical brain activity mapping shows topographically distinct temporal components or microstatesthat occur in rapid succession. For example, simple visual stimuli yield components at 80, 100, and 120 ms that reflect different brain processes.

Until a few years ago, there was a distinction between so-called exogenous and endogenous components of event-related brain activity. These were interpreted to index the processing of physical stimulus features or the influence of attention and cognitive processing. Recent publications have demonstrated that such a distinction is not warranted. The topography of ERPs components occurring as early as 100 ms after stimulus presentation is significantly influenced by attention, stimulus compatibility, or semantic meaning of language material. This suggests very rapid information processing of simple and complex stimuli in primary cortical areas.

A look at basic facts from sensory physiology and neurophysiology reveals that such results are far from surprising. Axonal conduction velocity is very high, distances within the brain are very small, and afferent routing to many different brain areas occurs in parallel pathways. There are many sensory, motor and cognitive processes that occur very fast: simple stimulus perception and processing of information contained in dynamic random-dot stereograms, motor reaction to simple stimuli or regular and ëxpress saccadesäs well as higher cognitive processing like reading (and understanding) words, or occur in fractions of

seconds.
Thus, in combination with electrical and fMRI brain imaging techniques, brain electrical activity mapping is an appropriate and useful tool for investigating sensory and cognitive functions of the human central nervous system.

The renaissance of the electrophysiological methods in schizophrenia research. S. Galderisi, *Department of Psychiatry, University of Naples SUN, Naples, Italy*
Recently, several factors contributed to the renascence of the electrophysiological methods in schizophrenia research; the most influential ones include: 1) the validation of previously reported electrophysiological findings by means of functional brain imaging techniques; 2) the possibility offered by electrophysiological techniques to study brain's systems physiological and pathological activity with a high temporal resolution; 3) a different conceptualizations of psychopathological phenomena, increasingly regarded as a consequence of the failure to integrate the activity of different brain areas. Main deliveries of such renascence include advances in the study of abnormal functional connectivity underlying schizophrenia symptoms and the identification of electrophysiological endophenotypes. In spite of the fact that electrophysiological abnormalities were shown to be related to diagnostic subtypes, risk factors, symptom dimensions and prognosis, electrophysiological methods are still of limited impact in clinical settings, and their application is confined to the exclusion of örganic"brain pathology.

New research potential of Mismatch Negativity: "Optimized"multifeature paradigms in clinical psychiatry. C. Norra (1), H. Thoennessen (2), *(1) Dept. of Psychiatry and Psychotherapy, Laboratory of Clinical Neurophysiology, Ruhr University Bochum, Germany, (2) Dept. of Child and Adolescent Psychiatry and Psychotherapy, University Hospital Aachen /Institute of Medicine, Research Center Juelich, Germany*

In neurophysiology, the mismatch negativity (MMN) of evoked potentials was consistently used to unmask deficits in pre-attentive information processing in schizophrenia - though not specific for this disorder. Traditionally,studies were performed with so-called öddballparadigms applying 10-20% of deviants within a series of standard tones. Instead, Näätänen et al. (2004)proposed an öptimizedmultifeature design with 50% of deviants operating 5 different deviants. These procedures were primarily employed in non-clinical samples only and extended to multiple assignments.

While we aimed at comparing the two procedures in EEG and MEG in schizophrenia, the optimized design was fastest to detect MMN changes. MMN was mostly reduced in schizophrenia if measured with MEG in the optimized paradigm reaching mean effect sizes of 0.85 (max. 1.5) as opposed to 0.65 in the traditional MMN profile recorded with EEG. Moreover, the MMNm of the left auditory cortex correlated significantly with positive symptoms for schizophrenia in both paradigms (Thönneßen et al. 2008). Especially the relationship of MMN deficits to psychopathology will have to be further clarified, and our results are currently replicated in patient samples with chronic schizophrenia as well as ADHD and substance abuse (Norra et al. in prep.) However, despite advantages of multifeature MMN

designs with shorter duration, higher sensitivity and multitude of characteristics to be analysed it remains open whether these new MMN tools are similar to the sensory memory trace build up by standard stimuli in the oddball MMN or rather reflect deficits in the central nervous representation of tonal characteristics. Therefore, minimal changes in the early auditory processing of multiple components would also be of relevance to the human speech including prosody (e.g. Kujala et al. 2005, Pakarinen et al. 2007). Thus, further investigation of pseudowords arranged in MMN pattern with either emotionally neutral or positive and negative intonation showed stronger bilateral MMNm of the latter, with predominance on the right hemisphere in the traditional and optimized designs in healthy individuals (Thoennessen et al. 2010). These findings will have implications for the early information processing and detection of physical and emotional contents of sounds, speech and social cognition of different psychiatric disorders as being studied.

Impact of EEG-vigilance on brain glucose uptake measured with [18F]FDG-PET in patients with depressive episode or mild cognitive impairment. T. Günther (1), P. Schönknecht (1), S. Hesse (2), S. Olbrich, C (1) . Sander (1), P. M. Meyer (2), G. Becker (2), J. Luthardt (2), U. Hegerl (1), O. Sabri (2), *(1) Department of Psychiatry and Psychotherapy, University Hospital Leipzig, Leipzig, Germany; (2) Department of Nuclear Medicine, University Hospital Leipzig, Leipzig, Germany*

[^{18}F]fluorodeoxyglucose positron emission tomography ([^{18}F]FDG-PET) is a well-established method for the examination of the cerebral glucose metabolism of patients with affective disorder or memory impairment. Building upon previous neuroimaging studies, we supposed an association between electroencephalogram (EEG)-vigilance and normalized brain [^{18}F]FDG-uptake (nFDGu) as measured by [^{18}F]FDG-PET. For the first time, the present study exploratively investigated this association in a routine diagnostic work-up.

Simultaneous EEG and [^{18}F]FDG-PET under resting conditions were acquired from 14 patients with depressive episode or mild cognitive impairment (MCI). EEG-vigilance was automatically classified by using the VIGALL algorithm (Vigilance Algorithm Leipzig). A nonparametric voxelwise simple linear regression with vigilance measure as predictor and nFDGu as criterion was performed using Statistical nonParametric Mapping toolbox.

The main finding was a significant negative correlation between vigilance measure and nFDGu in bilateral frontal and temporal regions, bilateral cingulate gyrus and right thalamus with vigilance-related changes of nFDGu between 17.1 and 44.4%.

Simultaneous EEG and [^{18}F]FDG-PET under resting conditions revealed that brain regions associated with EEG-vigilance partly overlapped with regions of impaired nFDGu in depression and MCI, as reported by previous studies. Vigilance-related changes of nFDGu were about the same size as disease-related metabolic changes in patients with affective disorder or memory impairment as reported in previous studies. Therefore, our data suggest that differences in EEG-vigilance might influence alterations of nFDGu in disorders such as depression or MCI. Whether this possible impact of vigilance on nFDGu should be taken

into account during the routine diagnostic application of [^{18}F]FDG-PET has to be explored in future studies with larger patient groups.

qEEG during trance healing: simultaneous results from healer and client.

P. L. Faber, P. Milz, F. Schlegel, D. Lehmann, *The KEY Institute for Brain-Mind Research, University Hospital of Psychiatry, Zurich, Switzerland*

Two experienced trance healers (Pascal Voggenhuber and Bahar Voggenhuber-Yilmaz who occasionally treat each other) were recorded simultaneously, each with 27 EEG channels. During no-task resting, their power spectra differed strongly: BV-Y showed an alpha power peak at 8.5 Hz, PV at 11.5 Hz. The two participants alternated their functions as trance healer and as client (8 sessions of 15 min: each participant 4 times as healer, 4 times as client). FFT spectral analysis was done using average reference. Spectra were averaged across the 27 channels. Power values were integrated for each of the eight frequency bands from delta through gamma. Resting states differed significantly from healing and client states. The eight simultaneous results of the healing sessions were statistically compared (band-wise block ANOVA). In their function as trance healer, both participants showed significantly less power in the delta and beta-3 EEG frequency bands than in their function as client. In sum, this pilot study of trance healing produced distinct qEEG states (that combined EEG characteristics of functional inhibition and functional facilitation) in healer and client that cannot be reduced to changes towards drowsiness or alertness.

EEG individual alpha frequency linked to functional and structural MRI.

K. Jann, A. Federspiel, M. Kottlow, T. Dierks, T. Koenig, *(1) Department of Psychiatric Neurophysiology, University Hospital of Psychiatry, University of Bern, Bern, Switzerland*

In this study we tried to find functional and structrural differences related to subjects individual alpha frequencies (IAF). IAF varies across subjects and is associated to a persons cognitive capabilities, especially in working memory processes. For this purpose we recorded simulatneous EEG-fMRI and diffusion tensor images (DTI). Functionally, we found that small intra-indiviudal temporal IAF fluctuations are positively related to increased BOLD signal in brain aras involved in working memory functions and the modulation of attention. Structural differences depending on interindividual IAF differences were found in fascicles connecting the above mentioned networks: subjects with higher IAF show increased DTI functional anisotropy (FA) values. These two observations taken together suggest that it is plausible that increased IAF improves task performance because there is increased activity and better connectivity in the relevant functional networks.

Analysis of ERP-data with matrix-wavelets and PCA.

A. Klein (1), T. Sauer (1), W. Skrandies (2), *Department of Mathematics, (2) Institute of Physiology, Justus-Liebig University, Giessen, Germany*

Whenever data from an array of EEG-electrodes is processed, the modelling of dependencies between electrodes tends to complicate the processing of the data significantly when each channel is processed separately as a scalar time-series. In this case, every pair of electrodes has to be handled

separately which becomes very cumbersome, even for moderate numbers of channels, since the number of pairs grows quadratically with the number of channels. This problem is remedied somewhat when the ensemble of channels is viewed as a multidimensional time-series that allows the dependencies to be modelled in the form of matrices operating on the time series via matrix-vector products, for example. However, a few things still remain to be considered: Time delays between channels cannot be modelled this way, as well as a number of more general dependencies that are not necessarily useful for EEG-analysis, but would be interesting in other settings. As a first step towards a general framework for multidimensional data analysis, we applied the novel method of matrix-wavelet-analysis to human SEP-data. The results of the matrix-wavelet-transform, which are complex-valued in this case, were further processed with principal component analysis, allowing us to test for:

1. Variations in the dimensionality of the data,

2. Shifting of spatial centroids of activity for certain components under different conditions,

3. Shifting of centroids of activity in time-frequency-space for certain components under different conditions.

The results were compared with the results that will be achieved when each channel is subjected to the scalar wavelet transform with PCA only applied to the aggregated transforms.

Print tuning during fast reading: a simultaneous EEG-fMRI study. J. Kronschnabel (1), U. Maurer (1), R. Schmid (1), D. Brandeis (1,2), *(1) Department of Child and Adolescent Psychiatry, University of Zürich, Switzerland, (2) Department of Child and Adolescent Psychiatry and Psychotherapy, Central Institute of Mental Health, Mannheim, Germany*

Tuning of visual activity for print yields an increased occipito-temporal N1 at about 150-250 ms in the event-related potential (ERP) to words compared to symbol strings. In functional Magnetic Resonance Imaging (fMRI) a corresponding specialization has been located in an occipito-temporal visual word form (VWF) system. In developmental studies specialization for print was reduced in adults compared to beginning readers. Yet, this was under slow presentation conditions that did not challenge adult reading skills adequately. Here, we test whether specialization for print increases if stimuli are presented under faster, more challenging conditions.

Words and symbol strings were presented to 8 adults for either 700 or 100 ms (long vs. short condition), while keeping SOA constant (1950 ms). ERP (59 channels) and fMRI data were collected simultaneously in a 3T scanner using a block design. Preliminary analyses revealed a larger left occipito-temporal N1 for words than for symbols, and a reversed pattern over the corresponding right hemisphere in both the short and long conditions. This tuning effect, however, was not further modulated by the presentation duration. Although the fMRI random effects analysis showed the expected activation pattern for the word and symbol conditions, no robust word-symbol differences emerged in VWF regions neither with

long nor with short presentation duration.
In conclusion, robust N1 effects indicating specialization for print could be obtained from the simultaneous recordings suggesting successful removal of scanner-related artifacts. Shorter presentations that challenge the reading system more strongly did not increase N1 print tuning in a sample of normally reading adults. The absence of any word-specific VWF activation in the fMRI data may be due to the small sample size, as previous studies using larger samples have found such effects to be weak. Alternatively, short presentations alone may not sufficiently challenge the mature reading system.
Supported by the Swiss National Science Foundation.

Functional sLORETA tomography of EEG during hypnotic and voluntary arm lifting. D. Lehmann (1), E. Cardeña (2), P. L. Faber (1), P. Jönsson (2), P. Milz (1), R. D. Pascual-Marqui (1), K. Kochi (1), *(1) The KEY Institute for Brain-Mind Research, University Hospital of Psychiatry, Zurich, Switzerland, (2) Center for Research on Consciousness and Anomalous Psychology (CERCAP), Lund University, Sweden*
What is the brain electric mechanism of hypnosis? The comparison of voluntary motor acts and motor acts under hypnosis can be used to compare hypnotic versus non-hypnotic brain states. In an earlier pilot study on four subjects [1], the dipole model source of the delta-theta (inhibitory) EEG frequency band was more posterior and the source of the alpha (routine function) and beta (facilitatory) bands was more anterior during hypnotic compared to voluntary arm lifting. - The present repeat study tested these findings in 30 volunteers (10 high, 10 medium, 10 low hypnotizables), applying sLORETA functional tomography analysis. As in the earlier study, only left arm movements were done (as is common in hypnosis studies as right hemisphere functions are apparently more amenable to hypnotic influence). Stronger in the hypnotic than voluntary condition was left prefrontal facilitatory activity and left central-superior temporal inhibitory activity, weaker was left inferior frontal-superior temporal inhibitory activity and right postcentral-temporo-parietal facilitatory activity. Results were similar over hypnotizabilty groups. - These results confirmed our earlier study, showing anterior facilitation and posterior inhibition in the hypnotic condition, and the opposite in the voluntary condition. Increase of self-rated hypnotic depth correlated with increased anterior inhibitory and decreased central facilitatory activity in the left hemisphere. Since only left arm data were available, the full role of the hemispheres remains to be clarified in future work. Reference: [1] Lehmann, D., Faber, P.L., Isotani, T. and Wohlgemuth, P. Source locations of EEG frequency bands during hypnotic arm levitation: a pilot study. Contemporary Hypnosis 18: 120-127 (2001). Erratum in: Contemporary Hypnosis 18: 220 (2001).
Supported in part by Bial Foundation

Preliminary tomographic neurofeedback results from children with ADHD. S. Maurizio (1), M. Liechti (1,2), H. Heinrich (3), G. Thalmann (1), L. Meier(1), Y. Schwitter (1), S.Hossmann (1), S. Walitza (1), H.-C. Steinhausen (5), L. Jäncke (2), R. Drechsler (1), D. Brandeis (1,6), *(1) Dept. of Child and Adolescent Psychiatry, University of Zürich, Switzerland; (2) Dept. of Neuropsychology,*

Institute for Psychology, University of Zürich, Switzerland; (3) Dept. of Child and Adolescent Psychiatry, University of Erlangen-Nürnberg and Heckscher-Klinikum, München, Germany; (4) Dept of Child and Adolescent Psychiatry, University of Leipzig, Germany; (5) Aalborg Psychiatric Hospital, Aarhus University Hospital, Aalborg, Denmark; (6) Dept. of Child and Adolescent Psychiatry and Psychotherapy, CIMH, University Heidelberg-Mannheim, Germany; and CIHP, University of Zürich, Switzerland

In this ongoing study, electroencephalogram (EEG) based tomographic neurofeedback (tNFB) is evaluated and compared to an EMG biofeedback training to clarify specific and nonspecific contributions to the treatment of attention deficit hyperactivity disorder (ADHD) in children. We hypothesised that region specific tNFB training leads to increased contingent negative variation (CNV; an event-related potential component reflecting preparation). A group of 13 children with ADHD (8.5-13y) was trained over 18 sessions to regulate their theta/beta-frequencies and slow cortical potentials (SCP) in the anterior cingulum (ACC). Thirty-one-channel EEG was used to calculate low-resolution electromagnetic tomographic (sLORETA) NFB. CNV changes were recorded as pre-/post-measurement in a cued continuous performance test (CPT).

Following tNFB training, we found improvement on behavioural rating scales and a tendency toward normalisation of the CNV. What aspects of regulation improved with tNFB training is currently being analyzed. Analyses of the EMG control group are also under way. Group comparisons will further clarify how specific this tomographic technique is.

Supported by the SBF COST B27 ENOC and by a grant to the GD, Kanton Zurich

EEG power and synchronization is differently linked to the BOLD signal in children and adults during working memory.

L. Michels (1), R.Lüchinger (2), T. Koenig (3), E. Martin (1,4), D. Brandeis (2,4,5), *(1) MR-Center, University Children's Hospital, University of Zurich, Zurich, Switzerland; (2) Department of Child and Adolescent Psychiatry, University of Zurich, Zurich, Switzerland; (3) Department of Psychiatric Neurophysiology, University Hospital of Psychiatry, Bern, Switzerland; (4) Center for Integrative Human Physiology, University of Zurich, Zurich, Switzerland; (5) Department of Child and Adolescent Psychiatry and Psychotherapy, Central Institute of Mental Health, Mannheim, Germany*

Increased theta band (4-7 Hz) activity is present typically when children and young adults performing a cognitively demanding task. Theta rhythms have been recently investigated in adults during short-term working memory (STWM) by simultaneous EEG-fMRI recordings, revealing an inverse relation to the BOLD (blood oxygen level dependent) signal. Yet, not only spectral power but also synchronization plays a fundamental role in cognitive processing, since the level of theta band synchronization is modulated during STWM. However, little is known about potential interactions between the BOLD signal and EEG synchronization during STWM. Further, it is unclear whether EEG-BOLD signal correlations differ between adults and children. In addition, the link between behaviour and physiological markers (i.e., power, synchronization, and the BOLD signal) during STWM

is not fully understood yet. In this study we asked in 18 young adults and 15 children whether EEG-BOLD signal correlations show age-dependent effects during a Sternberg STWM task. Our results reveal that frontal EEG theta power and theta-BOLD signal correlations were significantly enhanced in children compared to adults, i.e. the latter being visible as negative theta-BOLD signal correlations. In contrast, correlations between theta synchronization and the BOLD signal were exclusively positive but only significant ($p < 0.001$, uncorrected) in adults at midline frontal regions, right posterior parietal cortex, and posterior cingulate cortex. Synchronization but not power correlated positively with performance during the most demanding load condition in both groups of subjects, however, significantly stronger in the adults. Our results indicate that theta EEG-BOLD signal correlations depend differently on spectral power and synchronization and that they show age-dependent effects. Specifically, the weaker theta EEG and theta-BOLD signal synchronization effects in children might indicate not fully developed cognitive processing. This seems to be supported by the weaker coupling between synchronization and performance in children compared to adults.

Response control in patients with borderline personality disorder. M. Ruchsow (1), J. Karitzky (1), G. Grön (2), D. Brummer (2), M. Falkenstein (3), L. Hermle (1), *(1) Dept. of Psychiatry Christophsbad, Faurndauer Str. 6-28, D-73035 Göppingen, Germany; (2) Dept. of Psychiatry, University of Ulm, Leimgrubenweg 12-14, D-89075 Ulm, Germany; (3) Leibniz Research Centre for Working Environment and Human Factors (IfADo), Ardeystr. 67, D-44139 Dortmund, Germany*

Nogo-N2 and Nogo-P3 are supposed to be electrophysiological correlates of response control. Both ERP-components were measured in patients with borderline personality disorder (BPD, n = 17) and an independent sex-, age-, and education-matched control group.

Participants performed a hybrid flanker-Go/Nogo paradigm while a 64-channel EEG was recorded.

BPD patients showed reduced Nogo-P3 amplitudes compared to healthy controls; with respect to the Nogo-N2 there were no significant group differences. Possibly, the Nogo-P3 can be used as an electrophysiological marker indicating increased levels of impulsiveness. An additional study with healthy controls supports this view. Further research is needed to exactly determine the underlying neuropsychological and neurobiological mechanisms resulting in altered Nogo-P3 amplitudes in psychiatric patients.

Response control in patients with obsessive-compulsive disorder. M. Ruchsow (1), J. Karitzky (1), G. Grön (2), D. Brummer (2), M. Falkenstein (3), L. Hermle (1), *(1) Dept. of Psychiatry Christophsbad, Faurndauer Str. 6-28, D-73035 Göppingen, Germany; (2) Dept. of Psychiatry, University of Ulm, Leimgrubenweg 12-14, D-89075 Ulm, Germany; (3) Leibniz Research Centre for Working Environment and Human Factors (IfADo), Ardeystr. 67, D-44139 Dortmund, Germany*

Nogo-N2 and Nogo-P3 are supposed to be electrophysiological correlates of response control. Both ERP-components were measured in patients with obsessive-compulsive

disorder (OCD, n = 13) and an independent sex-, age-, and education-matched control group.
Participants performed a hybrid flanker-Go/Nogo paradigm while a 64-channel EEG was recorded.
OCD patients showed enhanced Nogo-N2 amplitudes compared to healthy controls; with respect to the Nogo-P3 there were no significant group differences. Possibly, the Nogo-N2 can be used as an electrophysiological marker indicating increased levels of compulsiveness. An additional study with healthy controls supports this view. Further research is needed to exactly determine the underlying neuropsychological and neurobiological mechanisms resulting in altered Nogo-N2 amplitudes in psychiatric patients.

The syntax of EEG microstates is sequence-inverted in skeptics and believers of paranormal phenomena. F. Schlegel, D. Lehmann, P. Faber, P. Milz, K. Kochi, *The KEY Institute for Brain-Mind Research, University Hospital of Psychiatry, Zurich*
Believers in paranormal phenomena have been hypothesized to have an increased vulnerability for schizophrenia. We tested this contention using microstate syntax analysis. The participants were selected from volunteer university students using a self-report scale for paranormal beliefs and experiences. Spontaneous brain electric activity (multichannel EEG) of believers (n=16) and skeptics (n=13) was recorded during closed eyes resting. EEG viewed as series of momentary potential distribution maps ('landscapes') can be parsed into segments of quasi-stable landscape, the microstates, the putative 'atoms of thought' that last about 100 ms. The microstates that were obtained from the present data were clustered into four microstate classes (A,B,C,D; Koenig et al., NeuroImage, 2002) that represent different types of information processing. Analysis of the temporal sequence (syntax) of these microstate classes revealed that believers showed a predominant sequence of microstate concatenations from A to C to B to A that was reversed in skeptics (A to B to C to A). - The present study demonstrated that subclinical differences in personality can be detected in resting EEG microstate syntax. The microstate concatenation sequences reported in a previous study that examined microstate syntax in medication-naive schizophrenics (Lehmann et al., Psychiatry Res, 2005) do not agree with the present results for believers. In sum, the studies did not reveal similarities in EEG microstate syntax between believers in paranormal phenomena and schizophrenics.

Aging, inhibiton measured by ERPs and intraindividual variability. C. Schmiedt-Fehr, S. Dühl, C. Basar-Eroglu, *Institute of Psychology and Cognition Research, University of Bremen, Germany*
ERPs are a valuable and common tool for studying changes of inhibitory function with age. This approach is based on the hypotheses that the detected signal in each single trial has stable characteristics, such as constant waveform morphology, amplitude, latency and spectral composition across all trials. Considering evidence for increased intraindividual variability (short-term trial-to-trial fluctuation) of behavior in later adulthood this assumption may not be unproblematic when applied to research in the field of cognitive aging. The present study aimed at verifying previously reported ERP results on inhibition-related sub-

processes in auditory and visual modality in single trial analysis. Commonly estimated Go- and NoGo ERP (N2/P3) components amplitude and latencies measures were compared with single trial estimations of time frequency magnitude and inter trial phase-locking in the delta and theta frequency range. In the auditory modality the single trial analysis mainly supported the previously reported ERP results, indicating inhibition-related changes with age in the P3 time range. In the visual modality main results also supported earlier ERP reports. In addition the results suggest that especially theta oscillations may be associated with age-related changes in response inhibition. The comparison of both the ERP and single trial time-frequency approach did not support the hypotheses that older age is related to increasing intraindividual variability in neural responses, at least during Go and NoGo processing.

Reliability of the STROOP interference task: An ERP study. T. Fehr(1,2), J. Wiechert (1), M. Herrmann (1,2), *(1) Dept. of Neuropsychology/Behavioral Neurobiology, Center for Cognitive Sciences, University of Bremen, Bremen, Germany; (2) Center for Advanced Imaging Bremen/Magdeburg, Bremen, Germany*

The STROOP-paradigm is one of the most consistent experimental approaches in psychological sciences. However, retest-reliability in individual physiological parameters has not been examined in both experimental intra- and inter-session arrangements. Based on previously published data, we applied an adapted form of the STROOP-task in an EEG-study to estimate individual intra- and inter-session reliability of behavioural and electrophysiological data. Behavioural data showed both consistent split-half as well as re-test reliability in 15 healthy young female study participants. There was an expected interference effect in the incongruent condition reflected in longer response times compared to both congruent and baseline conditions, and a facilitation effect in the congruent condition reflected in shorter response times compared to the baseline condition. Behavioural data will be discussed in relation to the respective electrophysiological findings.

The feeling of colors - semantic dimensions and topography of brain electrical activity. W. Skrandies, B. Rahimi, *Institute of Physiology, Justus-Liebig University, D-35392 Giessen, Germany*

The semantic differential technique is used in order to define dimensions of connotative meaning. We investigated the affective meaning of color words. 13 different words were rated on adjective scales of opposite meaning by a total of 1865 healthy young adults. We found three dimensions that reflected ”evaluation” (E, friendly, good, nice, etc.), ”potency” (P, strong, big, heavy, etc.), and ”activity” (A, fast, noisy, lively). Different colors had different factor scores that were used to classify colors in six different classes (E+/E-, P+/P-, A+/A-).

During ERP recordings, color words were presented in random order on a monitor. Attention was controlled by instructing subjects to could unrelated words appearing at random intervals. EEG was recorded from 42 healthy adults from 30 channels between the inion and Fz. ERPs were computed offline according to stimulus class. Repeated measurement ANOVAs were used for comparing experimental conditions.

Between 70 and 410 ms latency five components were identified by the occurrence of maximal Global Field Power (GFP). Between 70 and 130 ms different semantic classes yielded significantly different GFP ($F(2,82)=29.97$; $p<.00001$): colors judged as ”active” or ”passive” (yellow / orange or brown / black) were followed by high GFP while colors related to potency (P) showed smallest response amplitudes (red / gold or pink / silver). A very similar effect was seen between 130 and 190 ms ($F(2,82)=22.48$; $p<.00001$). This component displayed significantly different latencies ($F(2,82)=5.72$; $p<.0047$) where color words related to activity (A) had smallest latencies. In addition, there occurred a number of significant topographical effects. Our results show that color words can be consistently classified according to their connotative, affective meaning. Such differences are reflected by ERP components occurring after about 100 ms latency when color words are read by healthy adults.

W. Skrandies – Electrical Neuroimaging (Book Review)

W. Skrandies, Institute of Physiology, Justus-Liebig University, D-35392 Giessen, Germany
wolfgang.skrandies@physiologie.med.uni-giessen.de

This book is a tutorial text written by a group of ten experienced scientists who work in the field of multichannel EEG since a long time. The basis for "*Electrical Neuroimaging*" of human brain activity is the topographical analysis of brain electrical activity recorded from the surface of the head. A strictly topographical approach to the assessment of the electrical fields of the brain allows the dynamic mapping of functions of the central nervous system in both healthy subjects and patients with neurological or psychiatric symptoms.

The individual chapters aim at an overview of the neurophysiological basis for electrical imaging (see Chapter 1: "From neuronal activity to scalp potential fields") and on methodological questions of recording and data analysis. The reader also learns about practical problems with data acquisition and preprocessing, and the basic analysis of the electrical fields of the brain. The most instructive chapters explain the statistical analysis of multichannel scalp field data, neuroimaging in the time domain as well as methods of multichannel frequency and time-frequency analysis. In addition, source localization approaches and the imaging of the underlying neuronal generators of EEG (and MEG) are presented in detail. The last chapter gives an outlook on future developments and the integration of EEG with other functional brain imaging methods.

In this book, scientists in the field as well as experienced EEG-readers will learn about the quantitative and statistical spatio-temporal analysis of multichannel-recorded head surface potential fields

There are only a few (formal) shortcomings that can be easily corrected in a future edition of the book. As in many review publications, the cited literature is somewhat selective, and it contains a few errors. These are small shortcomings. However, there is no author index; this makes it impossible to search for individual contributors to the scientific literature. Most figures are clear and instructive, but some of the figures are very small, and in some instances the choice of color appears unfortunate.

In summary, this book enables researchers to apply appropriate analysis strategies to multichannel EEG data. This also helps to avoid mistakes when analyzing and interpreting head surface recorded electrical measurements. The book also contains detailed descriptions of the analysis procedures discussed. I trust that this volume can become an authoritative reference that gives a systematic overview of the theoretical and practical possibilities offered by a strictly topographical analysis of EEG and ERP data.

Electrical Neuroimaging. Edited by C. M. Michel, T. Koenig, D. Brandeis, L. R. R. Gianotti & J. Wackermann. Cambridge University Press, 2009, ISBN-13: 9780521879798, £ 70.00 / 85.40 / US$ 125.-

Announcements — Ankündigungen

- **ISBET Meeting**

  The annual meeting of the *International Society for Brain Electromagnetic Topography (ISBET)* will take place in Heidelberg, Germany, as a **Joint Meeting of ISBET / ISNIP / ECNS** from September 7 to 10, 2011.

  Information and Registration at: `http://www.isnip2011.unitt.de`

- **ISBET Workshop on Topographical Analysis of EEG/ERP Data (T. Koenig & W. Skrandies)**

  This workshop will take place during the **Joint Meeting of ISBET / ISNIP / ECNS**. It will explain the basics of topographical analysis. We will first outline the intrinsic relation between brain electric sources and scalp field measurement. Then, we introduce the possible methods quantify and compare scalp fields, to define components topographically, and to do subsequent statistical comparison. In the first part we will illustrate the theoretical bases of topographical analysis; for the second part it is planned to present a practical demonstration of analysis steps by the application of analysis software.

- **20. Deutsches EEG/EP Mapping Meeting / 20th German EEG/EP Mapping Meeting**

  Conference language is German; English contributions will be accepted.
  - 14. bis 16. Oktober 2011; Schloss Rauischholzhausen
  - Schwerpunkte / Themen
    - H.-R. Duncker (Gießen) Die Entwicklung der Menschen zu Sprach- und Kulturwesen
    - M. Ruchsow (Göppingen) Personale Identität aus Sicht der Neurowissenschaften und der (analytischen) Philosophie
    - M. Doppelmayr (Salzburg) Symposium über Neurokognitive Prozesse im Sport“
    - T. Fehr (Bremen) Symposium über Ëlektrophysiologie und Interferenzprozesse: Dynamik, Individualität und Stabilität“
  - Anmeldeschluss ist der 14. August 2011
  - Information und Anmeldung unter: `http://www.med.uni-giessen.de/physio/`